HSE

Health and Safety Executive

Assessment of electromagnetic fields around magnetic resonance imaging (MRI) equipment

Prepared by **MCL-T Ltd**
for the Health and Safety Executive 2007

RR570
Research Report

HSE

Health and Safety Executive

Assessment of electromagnetic fields around magnetic resonance imaging (MRI) equipment

Philip Chadwick
MCL-T Ltd
17B Woodford Rd
London
E18 2EL

This report describes the results of an investigation of operator exposure to static and switched-gradient fields from magnetic resonance imaging (MRI) systems. The project involves both computational modelling and the measurement of personal exposure using dedicated magnetic field dosemeters. The work was undertaken by Professor Stuart Crozier of the University of Queensland acting as an MCL consultant.

The computational modelling has three strands: modelling of the static and switched-gradient magnetic fields from MRI systems with 1.5 T, 4T and 7T magnets; modelling of induced current densities and internal electric field strengths arising from motion through static field spatial gradients; modelling of induced current densities and internal electric field strengths from time-varying switched-gradient fields.

Close to the ends of the three MRI systems modelled, relevant occupational exposure could be exceeded by movement through the static field, or directly by the switched-gradient fields.

This project has shown that the MRI personal dosemeter is capable of indicating, in real-time, situations which might lead to exposure guidelines being exceeded.

This report and the work it describes were funded by the Health and Safety Executive (HSE). Its contents, including any opinions and/or conclusions expressed, are those of the author alone and do not necessarily reflect HSE policy.

HSE Books

First published 2007

EXECUTIVE SUMMARY

This report describes the a project undertaken by MCL and the University of Queensland to investigate the magnetic field exposures of people working in magnetic resonance imaging (MRI) environments.

The project involved the use computational modelling to calculate the induced currents and voltages in target issues of people exposed to switched-gradient fields around 1.5, 4 and 7 T MRI systems, and also the induced currents and voltages in target issues of people moving through spatially-variable static fields of the magnets of the same systems. The project also included measurements of the actual magnetic field exposure of clinical staff in MRI facilities. These measurements were made with a personal magnetic field dosemeter designed specifically for the purpose.

The conclusions of the project are:

- Within a metre or so of the ends of the 3 MRI systems modelled, guidelines for occupational exposure could be exceeded by movement through the static field or directly by the switched-gradient fields. Faster movement through the static field than the modelled 1 m s^{-1} movement would exacerbate the exposure and slower movement would mean that the exposures would meet the ICNIRP restrictions at smaller distances. The calculated exposures from switched-gradient fields correspond to a worse-case field situation which would occur rarely in routine clinical practice, and real compliance distances may be somewhat less than this.
- Computational modelling of exposure indicates that it is not clear that use of different exposure guidelines would change the overall situation materially, even though this might be inferred from external field measurements.
- Although the size of the magnet does affect the compliance distance when movement through a static field is considered, it does not change the overall picture significantly. There is likely to be a potential problem with this exposure situation for any clinical MRI system. However, the extent to which the problem will be manifest will depend strongly on clinical practice. In particular, exposures to switched-gradient fields occur only when an image is being gathered, whereas exposures to static fields can occur at any time.
- The dosemeter could be used to give an indication of which clinical practices might lead to overexposures to the switched-gradient fields.

1 INTRODUCTION AND BACKGROUND

HSE commissioned from MCL an investigation of operator exposure to static and switched-gradient fields from magnetic resonance imaging (MRI) systems. An outstanding track record specific to MRI exposure modelling is a requirement for this project, as is the ability to dedicate significant effort to the project and to ensuring that it runs to the agreed timeframe. For these reasons, and with HSE's prior agreement, MCL used a Consultant-based project model for this work. The lead scientist was Professor Stuart Crozier of Brisbane University; MCL's Technical Director, Philip Chadwick, provided scientific project management and the interface with HSE.

In late April 2007, Professor Crozier provided his final report on the project. This is attached as an annex. This report is an overall summary of Professor Crozier's findings, intended to inform HSE's policy on occupational exposures to fields from MRI systems.

Professor Crozier's work is likely to provide some of the first published data on occupational exposures to magnetic fields from MRI systems, and will allow bounds to be put on the magnitude of any specific impact on MRI working practices of enforcement of both the EU Physical Agents Electromagnetic Fields (EMF) Directive and existing UK guidance.

MRI systems emit electromagnetic fields at a range of frequencies. There is a large magnet at the heart of the system, and this produces a *static magnetic field*. The health effects of static fields are not well-established, and this was one of the reasons why there is no *Exposure Limit Value* (ELV) for static fields in the EMF Directive. WHO published its Environmental Health Criteria Monograph "Static Fields" as EHC 232 in March 2006 and ICNIRP is expected to publish revised guidelines on static field exposures before the end of the year – these guidelines are, at the time of writing, out for external consultation and review.

When magnetic fields change with time (in strength or direction) they can induce electric currents in anything that conducts electricity, including people. If the currents are strong enough they can cause effects on the central nervous system, and also stimulation of peripheral nerves. These effects can range from almost imperceptible, though annoyance (and pain in the case of peripheral nerve stimulation) to (potentially at least) life-threatening. The EMF Directive, and current UK guidance from the Health Protection Agency- Radiation Protection Division (HPA-RPD; former NRPB), provides restrictions on the central nervous system, current density with appropriate safety factors.

Although there is no specific restriction on the EMF Directive for static fields, a worker moving though the field will experience time-varying current flow in the body as result of this movement. This current flow is addressed by the Exposure Limit Values of the Directive. The issue for the static field from MRI systems, then, is the movement of workers through the field.

MRI systems also use magnetic fields which deliberately vary with time. These are the so-called *switched-gradient fields* which are used to provide spatial data for the image reconstruction. The switched-gradient fields are effectively pulsed, with frequencies in the kilohertz (kHz) range. The same considerations of current flow in the body apply as for people moving through a static field, but in this case no movement is needed for the current to be induced. It is the changing field itself, rather than movement through a constant field that induces current flow.

The EMF Directive's Exposure Limit Values on current density (and the relevant Basic Restrictions of the HPA-RPD [NRPB] advice: they are equivalent) are expressed in milliamperes per square metre (mA m^{-2}). The exact value of the ELV varies with frequency.

The first part of Professor Crozier's work involves the computation of current density induced by movement through the static fields from typical and future MRI systems, and from their switched-gradient fields. The computation uses detailed models of the male and female human body developed by HPA-RPD - called NORMAN and NAOMI respectively - and data on the electrical properties of tissues that were established by MCL.

Although the EMF Directive is based on the guidance of the International Commission on Non-Ionizing Radiation Protection (ICNIRP), the possibility of applying the exposure guidelines of the Institution of Electrical and Electronics Engineers (IEEE) for MRI occupational exposures has been mooted. The reason is that, at the intermediate frequencies generated by the switched-gradient coils, the magnetic field Maximum Permissible Exposures (MPEs) recommended by IEEE are more than sixty times higher than the corresponding Action Values of the EMF Directive. However the IEEE MPEs, like the Directive's Action Values, are to be used as indicators that a more detailed analysis may be required.

IEEE specify Basic Restrictions analogous to those of ICNIRP and to the ELVs of the EMF Directive. Professor Crozier's analyses include a comparison with the underlying Basic Restrictions of IEEE.

[Technical note: there is not a factor of sixty between the IEEE Basic Restrictions and the EMF Directive's Exposure Limit Values; it is not possible to make a simple and direct comparison between them because the IEEE Basic Restrictions are on the electric field strength in tissues, rather than current density. The relationship between the two quantities involves the electrical conductivity of the tissue of interest, so it will vary quite widely with tissue type. There may well be some situations in which the IEEE Basic Restrictions are met when the EMF Directive's Exposure Limit Values are not, but the disparity is unlikely to be as great as indicated by the difference between the IEEE MPEs and the Directive's Action Values.]

Professor Crozier's analyses are intended to provide some indication as to the benefits to the MRI community of pursuing the use of the IEEE guidelines for occupational EMF exposures.

[*Technical note: the IEEE guidelines specifically address the issue of non-sinusoidal fields. They are based on the stimulation thresholds of different (modelled) nerve types, and these thresholds are calculated explicitly for the sorts of waveforms typical of MRI gradient fields – sawtooth, flat-tops and other very non-sinusoidal wave shapes. In contrast, the EMF Directive itself contains no specific guidance or limits for such waveforms. Indeed, the multifrequency summation formulae that ICNIRP included in its guidelines are not present in the EMF Directive. Below 100 kHz, the ICNIRP guidelines themselves generally are based on considerations of steady-state sinusoidal exposure, which are extended by default to non-sinusoidal waveforms in the 1998 ICNIRP Guidance on Determining Compliance of Exposure to Pulsed and Complex Non-sinusoidal Waveforms Below 100 kHz with ICNIRP Guidelines (Health Physics* ***14****, 74).*

The EMF Directive itself does not include this extension, or any other explicit advice on non-sinusoidal fields, and therefore it is not clear quite how - or perhaps even if - it should be applied to exposures from MRI switched-gradient fields. This issue was discussed in some depth at an ICNIRP/WHO/EMFNET workshop in Milan in February 2007, and it is clear from the proceedings of that workshop (in press at time of writing) that the application of the EMF Directive to the sorts of waveforms that are typical of MRI switched-gradient fields is not necessarily defensible. ***For the purposes of this report we have therefore made comparisons between measured and calculated exposures and the ICNIRP guidelines for occupational exposure rather than with the action vales and exposure limit values of the EMF Directive****]*

The second part of the project involves the use of personal dosemeters to measure the exposure of MRI workers to static and gradient fields during 30 working shifts at three MRI facilities. The dosemeters were used to compare the calculated field distributions and gradients around the MRI systems with the actual corresponding values, and to provide information on what levels of magnetic field exposure MRI staff encounter during their normal duties.

2 COMPUTATIONAL MODELLING

2.1 CALCULATION AND PLOTTING OF FIELD DISTRIBUTIONS AROUND 1.5, 4 AND 7 T MRI MACHINES

1.5 tesla (T) magnet MRI systems are common clinical instruments; 4 T systems exist, although they are rarer, and whilst 7 T MRI is currently mainly used for research purposes, this and higher field systems may become more common in the future. The three systems modelled are a 1.5 T Infinion (actively shielded,), 4T Siemens (actively shielded) and 7 T EMI research magnet (unshielded and designed in-house). The three field strengths were chosen to reflect a range of likely exposures rather than to be representative of instruments in common clinical use.

Professor Crozier has modelled the distributions of the static fields around the machines; the results are shown graphically in Figure 1. It is not surprising that the higher strength magnet has the higher fields, but it is interesting that the fields from the smaller magnets show much less uniformity than the field from the 7 T system. This is because the smaller magnets use active shielding, which involves the use of secondary magnetic coils to shape the field from the primary.

Similar plots have been provided for the fields from the gradient coils. *[These can be seen in Figure 1 of Section 2 of Professor Crozier's final report, attached as an Annex to this report.]*

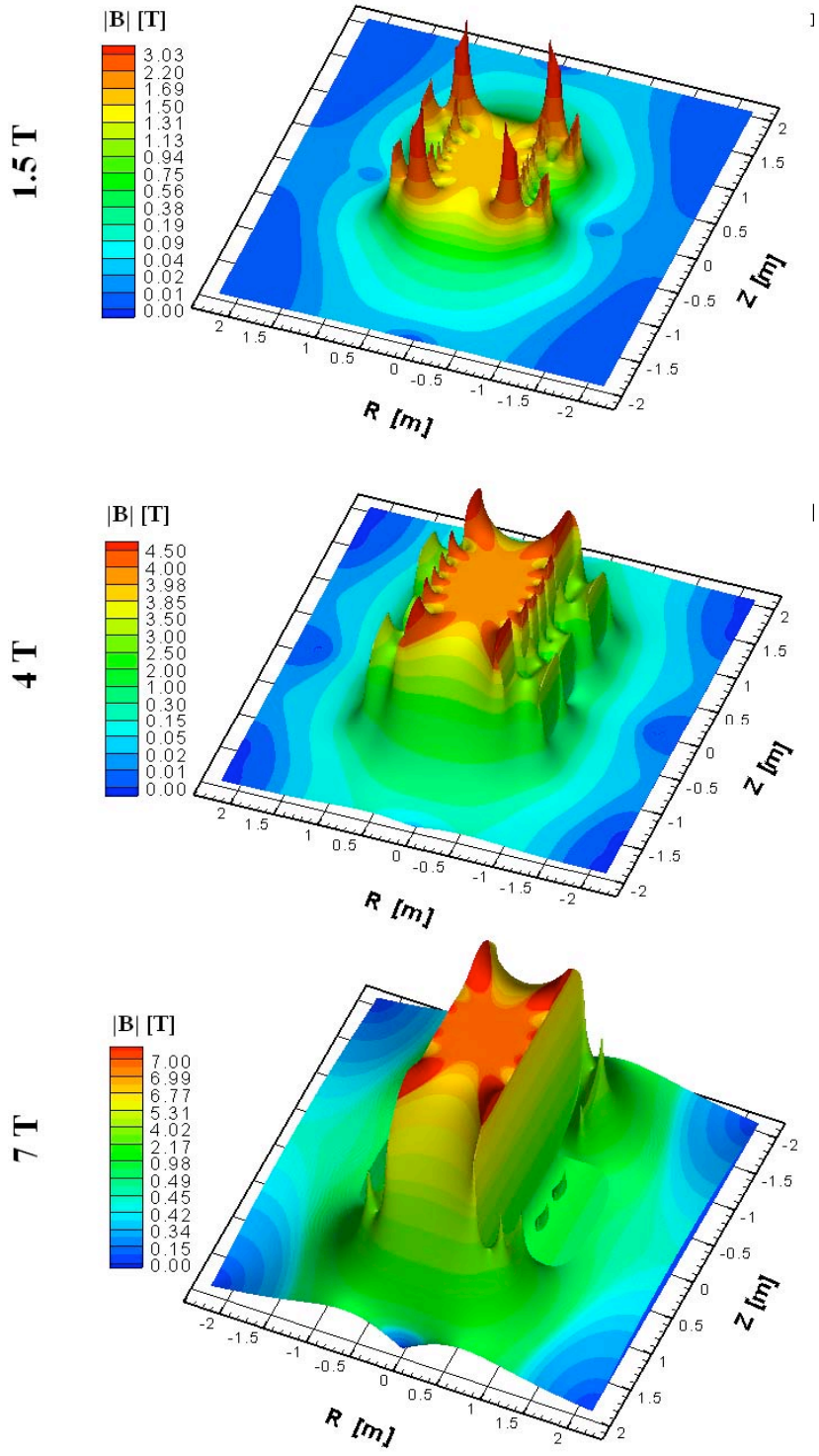

Figure 1 Static field distributions around MRI magnets

2.2 CALCULATION OF INDUCED CURRENT DENSITIES AND INTERNAL ELECTRIC FIELD STRENGTHS FROM MOVEMENT THROUGH STATIC FIELDS

Four types of movement through the static fields from the MRI systems have been modelled:

I Moving parallel to the magnet's long axis

II Moving transverse to the magnet's long axis

III Jumping whilst facing a direction parallel to the magnet's long axis

IV Jumping whilst facing a direction transverse to the magnet's long axis

These defined movements are illustrated in Figure 2.

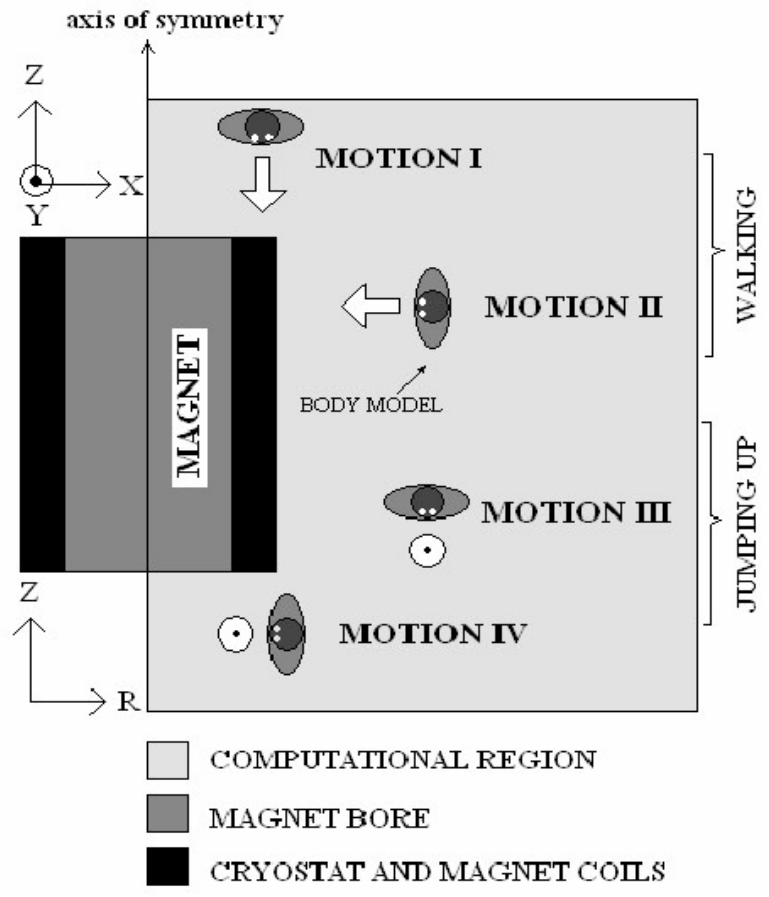

Figure 2 Modelled movements around MRI systems

The four movement directions and the genders of the body models give eight computational permutations for each position around the magnets. To map out the areas of highest exposure in detail, calculations were made over a 0.1 m square grid covering 8.8 square metres. This

corresponds to 880 positions, and therefore 7040 total computational permutations. To make the overall assessment tractable, the body models were run at a comparatively low resolution of 8 mm for this part of the assessment. Figure 3 shows the way in which the maximum computed current density at any point in the male model for each of the four defined movements varies with position around the magnets.

[*Technical note: in fact this is not quite the maximum current density; to avoid artefacts associated with the low resolution of the model, the top 1% of calculated values are excluded*.]

The low resolution spatial information shown in Figure 3 was used to identify the locations where the highest induced currents and internal electric field strengths were to be expected for each gender and each movement around each magnet. This gives 24 computation permutations, which were investigated using the body models at high resolution (2 mm).

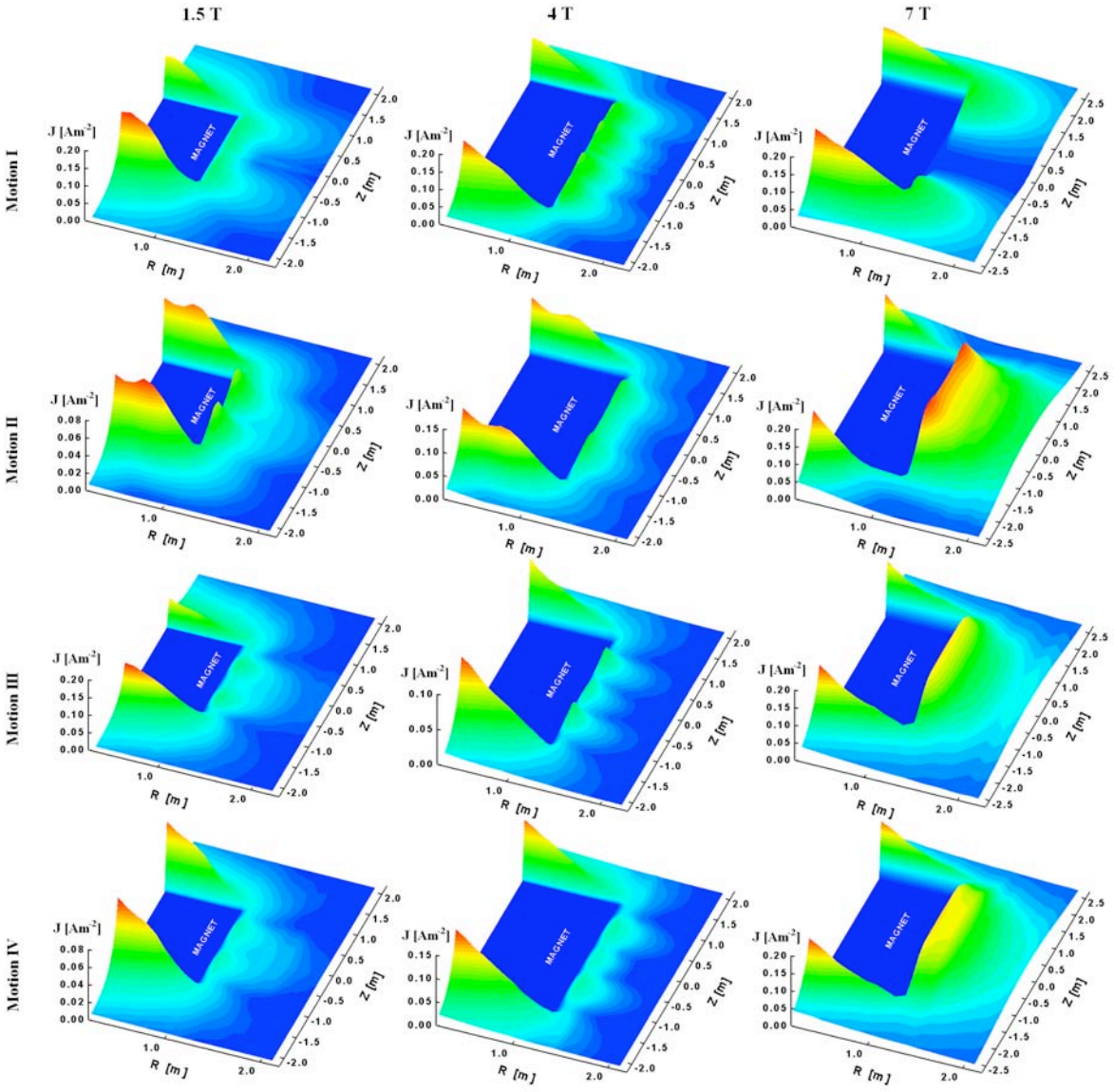

Figure 3 Calculated maximum (99% threshold) current densities in the male body model for the four defined movements around the three magnet systems

Figure 4 shows the distributions of induced current density in the two body models during "Movement 1", moving along the magnet axis toward its end at a distance of 0.3 m from the cryostat.

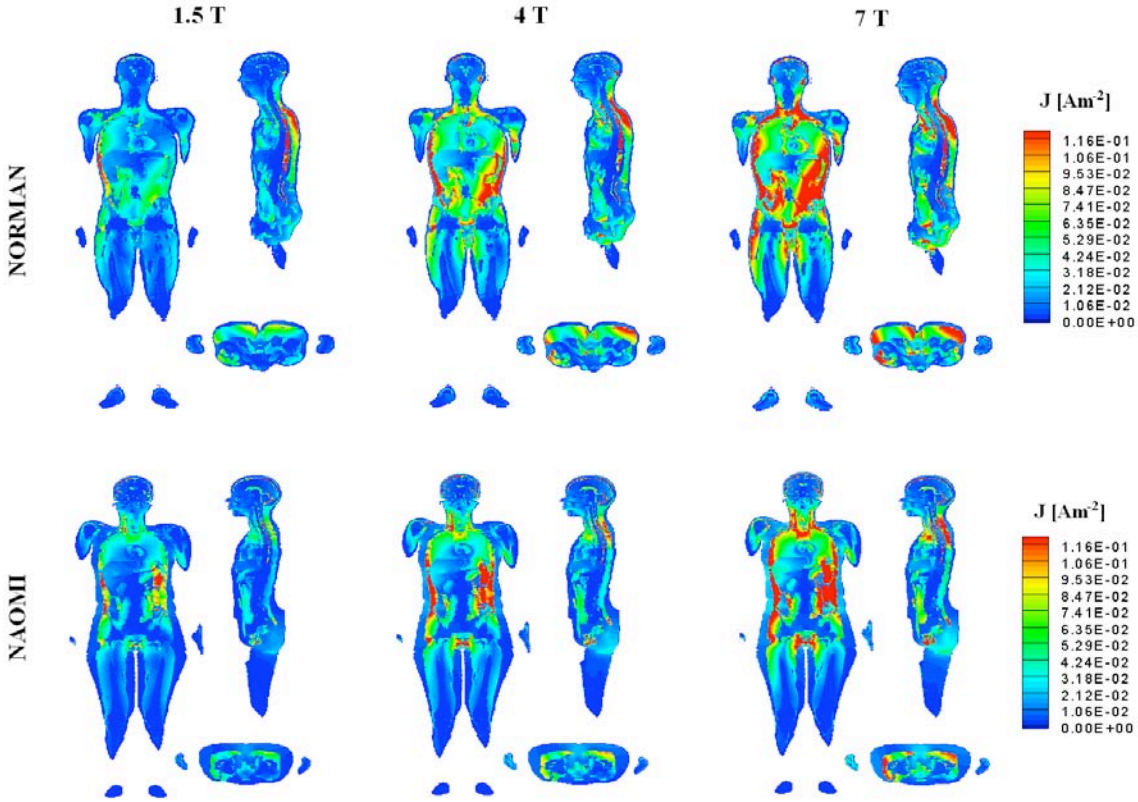

Figure 4 Representative high resolution induced current density distributions

The calculated exposures are for movement through the static field at 1 metre per second; the calculated current densities and internal electric field strengths scale directly with speed.

Professor Crozier's tabulated results indicate that in almost all these worst-case assessment locations, the Basic Restrictions of the ICNIRP Guidelines could be exceeded for any of the four defined movements in either gender. The same is true of the IEEE Basic Restrictions. This is probably no great surprise, as these are by definition worst-case locations. However, it is clear that the ELVs can be exceeded very significantly in some situations.

[*Technical note: In Tables V and VI of Appendix 1 of his report, Professor Crozier provides maximum 1 cm*^{2}-average *current density in various target tissues. These averages are across heterogeneous (multi-tissue) cross sections. Where there are high conductivity materials such as cerebrospinal fluid around a tissue of interest (such as spinal cord) the* 1 cm^2-average *current density will be much higher than the true current density in the tissue of interest. Conversely, where low conductivity tissues (such as bone) surround the tissue of interest, the calculated average current density may be lower than that in the target tissue. The problem of course is that the target tissue does not always have a 1 cm*^{2}- cross section. C*alculations of induced current density by other researchers sometimes follow a suggestion made by ICNIRP to CENELEC (although never officially published) that the averaging is done over an artificial*

cross section made up entirely of the target tissue, even where this is not physiologically realistic. Professor Crozier's calculations do not do this, as he was pursuing worst-case exposure parameters in this investigation. The IEEE's use of internal electric field strength as a basic restriction avoids this problem, and this is one area where it is superior to ICNIRP's use of current density.

The overall message here is that the very calculated high current densities in, for example, cerebrospinal fluid may be of less significance than they appear, and that some of the apparently high current densities calculated for nervous system tissues may be unduly weighted by the inclusion of cerebrospinal fluid into the averaging area.]

One of the most useful parts of Professor Crozier's analysis of exposures arising from movement through static fields is his calculation of likely "compliance distances" based on meeting the IEEE or ICNIRP restrictions in various tissues. He has provided a series of graphs in Figure 9 of Section 1 of his final report to illustrate this, one of which is reproduced below as Figure 5.

The calculated distances are all for Movement 1 at a radial distance of 0.3 m from the magnet's axis as the earlier calculations indicate that this would be, in general, the worst case.

[*Technical note: the reason that the indicated Basic Restriction in Figure 5 is a little above 50 mA* m^{-2} *rather than 40 is because these are temporal peak (as opposed to rms) current densities*]

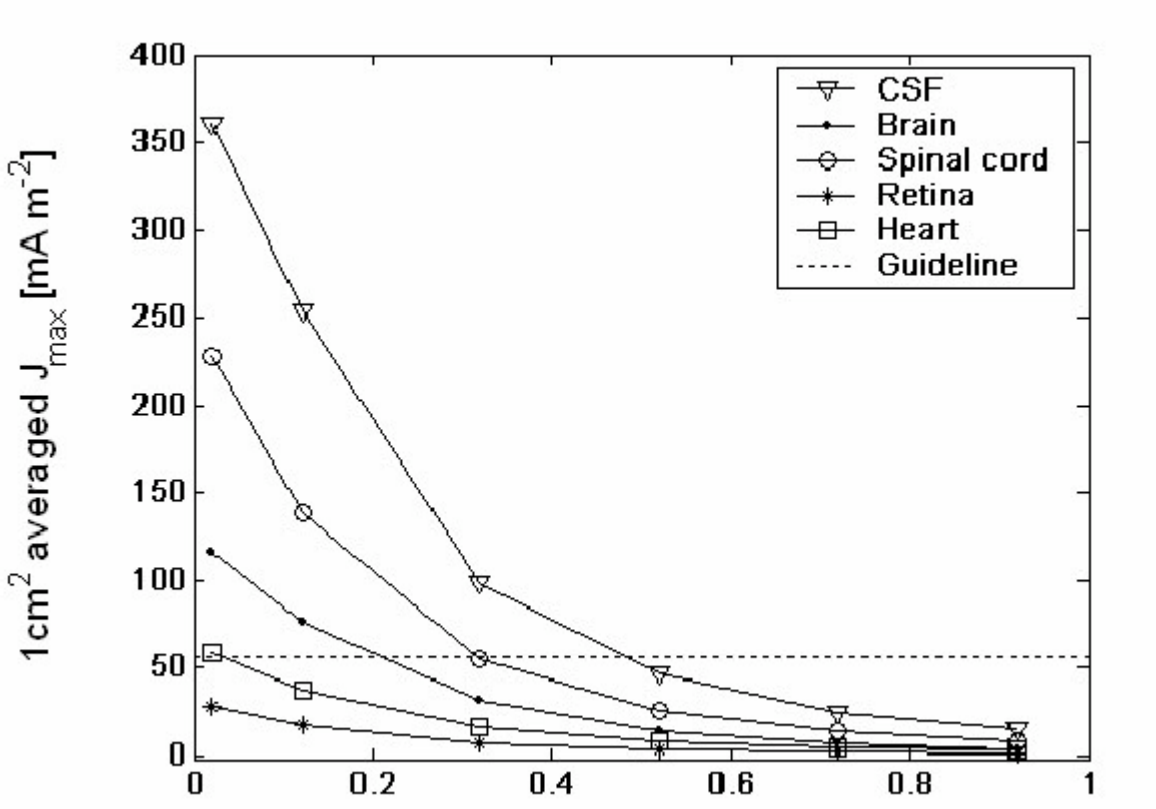

Figure 5 1 cm^2-averaged current densities induced in the central nervous system and heart tissues of the male body model *versus* axial distance away from 1.5 T magnet end (including cryostat vessel)

Summary

- Calculated 1 cm^2- averaged current density magnitudes for people moving at 1 m s^{-1} are below the ICNIRP occupational basic restrictions at approximately 0.5 - 1.0 m from the cryostat end of 1.5 - 7 T MRI systems.
- Use of the IEEE guidelines would not materially affect these distances.
- Faster movement would increase these distances – 1 m s^{-1} is used for illustrative purposes - and a true estimate of likely exposure would require consideration of actual speed of movement during various clinical and maintenance practices including patient emergencies. The current density *vs* distance graphs provided by Professor Crozier allow this scaling to done easily: doubling the speed would double current density, for example, and this would shift the compliance distance indicated in Figure 5 by perhaps 20 cm. Conversely, moving more slowly would mean that the ICNIRP basic restrictions would be met closer to the magnet than 1 m.

2.3 CALCULATION OF INDUCED CURRENT DENSITIES AND INTERNAL ELECTRIC FIELD STRENGTHS FROM SWITCHED-GRADIENT FIELDS

The first part of this work involves the modelling of the magnetic fields from the gradient coils and the plotting of their distributions, as with the static fields. Because of the shapes of the coils and the shielding effect of the cryostats, the regions of strongest field are concentrated around the ends of the MRI system and the directions of the gradient fields will be primarily axial.

For these reasons the initial low-resolution assessments, in which the body models are run at multiple locations to find the worst-case position as was done for the static fields, were carried out in regions around the ends of the coils and with the body models stationary and facing the magnets' bores. The assessment geometry and the area over which the low-resolution computations were made is shown in Figure 6; the area indicated is approximately 2 m square, and the assessment grid has a 0.2 m spacing, which was reduced to 0.1 close to the magnet. This gives more than 100 computational assessment combinations for each of the body models.

[Technical note: this is fewer than for the static field assessments because the multifrequency nature of the switched-gradient fields (Fourier components) makes each computation much more resource-intensive. ***This is a procedure that is predicated upon the use of the ICNIRP summation formulae and cannot, strictly, be done with the EMF Directive alone****]*

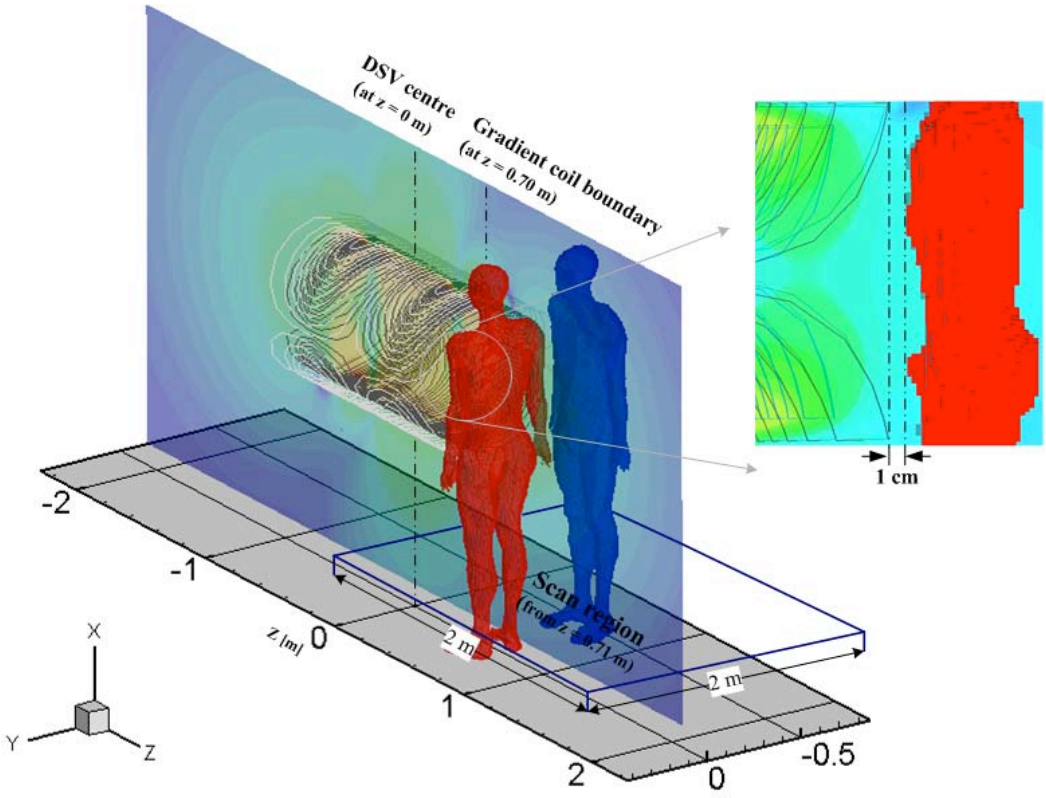

Figure 6 Gradient coil geometry and low resolution assessment region

[Note: Professor Crozier's report (3.2 of Section 2) says: "In order to evaluate the induced

fields due to each gradient individually under similar conditions, all three gradient coils have been designed to have approximately same axial length of ~ 1.4 m, ...The axial length of ~ 1.4 m has been chosen so that the gradient coils would fit inside most conventional 1.5T MRI magnets...and yet be able to provide maximum (i.e. worst-case) exposure to the worker. Table 1 lists some important parameters while Figure 1 (first column) illustrates the geometries of the three gradient coils. We note that the distance from the end of the gradient coil set to the end of the magnet varies between MRI systems and, for cylindrical systems, is typically smallest in short 1.5T magnets and larger in higher field systems. We therefore use the end of the gradient set as a reference point for model positioning"

On this basis, the calculated exposure levels from the theoretical gradient coils may be overestimates for the larger magnets, where the actual gradient coils do not reach the ends of the magnet bore.]

The moving couch that is positioned on a pedestal at one end of the housing will tend to restrict close approach of a vertical body in many cases and this will tend to make real exposures somewhat less than those calculated. This varies from system to system, and to address this Professor Crozier's team have run the simulations to include the worker at 90 degrees to the gradient coil (in blue in Figure 6) as well as facing it (in red in Figure 6. The distribution of induced fields and currents changes between the two body orientations but the maxima remain of very similar magnitude.

The exposures have been calculated for a normalised spatial field gradient of 1 mT m^{-1} and a trapezoidal waveform with a frequency of 1 kHz.

The calculated current densities and internal electric strengths at the worst-case exposure positions are tabulated (Tables 2 -5 of Section 2 of Professor Crozier's final report), and they appear to be below the ICNIRP and IEEE restrictions. However, Professor Crozier makes the point that typical clinical spatial gradients are 40 mT m^{-1}, so the values in the tables all should be multiplied by 40 for a realistic comparison between occupational exposures to switched-gradient fields and the relevant basic restrictions. When this is done the exposure levels close to the MRI systems would exceed the ICNIRP levels and the IEEE levels quite significantly.

The switching time of the switched-gradient field also influences the induced current density; Professor Crozier has calculated scaling factors for a different switching time (250 μs) *via* the Fourier expansion. To scale to a gradient strength of 40 mT m^{-1} and a rise-time of 250 μs with a pulse repetition rate of 1 kHz, the scaling factor is approximately 32.

As with the static field situation, Professor Crozier has provided analyses of how likely exposure levels would change with distance from the the ends of the magnet. He has provided a series of graphs (his Figure 10 of Section 2) to illustrate this, one of which is reproduced below as Figure 7.

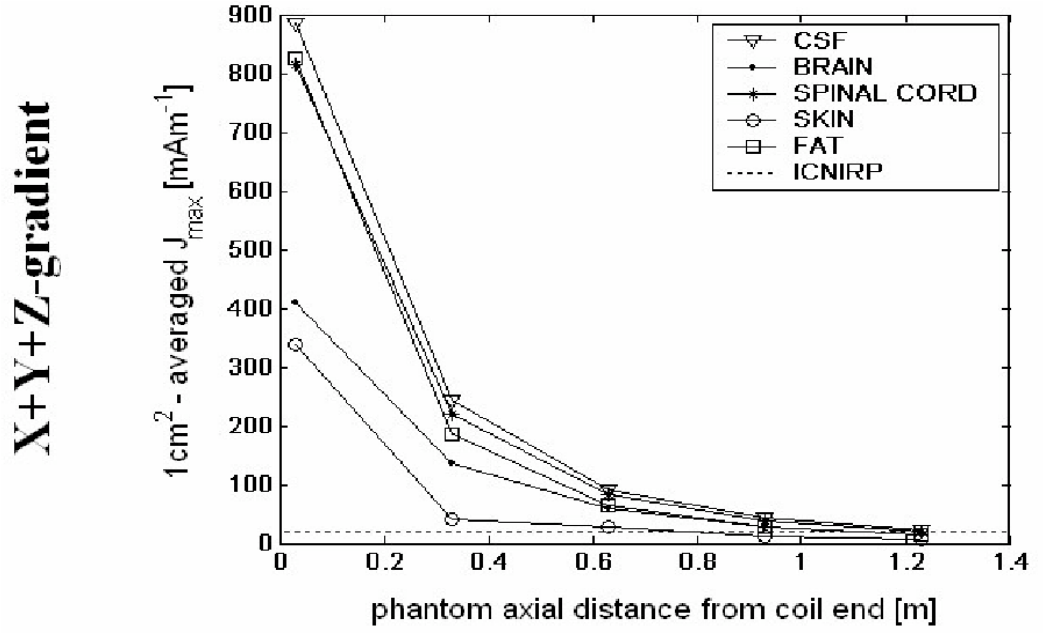

Figure 7 1 cm^2-averaged current densities induced in the central nervous system and heart tissues of the male body model *versus* axial distance away from magnet end (including cryostat vessel)

It can be seen that the ICNIRP occupational basic restrictions would be met at distances greater than approximately 1 m from the MRI system.

Summary

- The ICNIRP occupational basic restrictions would be met at distances greater than approximately 1 m from the MRI system. However, this corresponds to the absolute worst-case of all gradient fields at maximum value. This occurs rarely in routine practice. The distance also would be affected by switching times: longer switching times would decrease the distance at which the ICNIRP levels would be met.
- Using the IEEE guidelines would not necessarily change the compliance distance significantly
- The distance from the end of the gradient coil set to the end of the magnet varies between MRI systems and, for cylindrical systems, is typically smallest in short 1.5T magnets and larger in higher field systems.
- The methodology described in this work is able to be used to calculate regions of compliance for specific magnet/gradient coil combinations.

2.4 RECOMMENDED FURTHER MODELLING WORK

- **Examining exposures during a variety of work postures**. In clinical practice the workers currently often lean into the MRI magnet to attach accessories to the patient or to comfort or communicate with a patient who may be nervous or anxious. Workers also currently lean into the magnets to assess sedated or intubated patients. In these cases, exposure due to both mechanisms; movement through static gradients and residing in strong pulsed gradients needs to be simulated. From a modelling viewpoint, maintaining integrity in the human models with variable posture is not trivial.

- **Exposures in systems used for interventions**. Interventions are performed either with short cylindrical (conventional) magnet systems (such as, for example, The Siemens ESPREE or Toshiba VANTAGE) or in "open" MRI systems. In both cases workers (surgeons, nurses, radiographers) perform movements in static field gradients – some of which require precision, and are exposed to pulsed field gradients. A full modeling analysis of these systems is recommended as a priority.

- **Actions of workers in OEM companies and magnet manufacturers** who frequently enter magnet systems in field servicing or magnet installation/construction phases should be simulated to deduce practices that may be above recommended guidelines.

3 PERSONAL DOSIMETRY

3.1 THE DOSEMETER

The patented magnetic field dosemeter measures exposure to magnetic fields, rate of change of magnetic fields, and enables ambulatory monitoring of instantaneous and cumulative exposure to a wide range of static magnetic fields. It also monitors and measures the cumulative amount of static field gradient that the monitored person is exposed to, thus providing field gradient dosimetry.

A combination of Hall sensors and dB/dt (rate-of-change-of-field) loop sensing coils allow high sensitivity measurements over a large dynamic range of magnetic fields otherwise unattainable by use of a Hall sensor alone. Hall sensors are either limited in dynamic range due to saturation and are unable to measure or record high field strengths accurately, or have wide operating ranges but lack resolution at low field strengths. Loop sensors alone are insensitive to static fields and low frequency fields. Using a hybrid measurement system avoids these problems. The dosemeter measures instantaneous magnetic field strength with the Hall sensor and simultaneously measures rate of change of the magnetic field with the loop coil, located adjacent to and orientated in the same direction as the Hall sensor. At low field strengths within the normal operating range of the Hall probe, the dosemeter uses the Hall sensors' high sensitivity measurements, but at a predetermined field strength below the Hall sensor saturation point loop coil (with an integrator) is used instead.

The dosemeter can provide accurate measurements over a wide range of magnetic field strengths between 0 and +/- 7 T, whilst maintaining high resolution of 0.25 mT at low field strengths. It has a bandwidth of 0 Hz to several tens of kilohertz.

The dosemeter uses a three-axis system orientated in three orthogonal directions, allowing isotropic measurements over a 1 cm^3 volume. The dosemeter has an onboard FLASH memory disk and connects to a PC though a USB interface. A dedicated PC software application uploads the data and presents the data showing cumulative exposure to magnetic field, rate of change of magnetic field, peak values, time-weighted-average exposures, and periods of exposure over any preset value.

3.2 STATIC MAGNETIC FIELDS, AND MOVEMENT IN THEM

A measurement bandwidth from 0 Hz to 7 Hz was chosen for this part of the dosimeter investigation: in a static magnetic field the kinematics of normal human gait and lateral motion, such as leaning forward and bending over, produce effective frequency components within this range. In this configuration the dosemeter has a total active battery life of more than 50 hours and is able to retain 75 hours worth of data.

The device has been used at various MRI sites in Brisbane, Australia and overall 240 hours of measurements were collected. Workers used the dosemeter during their normal working shifts in a 1.5T Siemens Magnetom Sonata clinical system at the UQ research facility at the Wesley Hospital, a 1.5T Siemens Vision clinical system in a private radiology firm at the Wesley hospital, a 1.5T Siemens Vision Plus system at the Royal Brisbane Hospital, a Bruker S200/Oxford Magnet Technology 2T research system at UQ, and a Bruker 4T Siemens clinical

imaging system at the Wesley Hospital. All studies conformed to the ethical standards set down by The University of Queensland ethics board.

Figures 8 illustrates an example of a magnetic field exposure plot measured during a working shift in a 1.5 T clinical MRI facility. It shows the absolute value of the total magnetic flux density, as well as the absolute value of the dB/dt of the magnetic field exposure. From these data, the cumulative exposure and the time weighted average exposure can be calculated, and this was done for each of the thirty working shifts. Peak dB/dt and peak B field were also recorded. This results are shown in Table 3, together with information about the number of patients attended to during the shift, and the site in which the measurements were taken.

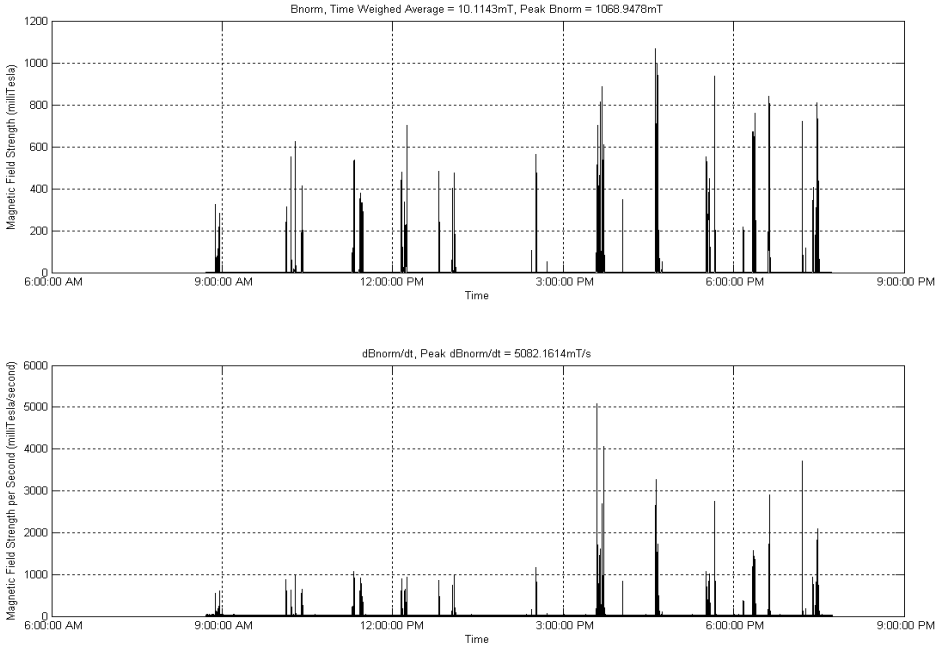

Figure 8 Typical recorded dosemeter data (shift 30)

Table 1 Static field dosimetry results

Shift	*Location*	*Magnet strength (T)*	*|B| Peak (T)*	*|dB/dt| Peak(T s^{-1})*	*|B| Time weighted average (mT)*	*Cumulative |B| (Ts)*	*Number of patients*	*Duration of shift (HH:MM)*
1	Wesley- UQ	4	0.616	1.2	9.92	305.29	8	08:33
2	Wesley- UQ	4	0.429	1.65	1.95	45.67	6	06:31
3	Wesley- UQ	1.5	0.478	5.98	9.05	318.32	12	09:46
4	Wesley- UQ	1.5	0.321	0.56	2.78	80.26	8	08:02
5	Wesley- UQ	1.5	0.569	0.96	12.54	259.51	9	05.44
6	Wesley- UQ	1.5	0.494	1.17	4.28	123.12	6	08:00
7	RBH	1.5	0.446	1.27	7.38	192.41	9	07:14
8	RBH	1.5	0.713	2.77	2.90	96.22	6	09:12
9	Wesley	1.5	0.575	1.56	2.88	127.58	11	12:19
10	Wesley	1.5	0.315	1.24	1.77	78.19	7	12:18
11	RBH	1.5	1.281	2.71	8.82	313.45	10	9:52
12	RBH	1.5	0.592	2.14	3.44	99.75	6	8:03
13	RBH	1.5	0.982	3.85	9.69	392.71	12	11:15
14	RBH	1.5	0.526	4.59	2.50	117.49	9	13:03
15	RBH	1.5	0.334	0.92	1.52	47.62	7	8:41
16	RBH	1.5	0.743	1.96	1.52	54.50	8	9:56

Shift	*Location*	*Magnet strength (T)*	*|B| Peak (T)*	*|dB/dt| Peak(T s^{-1})*	*|B| Time weighted average (mT)*	*Cumulative |B| (Ts)*	*Number of patients*	*Duration of shift (HH:MM)*
17	Wesley	1.5	0.542	0.85	3.02	86.83	12	7:59
18	Wesley	1.5	0.694	1.37	4.93	159.05	9	8:58
19	Wesley- UQ	4	0.516	2.04	6.63	195.62	10	8:11
20	Wesley- UQ	4	0.493	2.50	7.15	208.83	11	8:06
21	Wesley- UQ	4	0.511	1.27	6.24	183.00	8	8:08
22	UQ-CMR	2	0.584	1.15	6.03	184.56	8	8:30
23	UQ-CMR	2	0.538	1.75	7.67	234.38	8	8:29
24	Wesley	1.5	0.570	1.95	4.49	114.64	9	7:05
25	Wesley	1.5	0.366	1.11	4.20	199.69	20	13:13
26	Wesley	1.5	0.474	0.68	3.61	153.27	18	11:47
27	Wesley	1.5	0.589	2.12	5.23	194.55	14	10:19
28	Wesley	1.5	0.704	2.00	7.73	273.29	11	9:49
29	Wesley	1.5	0.439	3.20	3.61	117.46	11	9:01
30	RBH	1.5	1.070	5.08	10.11	401.22	15	11:01

The average worker at these sites attended to 9.9 patients per shift on average during this study, and worked an average of 9.3 hours per shift. However typical workloads experienced by medical personnel are two to three patients an hour, and working shifts can be as long as 14 hours.

The time-weighted-average magnetic field exposure ranges between 1.5 mT and 12.5 mT. The maximum and minimum cumulative exposure values are 401 T s and 46 T s, and are not dependant on the magnet strength but rather on the amount of time spent at high fields, the number of patients attended to, and the nature and position of movements inside the magnet room.

The peak |B| and |dB/dt| values are approximately 1.3 T and 5.1 T s^{-1} respectively, and are independent of the magnet strength because these values largely depend on the positioning of the person within the magnet room and the nature of the body movements whilst in the magnet room. Higher field magnets do, though, have the potential to cause higher peaks in both |B| and |dB/dt|, due to their higher field profile outside the bore. 28 out of the 30 peak values of |db/dt| recorded exceeded 767.9 mT s^{-1} within the measurement bandwidth.

[Technical note: the value of 767.9 mT s^{-1} is referred to several times in Professor Crozier's report, as a maximum allowable dB/dt. This value is calculated from the IEEE standard (C95.6-2002). Section 5.2.4.1.2 of that standard, Peak Environmental Field, describes the procedure used to calculate this value. For the frequency range 0-7 Hz, because the MPE is frequency dependant, the peak dB/dt value remains constant. The derived value is for head and torso exposures.

*The 1998 ICNIRP Guidance on Determining Compliance of Exposure to Pulsed and Complex Non-sinusoidal Waveforms Below 100 kHz with ICNIRP Guidelines (Health Physics **14**, 74) gives the basis for deriving similar dB/dt values corresponding to the ICNIRP guidelines. If it could be argued that this approach also could be applied to the exposure limit values of the EMF Directive (see Section 2 for further discussion on the validity of this) then the corresponding value for the torso at 7 Hz would be 220 mT s^{-1}. The basic restrictions are frequency-dependent between 0 and 7 Hz, and for example at 1 Hz dB/dt would be 883 mT s^{-1}. The ICNIRP Guidance makes the point that a different sized current loop dosimetric model would be appropriate for head exposures. If, conservatively, this were taken to be half the radius of the torso current loop then these values would become* 440 mT s^{-1} *at 7 Hz and 1.8 T s^{-1} at 1 Hz.]*

The peak |B|-fields and spatial gradients of |B| are encountered near the inner edges of the magnet ends and this location is where maximum dB/dt values occur as the radiologist is undergoing a fast translational or bending motion near the magnet bore's inner edges. To investigate this further, exposures at these specific locations were analysed in more detail. These would be, specifically, exposures of the head.

The instantaneous peak magnetic fields measured during the head exposure studies during bending movements at the inner edges of the magnet ends, for the 1.5, 2 and 4 T magnet systems, are presented in Figures 14 to 16 of Section 3 of Professor Crozier's report. Figure 9 of this report, below, shows a typical dosemeter trace for a 1.5 T system

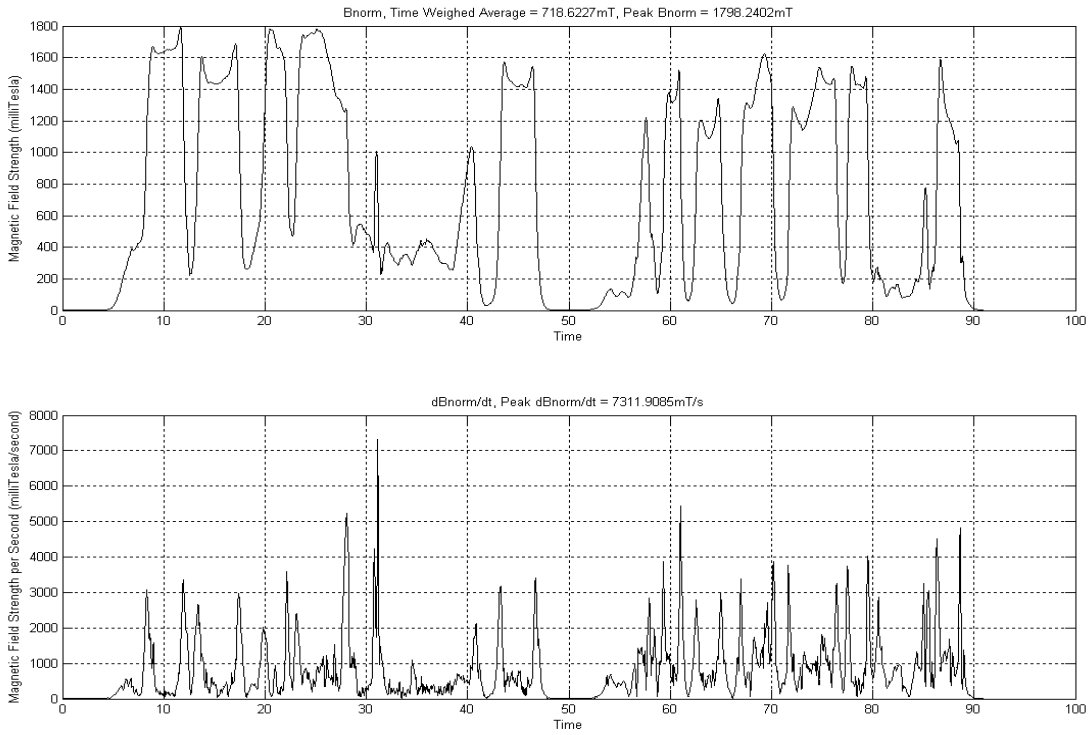

Figure 9 Detailed exposure of head during movement close to bore end of 1.5 T magnet

The peak B fields are 1.798 T, 1.713 T, and 3.646 T for the 1.5 T, 2 T, and 4 T magnets respectively. However for the 2T system it was not possible to measure immediately against the inner bore due to the physical structure magnet enclosure. This may explain why the maximum instantaneous peak for the 2 T system is slightly lower than for the 1.5 T system.

The measured isotropic magnetic flux density strengths and profiles correspond quite well with the calculated field magnitudes and distributions described in Section 3.1. The peak dB/dt values are 7.3 T s^{-1}, 4.4 T s^{-1}, and 6.17 T s^{-1} for the 1.5 T, 2T , and 4 T systems respectively. It can be concluded that as an MRI worker's head is undergoing a fast translational or bending motion near the magnet bore inner edges, the likelihood for significant *in situ* current induction increases due to the spatial (non-uniform field profile) and temporal (movement) change in the impressed magnetic flux density. It is interesting to note that the peak dB/dt values experienced by workers can approach the types of magnitudes that the measured pulsed gradient fields produce (see section 4.3).

The dosemeter will be useful in further scientific studies to explore the potential health effects of EM exposure at low frequencies related to movement through a spatially-varying static field.

3.3 SWITCHED-GRADIENT FIELDS

For switched-gradient measurements the bandwidth of the dosemeter was extended to a sampling frequency of 40 kHz per channel. In this configuration the active battery life of the dosemeter is reduced down to 1.5 hours and it is able to retain 2 hours' worth of information.

Exposures to gradient-switched magnetic fields have been measured during echo-planar imaging (EPI) sequences at the Siemens Magnetom Sonata whole-body MRI clinical system, and at the Bruker S200/Oxford Magnet Technology 2 T research system.

[*Technical note: echo-planar imaging is a specific MR imaging technique that is considered particularly rapid. It uses a standard pulse sequence. Because of its speed and comparative insensitive to motion, echo-planar imaging a popular choice for imaging dynamic physiological processes.*

The standard EPI gradient waveforms are shown in Figure 10; the total "switched gradient field" is a summation of these. The slice-selection gradient is primarily an axial (z) component field that is used to select an imaging slice in a given x-y (transverse) plane. The read-out gradient field is applied to give a transverse (x) gradient in the axial field and the phase-encoding gradient is applied to give a transverse (y) gradient in the axial field. Between them, the three switched-gradient fields can be used to interrogate an imaging voxel.]

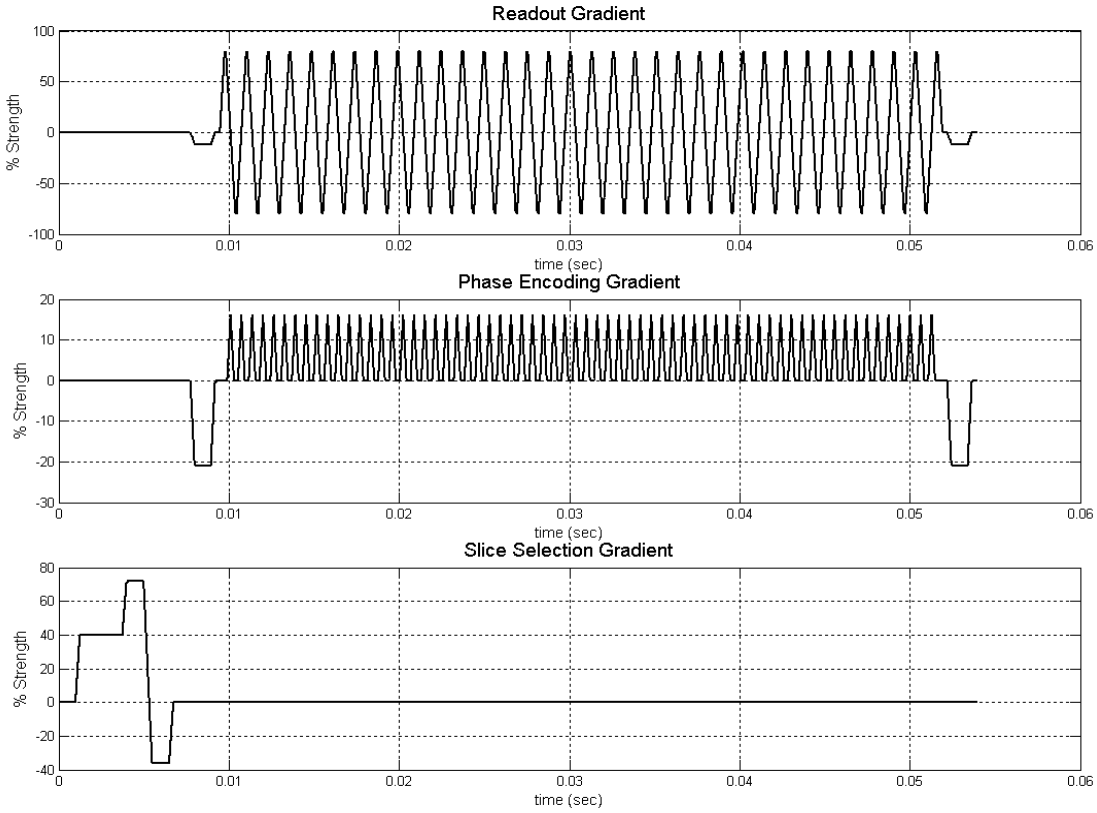

Figure 10 The standard echo-planar imaging switched gradient waveforms

Because the three EPI gradients waveforms are applied in mutually orthogonal directions, then if the dosemeter is aligned so that the axes sensors coincide with the coordinate axes of the gradient fields, it should be possible to identify each of the EPI gradient waveforms with a separate dosemeter sensing direction. Figure 11 shows a dosemeter dataset where this can be seen clearly; in other datasets the alignment is less good – but since the dosemeter is intended to be used in arbitrary orientations with respect to the MRI coordinate system, this is of little more than academic interest.

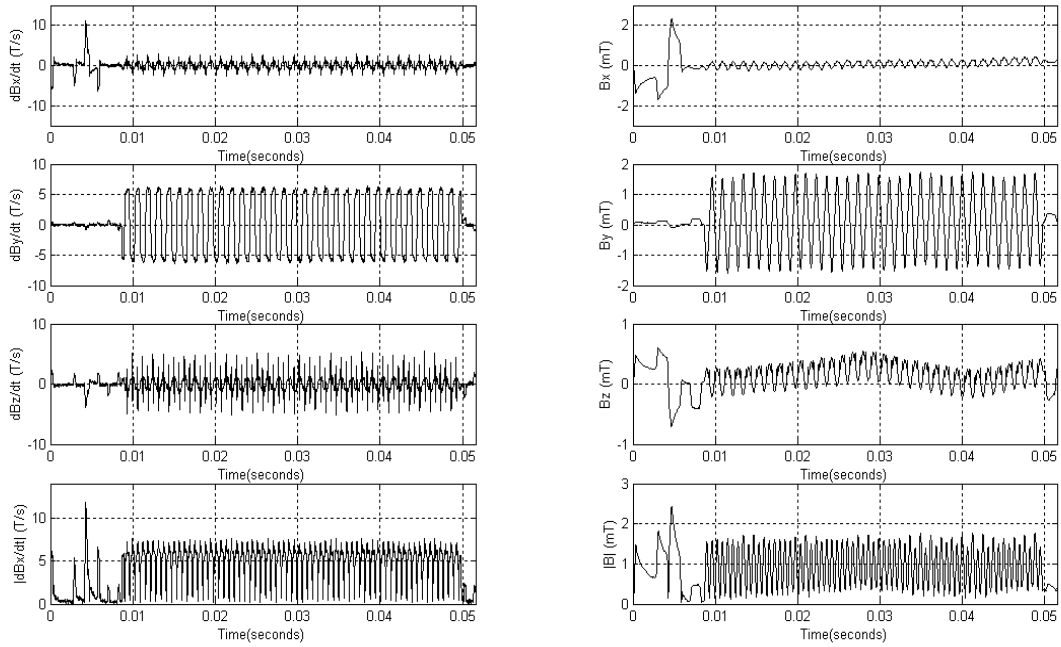

Figure 11 Measured switching gradient dosemeter data during the EPI sequence at position z = 120cm, x = 3cm, and y = 0cm

Section 3.3 contains results of the numerical modelling of switched-gradient exposures using a simple trapezoidal waveform and assumed gradient coil geometries for a series of MRI systems. Because of the strong spatial variation of the switched-gradient fields, exposure close to the end of the magnet bore will be very dependent on actual gradient coil geometry. The dimensions of the gradient coils of the Bruker system are known, and for this reason, and also to assess the performance of the dosemeter when used to measure real gradient fields, it was decided to model the switched-gradient fields from this system specifically so that direct comparisons could be made with measured data. The exact current pattern that generates the field is not

provided by the manufacturer so instead the dimensions of standard theoretical actively shielded, symmetric gradient coils were appropriately scaled to conform to the actual size of the gradient set in the Bruker system. This will not give a perfect match to the measured dosemeter data, but it should be reasonably informative.

Measurements were taken on the XZ plane at Y = 0cm, from X = 0 to 60cm and Z = 120cm to 175cm. Figure 12 shows the region over which the measurements were taken.

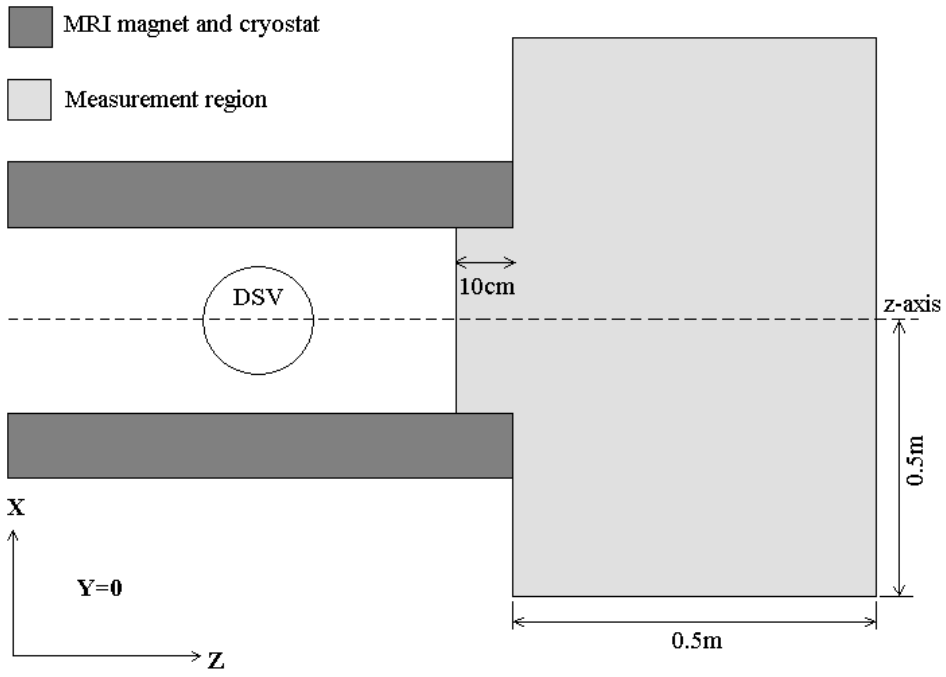

Figure 12 The measurement region for the switched-gradient fields

Figure 13 shows comparisons between measured (with the dosemeter) and theoretical distributions of rms magnetic flux density (B) and dB/dt for the Bruker 2 T system with the EPI gradient sequence.

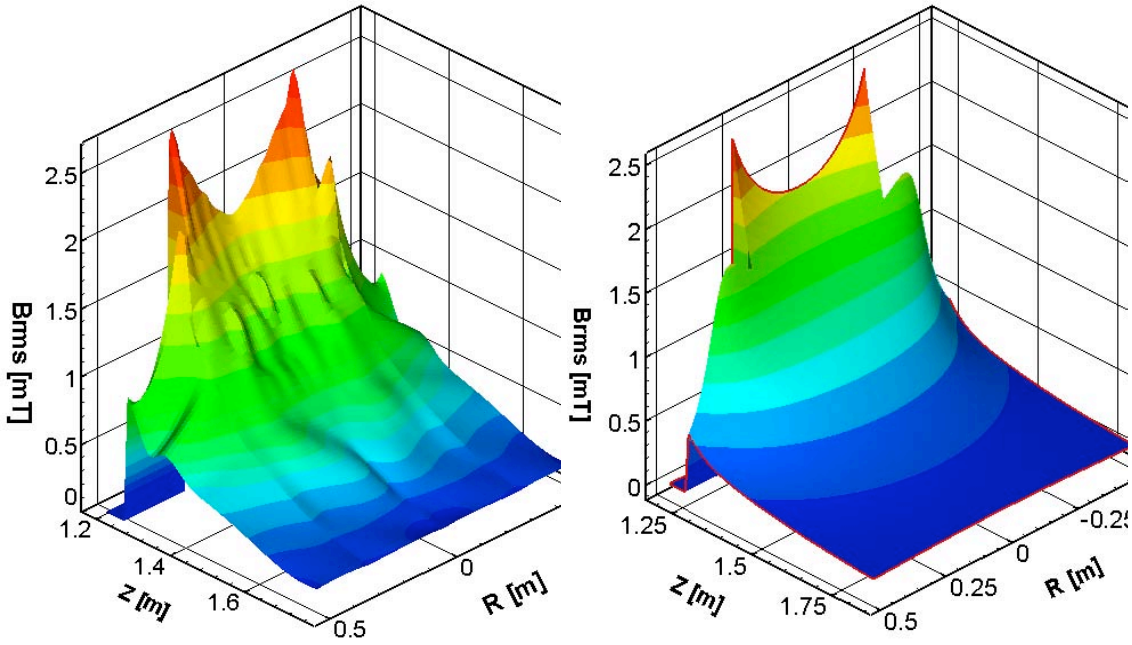

Measured |Brms| Numerically computed |Brms|

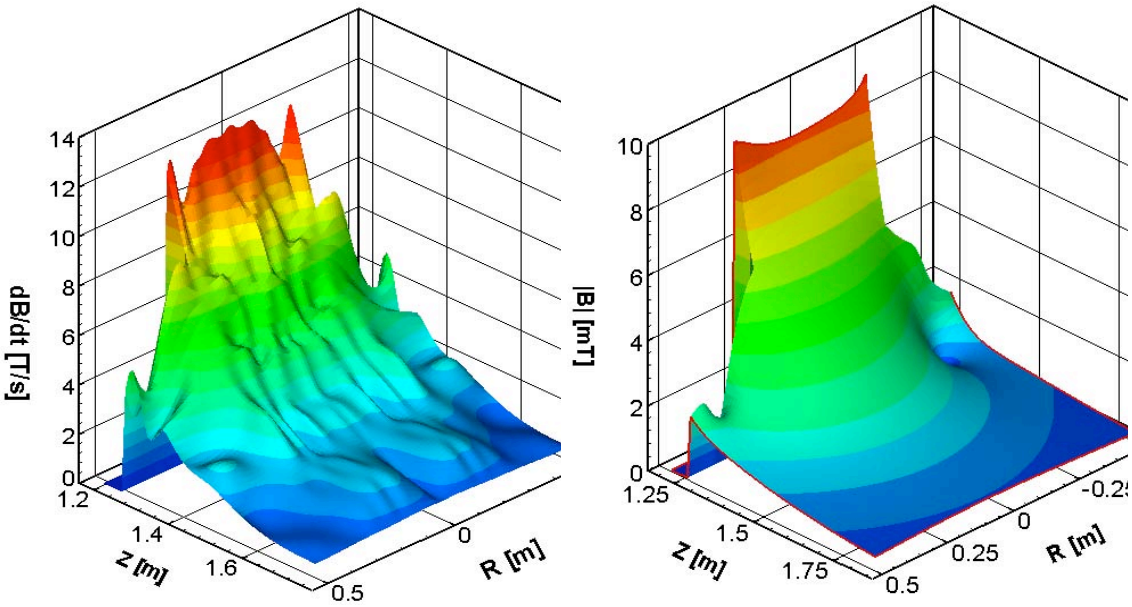

Experimentally measured |dB/dt| Numerically computed |dB/dt|

Figure 13 Comparisons between measured and theoretical distributions of rms magnetic flux density (B) and dB/dt for the Bruker 2 T system with the EPI gradient sequence

There is good agreement between the measured and calculated B and dB/dt distributions shown in Figure 13. The slight discrepancies in spatial distributions probably reflect differences between the theoretical and actual gradient coil current distributions and therefore somewhat different magnetic field profile to that of the 2T Bruker's gradient set. The results indicate that there is a good corroboration between measured and calculated B field profiles even though a temporally challenging EPI time sequence was engaged during both simulation and measurement. Furthermore, this particular result confirms the validity of the numerically evaluated male and female occupational worker exposures to magnetic fields produced by trapezoidally switched gradient coils that are described in Section 3.3. There is more variability between the measured and calculated dB/dt values than between the B values. The values are similar, but as well as differences between real and modelled gradient coils the discrepancies may well arise because the largest numerical values occur at sharp corners and are therefore susceptible to changes to the cryostat vessel parameters (i.e. a 5 mm deviation in cryostat vessel position can noticeably change the dB/dt values).

When it comes to comparison between the switched-gradient fields and human exposure guidelines, there are two issues to consider. One is the rms magnetic field strength and the other is dB/dt. Both IEEE ad ICNIRP specify frequency (or duration)-dependent restrictions on these quantities. Table 2 lists these for the waveform parameters of the EPI gradient sequence. It should be noted that these are external field quantities rather than internal currents and *in situ* field strengths as calculated in Section 3.3, and as such can be measured directly using the dosemeter.

Table 2 IEEE controlled exposure and ICNIRP occupational levels for the EPI gradient sequence

Parameter		*Read-out gradient*		*Slice select gradient*		*Phase encode gradient*	
		IEEE	*ICNIRP*	*IEEE*	*ICNIRP*	*IEEE*	*ICNIRP*
Brms	*Extremities*	2.1 mT		1.9 mT		1.5 mT	
	Head/Torso	1.1 mT	30.7 µT	1.0 mT	30.7 µT	0.82 mT	30.7 µT
Peak B	*Extremities*	2.9 mT		2.7 mT		2.1 mT	
	Head/Torso	1.6 mT	43.4 µT	1.5 mT	43.4 µT	1.2 mT	43.4 µT
Peak dB/dt	*Extremities*	10.7 T s^{-1}		10.7 T s^{-1}		10.7 T s^{-1}	
	Head/Torso	5.8 T s^{-1}	0.16 T s^{-1}	5.8 T s^{-1}	0.17 T s^{-1}	5.8 T s^{-1}	0.22 T s^{-1}
Frequency		1.8 kHz		2 kHz		2.5 kHz	

Figure 14 shows the areas of the calculation region defined in Figure 12 in which the IEEE and

ICNIRP occupational field levels are exceeded for the various components of the gradient sequence. The darkest blue areas of each field plot are where the field value is not exceeded. It can be seen that the IEEE values are exceeded within perhaps 10 to 20 cm of the end of the magnet but that the ICNIRP values are exceeded over most of the calculation region. This is a somewhat different result than that of Section 3.3, where it is shown that when internal currents and fields are calculated, the compliance areas for the IEEE and ICNIRP guidelines are not dissimilar. The difference reflects the rather large level of conservatism built into the dosimetric model used to derive the ICNIRP reference levels.

3.4 SUMMARY

Dosemeter

- An ambulatory tri-axial magnetic field dosemeter has been used experimentally to quantify exposures of MRI personnel to both static and dynamic magnetic fields during normal working shifts within clinical MRI settings
- There is good agreement between dosemeter measurements and calculated field distributions around MRI systems
- Magnetic field dosimetry can be achieved in a practical manner and will be extremely useful in further scientific studies. There is scope for a larger and more detailed study, investigating how details of clinical procedures and practice affect recorded levels of exposure.

Static magnetic field measurements

- Time-weighted-average static magnetic field exposures are quite small for the sets of 30 shift data analysed
- dB/dt values experienced by workers as they move around the magnet room, especially during bending motions near the inner bore at the magnet ends often exceed guideline levels.

Switched gradient magnetic field measurements

- Both |Brms| and dB/dt have been calculated and measured around a 2T MRI system
- There is good agreement between measured and calculated field quantities
- IEEE field-strength guidelines for controlled areas are exceeded in regions near the gradient coil ends, as predicted in the numerical models
- ICNIRP occupational field strength guidelines are exceeded through the whole region that was measured, reflecting the conservatism in the ICNIRP dosimetric model used to derive reference levels

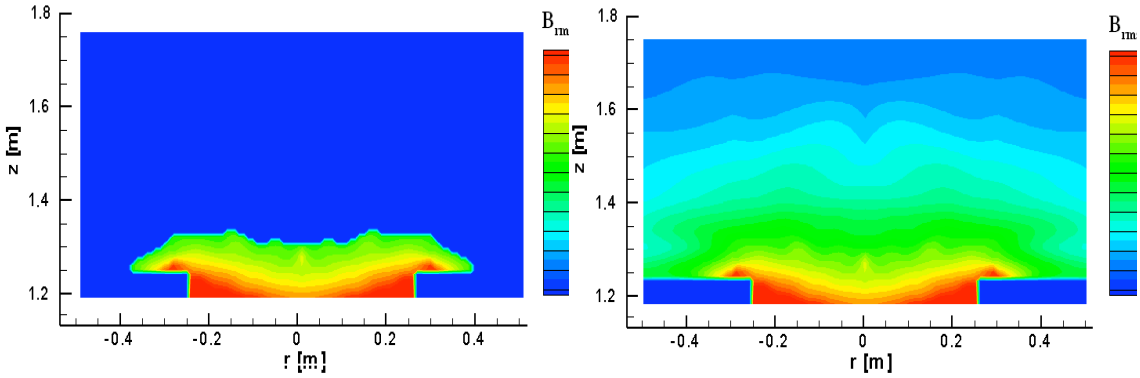

Positions where |Brms| exceeds IEEE, head & torso: readout gradient

Positions where |Brms| exceeds ICNIRP, all three gradients

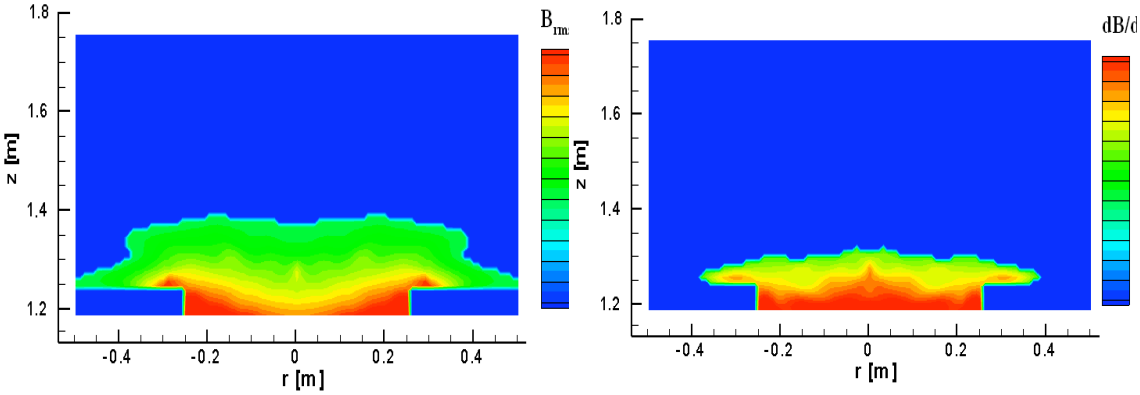

Positions where |Brms| exceeds IEEE, head & torso: phase encode gradient

Positions where |dB/dt| exceeds IEEE, head and Torso

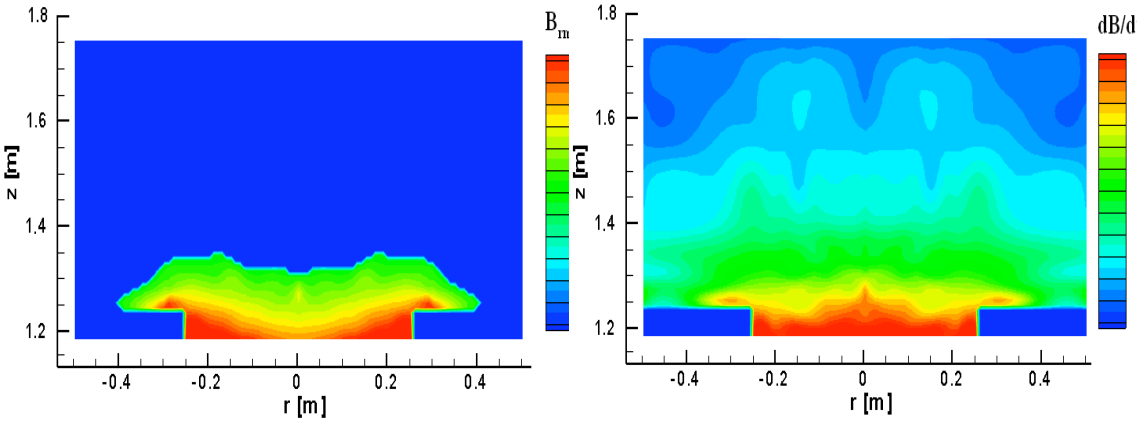

Positions where |Brms| exceeds IEEE, head & torso: slice select gradient

Positions where |dB/dt| exceeds ICNIRP

Figure 14 Areas in which the IEEE and ICNIRP occupational field levels are exceeded

4 OVERALL CONCLUSIONS

Within a metre or so of the ends of the 3 MRI systems modelled, the ICNIRP basic restrictions for occupational exposure could be exceeded by movement through the static field or directly by the switched-gradient fields. Faster movement through the static field than the modelled 1 m s^{-1} would exacerbate the exposure and slower movement would mean that the exposures would meet the ICNIRP restrictions at smaller distances. The calculated exposures from switched-gradient fields correspond to a worse-case field situation which would occur rarely in routine clinical practice, and real compliance distances may be somewhat less than this.

Computational modelling of exposure indicates that it is not clear that use of the IEEE guidelines rather than those of ICNIRP would change the overall situation, even though this might be inferred from external field measurements.

Although the size of the magnet does affect the compliance distance when movement through a static field is considered, it does not change the overall picture significantly. There is likely to be a potential problem with this exposure situation for any clinical MRI system. However, the extent to which the problem will be manifest will depend strongly on clinical practice. In particular, exposures to switched-gradient fields occur only when an image is being gathered, whereas exposures to static fields can occur at any time. This project has shown that the UniQ dosemeter is capable of indicating, in real-time, situations in which movement through a static field might lead to exposure guidelines being exceeded.

The results indicate also that the dosemeter could be used to give an indication of which clinical practices might lead to overexposures to the switched-gradient fields.

Health and Safety Executive

An investigation into occupational exposure to electromagnetic fields for personnel working with and around magnetic resonance imaging equipment

Annex

Stuart Crozier B.Eng (Hons), MSc (Med Phys), PhD, D. Eng, FInstP (UK)
School of Information Technology and Electrical Engineering
The University of Queensland
St Lucia, Brisbane
Qld 4072
Australia

This report provides modelling and measurement studies of the exposure experienced by healthcare workers around MRI equipment due to movement through static magnetic field gradients and pulsed magnetic field gradients.

This report and the work it describes were funded by the Health and Safety Executive (HSE). Its contents, including any opinions and/or conclusions expressed, are those of the author alone and do not necessarily reflect HSE policy.

HSE Books

First published 2007

ACKNOWLEDGEMENTS

The author would like to thank the following researchers at The University of Queensland who contributed to this work: Drs Feng Liu, Adnan Trakic, Hector Sanchez, Stephen Wilson, Mr Miguel Fuentes and Mr Hua Wang. Further acknowledgements are given at the end of each of the three sections.

CONTENTS

SECTION 2

NUMERICAL EVALUATION OF HEALTHCARE WORKERS EXPOSURES TO PULSED MAGNETIC FIELD GRADIENT COILS IN MRI 30

SECTION 3

THE MEASUREMENTS OF MAGNETIC FIELD EXPOSURES FOR HEALTHCARE WORKERS IN SELECTED MR ENVIRONMENTS 58

EXECUTIVE SUMMARY

This report describes investigations into the exposure of healthcare workers due to low frequency electromagnetic fields around MRI systems. The first two sections report on theoretical modelling studies of workers moving around MRI magnets and when exposed to the fields produced by switched field gradients, the components responsible for spatial location in MR imaging. The final section reports measured values.

The results of the movement through static field simulations indicate that the ICNIRP threshold of $40\ mAm^{-2}$ - rms in the head and trunk can be easily exceeded when the worker is moving close to any of the three MRI magnets used in this study. Since the velocity of motion has been normalized to $1\ ms^{-1}$ in all designated cases, the results can be scaled linearly for other velocities. It is shown that the levels of induced electric fields and current densities clearly increase for increasing static magnetic field strength. In order to limit the induced current densities to less than $40\ mAm^{-2}$ - rms in the tissues of the central nervous system when walking along the magnet bore, the simulation results suggest that the worker should be at least ~0.5-1.0 m axially away from the ends of 1.5-7 T magnet cryostats respectively, or should be moving at correspondingly lower velocities than 1 m/s. Further theoretical and experimental studies will need to be conducted to completely describe the regions around specific magnets where guidance should be given to occupationally exposed healthcare workers.

Similarly, studies of the induced fields and currents due to switched field gradients show that when the worker is standing near the gradient coil entrance, the levels can be above the relevant EU, ICNIRP and IEEE standards. The calculations show that to be within regulatory limits the workers need to be some distance away from the gradient coils when they are all pulsed simultaneously so as to generate 40mT/m each in the dsv. This is the worst case scenario. Experimental work into the typical gradient field exposures used in routine scanning is underway and will further inform these results. We note that the distance from the end of the gradient coil set to the end of the magnet varies between MRI systems and, for cylindrical systems, is typically smallest in short 1.5T magnets and larger in higher field systems.

For the measurement studies we have used an ambulatory tri-axial magnetic field dosimeter to experimentally quantify exposures of radiology personnel to both static and dynamic magnetic fields during normal working shifts within clinical MRI settings. Measurements were made around 1.5T, 2T, and 4T magnets during routine patient procedures. Exposures to pulsed commercial gradient coils were measured using a practical Echo Planar Imaging (EPI) sequence. Apart from comparing the static and dynamic field exposures to most-recent international regulatory standards (IEEE, ICNIRP and EU-Directive 2004/40/EC), the field measurements from the gradient field sub-study were assessed against the numerical simulations of the first two sections with a high degree of corroboration. Our measurements confirm that workers can be exposed to magnetic fields exceeding the guidelines at positions near the main magnet and gradient coil ends during clinical imaging. The time weighted average magnetic field exposures in 1.5T, 2T, and 4T were all within the regulatory limits during static magnetic field measurements. More data and detailed situational studies need to be undertaken and compiled to fully understand the extent and nature of these exposures. We have shown that magnetic field dosimetry can be achieved in a practical manner and could be useful in providing workers with instantaneous warnings about over-exposure to magnetic fields.

It is hoped that these results will better inform the MRI community concerning compliant activity around MRI systems.

1 INTRODUCTION

This introductory section provides a summary of the results of both simulations and measurements around Magnetic Resonance Imaging (MRI) systems and brief recommendations for further studies. Full technical details of the modelling and measurement studies can be found in Sections 1-3.

1.0 MODELLING SIMULATIONS

Section 1 details the simulations of workers moving through the static field gradients inherent in MRI magnets. Section 2 details the simulations of workers exposed to pulsed field gradients when scanners are in operation. Both Sections contain literature reviews and explanations of the methodologies used. Note that bending, twisting or other actions taken by healthcare workers, particularly around the patient bed are acknowledged to be important but were beyond the modelling scope of this study.

The following is a summary of the findings relative to regulatory guidelines and also recommendations for future studies.

2.0 SUMMARY OF RESULTS

Movement around model 1.5T, 4T and 7T magnet systems (see Section 1).

2.1 Current Standards

The **I**nstitute of **E**lectrical and **E**lectronics **E**ngineers (IEEE) standard for exposure to magnetic fields at frequencies below 1 Hz assumes adverse biological reactions in 50% of human subjects at 1.5 T-peak or larger [12 in Section 1]. The same standard restricts the induced *in situ* electric fields in the brain and heart to 25.03 mV/m (below 20 Hz) and 1.33 V/m (below 167 Hz) for controlled environments, respectively. At the same time, the *in situ* magnetic flux density is restricted to 500 mT (below 10 Hz). In the IEEE guidelines, the *in situ* electric field is used as the fundamental metric, rather than the current density, as the later introduces an additional parameter (conductivity), and thus adds uncertainty beyond that which already existed in deriving the electric field *itself*. However, the **I**nternational **C**ommission for **N**on-ionizing **R**adiation **P**rotection (ICNIRP) [23 in Section 1] and the Directive 2004/40EC of the European Parliament and Council [24 in Section 1] state that the current density averaged over a $1\ cm^2$ surface must not exceed a threshold of $40\ mA/m^2$ - rms. (at frequencies below 1 Hz) in the head and trunk.

2.2 Results

The simulations show that for workers moving at a nominal speed of 1m/s, the maximum $1\ cm^2$ - averaged current densities (tables V and VI in Section 1) for most combinations of magnets and motion type can be larger than the threshold of $40\ mAm^{-2}$ -rms. (or $56.57\ mAm^{-2}$ - peak) defined in the ICNIRP guideline and EU Directive. The worst-case maximum electric fields induced in the brain exceed the IEEE standard of 25.03 mV/m-peak, while in some circumstances the electric fields exceed the value of 0.75 V/m-peak that is attributed to experimentally observed alternation of neural activity in hippocampal slices of the rat brain [20-21 in Section 1]. The pre-synaptic depolarization threshold of 74.95 mV/m-peak for retina [13-14 in Section 1] might be exceeded at very high and ultra-high field strengths for both male and female. However the magnitudes of maximum induced electric fields in the heart are below the

IEEE threshold of 1.33 V/m-peak for all examined field strengths [12, 22 in Section 1]. The results detailed in the appendix show that the electric field thresholds that result in peripheral nervous stimulation can be exceed in the tissues of fat and skin at very high and ultra high field strengths [12 in Section 1].

We have estimated the axial distances away from the three assumed magnets at which the induced maximum 1 cm^2 - averaged current density magnitudes would drop below the ICNIRP threshold of 56.57 mAm^{-2} - peak in the head and trunk. According to selected results shown in figure 10 (for tissues of CNS and heart), the maximum 1 cm^2 - averaged current density magnitudes are below the 56.57 mAm^{-2} - peak threshold at distances from cryostat end of ~0.5-1.0 for the static magnetic fields between 1.5-7 T. The same holds true for all other tissues. This means, that for higher field strengths, workers moving at the same velocity should be further away from the magnet to be compliant . We note here, that these values are only representative of motion velocities normalized to 1 ms^{-1} and obviously, slower is better.

Therefore, it seems that to comply with regulatory limits occupational workers need to move slowly in specified regions around magnets; each type of magnet having a different profile for this "reduced speed" region.

2.3 Pulsed Field Gradient Induction

See Section 2.

2.4 Current Standards

Regulatory agencies such as the IEEE and the ICNIRP) have defined limits on the time-varying electric, magnetic and electromagnetic field exposures to the general public and in controlled environments. According to the IEEE standard [17 in Section 2], the *in situ* electric field stimulation thresholds for most CNS and PNS neurons are around 12.3 V/m and 6.15 V/m for exposure durations of 0.128 ms, respectively. However, heart and other tissues are limited to electric field exposures of 7.98 V/m and 0.86 V/m respectively, at a frequency of 1 kHz (for controlled environments). The ICNIRP guideline [18 in Section 2] and the Directive 2004/40/EC of the European Parliament and Council [19 in Section 2] on the other hand, state that the current density averaged over a 1 cm^2 surface must not exceed a threshold of 10 mA/m^2 - rms. in the head and trunk at a frequency of 1 kHz.

2.5 Results

The simulations model the exposures of male and female occupational workers to pulsed field gradient gradients typically used in MRI. These gradients are intended to be typical of currently available cylindrical MRI systems, but do not cover all gradient sets on the market and therefore provide indicative results only. The simulations show that the induced fields and currents can be in the same order of magnitude as those induced in the patients during MRI imaging and therefore should not be ignored. The normalized simulation results obtained can be extrapolated to evaluate the potential safety issues at different gradient strengths and distances away from transverse and longitudinal coils. The longitudinal gradient tends to induce more fields in workers than the transverse coils. The strongest levels of field exposure are observed when all three gradient coils are operated simultaneously. As suspected, the induced current densities and electric fields, when the occupational worker is standing near the gradient coil entrance, can be well above the relevant EU, ICNIRP and IEEE standards. The calculations show that to be within regulatory limits, the workers need to be approximately 1 metre away from the gradient coils (note this is not the end of the magnet, the distance between the end of the gradient coil set and the magnet varies between installations) when they are all pulsed simultaneously so as to generate 40mT/m each in the dsv. We note that the distance from the end of the gradient coil

set to the end of the magnet varies between MRI systems and, for cylindrical systems, is typically smallest in short 1.5T magnets and larger in higher field systems. The methodology described in this work is able to be used to calculate regions of compliance for specific magnet/gradient coil combinations. Further modeling work is required to better understand exposures in a variety of occupational situations including bending around the patient bed.

3.0 MEASUREMENT STUDIES

The technical details of the measurement methods are included in Appendix 3 details the use of a dosimeter for B and dB/dt exposure measurements in a small number of healthworker shifts (30 shifts). This is only an indicative set of measurements.

The following is a summary of the finding relative to regulatory guidelines and also recommendations for future studies.

3.1 Results

The dosimeter measured three axis B fields and three axis dB/dt measurements. From these measurements peak and time weighted average values can be calculated.
The root-mean-square (RMS) values of the dynamic magnetic fields were evaluated and compared against the numerical simulations and the most recent IEEE, ICNIRP and EU-Directive 2004/40/EC standards. The measurements confirm that workers can be exposed to magnetic fields exceeding the guidelines at positions near the gradient coil ends during clinical imaging and a high degree of correlation exists with the numerical results presented in Appendices 1&2. Exposures due both to movement through static magnetic field gradients and to pulsed magnetic field gradients can exceed guidelines in some routines practices. While the time weighted average magnetic field exposures in 1.5T, 2T, and 4T were all within the regulatory limits during static magnetic field measurements, the peak limits for the head were exceeded in some circumstances.

The small number of routine shifts acquired provide indicative results only and more extensive studies are needed. We have shown that magnetic field dosimetry can be achieved in a practical manner and will be useful in providing workers with instantaneous warnings about over-exposure to magnetic fields.

3.2 Recommendations for Further Modeling/Measurement

There are a number of important scenarios that are relevant to clinical practice that were outside the scope of this initial investigation and should be the subject of further modeling studies. It is recommended that further modeling studies be carried out, along the lines of :

- Examining exposures during a variety of work postures. In clinical practice the workers currently often lean into the MRI magnet to attach accessories to the patient or to comfort or communicate with a patient who may be nervous or anxious. Workers also currently lean into the magnets to assess sedated or intubated patients. In these cases, exposure due to both mechanisms; movement through static gradients and residing in strong pulsed gradients needs to be simulated. From a modeling viewpoint, maintaining integrity in the human models with variable posture is not trivial.

- Exposures in systems used for interventions. Interventions are performed either with short cylindrical (conventional) magnet systems (such as, for example, The Siemens ESPREE or Toshiba VANTAGE) or in “open” MRI systems. In both cases workers (surgeons, nurses, radiographers) perform movements in static field gradients – some of

which require precision, and are exposed to pulsed field gradients. A full modeling analysis of these systems is recommended as a priority.

- Actions of workers in OEM companies (eg, Siemens, Philips, GE) who frequently enter magnet systems in field servicing or magnet installation/construction phases should be simulated to deduce practices that may be above recommended guidelines.

- A measurement study of a much larger population is recommended based on the preliminary measurement data and detailed situational studies need to be undertaken and compiled to fully understand the extent and nature of these exposures. Interventional systems and practices should be included in the larger study.

SECTION 1

NUMERICAL STUDIES OF CURRENTS IN WORKERS INDUCED BY BODY- MOTION AROUND MRI MAGNETS

1.0 ABSTRACT

In modern magnetic resonance imaging (MRI), workers are exposed to strong, non-uniform static magnetic fields generated by the main superconducting magnet. Previous studies have indicated that movement of the body through these fields can stimulate *in situ* electric fields/ current densities of physiological significance. The relationship between the magnetic field pattern/strength and the current distribution/level induced in the body is not well understood. This study presents numerical evaluations of electric fields/currents in tissue-equivalent, whole-body male and female human models (workers) at various positions and variety of body motions around three real superconducting magnets with field strengths of 1.5T, 4T and 7T.
Note that bending, twisting or other actions taken by healthcare workers, particularly around the patient bed are acknowledged to be important but were beyond the modelling scope of this study. Reported data includes electric fields and current densities induced in selected tissues, as well as current density averaged over $1\ cm^2$ areas normal to the current flow. A value of latter quantity of 40 mA/m^2 - rms. is suggested as a threshold for head and trunk in international regulations. Possible correlations between the magnetic field characteristics and the induced current density distribution are discussed and simulations show that it is possible to induce electric fields/current densities above recommended levels when the worker is moving very close to the MRI machines. Furthermore, the results indicate that the worker should be at least ~0.5-1.0 m axially away from the cryostat end for field strengths between 1.5-7 T to limit the exposure according to the suggested safety standards when moving at a nominal 1 m/s. A strict scaling law between induced *in situ* electric field/ current densities and respective static field strengths investigated *herein*, could not be established, however, due to the effect of differing field profiles. The numerical calculations are based on an efficient, quasi-static finite-difference scheme and the methodology presented can be extrapolated to other ultrahigh static field strengths for the evaluation of the effects of motion at a variety of body orientations and velocities.

Keywords: *MRI, superconducting magnet, human models, worker, quasi-static finite-difference.*

2.0 INTRODUCTION

In the past decade, there has been a concerted effort to enable magnetic resonance imaging (MRI) at very high field strengths. The most common system in current clinical use has a 1.5 T central field, but research systems from 4 T to 9.4 T are now being developed for clinical imaging. As the field strength of the MRI system increases, so does the potential for tissue/field interactions of a variety of types. Therefore the safety issues for patients and healthcare workers exposed to such strong magnetic fields needs to be carefully considered. Understanding the interactions between the electromagnetic fields generated by MRI systems and the human body has become more significant in recent years [1-5].

The strong static magnetic field generated by the main MRI magnet can induce magneto-hydrodynamic forces on the moving charge carriers of the human vascular system (i.e. haemoglobin of the red blood cells, ions of different salts, etc). For instance, Jehesen and associates [6] have observed a 17% increase in human heart-rates under laboratory conditions of 2 T exposure, which might be at best harmless in healthy human subjects, but its safety in dysrhythmic subjects can not be ascertained. Other studies indicated a change in blood velocity of 0.2-3% between 1-10 T [7-8].

Another concern in high-field MRI is related not to the strength of the static field and resulting magneto-hydrodynamic forces, but to induction of *in situ* electric fields and associated current densities caused by rapid movement of the body within the non-uniform, strong static magnetic field. A number of adverse effects were noted at 1.5 T, including but not limited to: headaches, nausea, vertigo, phosphenes (light flashes), numbness and tingling, loss of proprioreception and balance, and a metallic taste in the mouth associated with the head movement. Much more marked reactions were observed at 4T and higher [9]. It is believed that these biological responses are most likely results of nerve and synapse excitations in the central and peripheral nervous system. The central nervous system (CNS) contains the tissues of the brain, spinal cord, retina and cerebral spinal fluid (CSF), where as the peripheral nervous system (PNS) is mostly embedded in the tissues of the skin and subcutaneous fat. The stimulation of peripheral nerves is a well-known phenomenon encountered during pulsing of magnetic field gradient coils at a frequency of 1 kHz or so [10] and it is associated with the twitching of muscles and tingling in the skin. However, there is some indication that this effect can extend to much lower frequencies, even during body motion in static magnetic fields [11]. The *in situ* electric field stimulation thresholds for most CNS and PNS neurons are around 12.3 V/m and 6.15 V/m for a time duration of 0.128 ms, respectively [12]. However, membrane depolarization of nerve cells in the retina (eye) is much more sensitive to the electric and magnetic field induction [13-14]. This synaptic polarization effect in retina, rather than the excitation of the optic nerve or the visual cortex, is attributed to the phenomenon of electro- and magneto- phosphenes, which are visual effects resulting from electric and magnetic fields applied to the head [13-18]. Alternation of pre-synaptic membrane potentials in retina synapses with *in situ* induced electric fields of around 53 mV/m-rms. (with corresponding current density of $8\ mA/m^2$), at the most sensitive frequency of 20 Hz, can result in electrophosphenes [18-19]. The electric field stimulation threshold for neural response in the brain is reported to be around 750 mV/m-peak, a factor of 16 below the threshold of 12.3 V/m for excitation of a large CNS nerve [20-21]. On the other hand, heart tissue requires a 12 V/m *in situ* electric field to trigger cardiac excitation [12, 22].

The IEEE standard for exposure to magnetic fields at frequencies below 1 Hz assumes adverse biological reactions in 50% of human subjects at 1.5 T-peak or larger [12]. The same standard restricts the induced *in situ* electric fields in the brain and heart to 25.03 mV/m (below 20 Hz) and 1.33 V/m (below 167 Hz) for controlled environments, respectively. At the same time, the *in situ* magnetic flux density is restricted to 500 mT (below 10 Hz). In the IEEE guidelines, the *in situ* electric field is used as the fundamental metric, rather than the current density, as the later introduces an additional parameter (conductivity), and thus adds uncertainty beyond that which already existed in deriving the electric field *itself*. However, the ICNIRP [23] and the Directive 2004/40EC of the European Parliament and Council [24] state that the current density averaged over a $1\ cm^2$ surface must not exceed a threshold of $40\ mA/m^2$ - rms. (at frequencies below 1 Hz) in the head and trunk.

In this theoretical investigation, we have computed the electric fields and current densities induced in whole-body male and female models of workers during motion around magnets with static field strengths of 1.5T, 4T and 7T. Actions such as walking and upward motion in the

MRI room have been considered. The objectives of the research reported here are to evaluate several worst-case exposure scenarios and to understand the relationship between the field pattern generated by the superconducting coils and the positions around the magnet where largest electric fields and current densities are induced in the body. Various measures of electric field and $1\ cm^2$ - averaged current densities are reported for tissues of CNS and heart and the results are compared to the aforementioned international standards. Table V includes selected worst-case results for other body-identified tissue types. In addition, the axial distances from the three model magnets where the maximum induced $1\ cm^2$ averaged current densities are below the ICNIRP threshold have been evaluated. This study does not consider magneto-hydrodynamic forces on the vascular system and any thermal effects attributed by the induced current densities, as the later is not dominant at frequencies below 100 kHz and the former requires a detailed model of the vasculature, which is beyond the scope of the current body model resolution of ~2 mm used in this investigation. The reader is encouraged to refer to following publications on these topics [12, 25]. It is hoped that this study will help in the evaluation of the regulatory compliance ofhealth workers and patients when moving through non-homogeneous, intense, static magnetic fields.

3.0 MATERIALS AND METHODS

3.1 Human body models and superconducting main magnets

To accurately model realistic workers subject to static magnetic fields, both male and female inhomogeneous voxel phantoms NORMAN and NAOMI [26-27] were engaged in this numerical study. The dimensions of the models are very close to ICRP 89 reference adult male and female [28]. The models have some forty tissues identified, with each voxel assigned (where possible) a recently measured [29-30] conductivity value corresponding to its dominant tissue type and appropriate to the required DC frequency. The model resolution of *~2 mm* used in this study is sufficiently high to resolve all major body components, as well as some of the smaller organs and tissues.

The simulations involved are computationally intensive. Therefore, a lower resolution body model is employed first to efficiently estimate the fields induced in the tissues at various positions around the MRI magnet, after which a higher resolution body model is used for more detailed field evaluations. The conductivities of the downscaled cells in the low-resolution models were taken as the volume average of the component voxels. Table 1 details the body model resolutions used in this work.

Table I
Body model properties

		Body model	
		NORMAN (male)	**NAOMI (female)**
Low resolution	***No. of cells x-y-z***	70 x 37 x 218	74 x 31 x 198
	Cell size [mm]	8.219 x 8.308 x 8.075	7.739 x 7.792 x 8.234
High resolution	***No. of cells x-y-z***	277 x 148 x 871	294 x 124 x 791
	Cell size [mm]	2.077 x 2.077 x 2.021	1.948 x 1.948 x 2.061
Height [m]		1.76	1.65
Weight [kg]		73	58

For whole-body MRI systems, magnetic field strength might be divided into high field (1.0-3.0 T), very high field (3.0-7.0T) and ultra high field (≥ 7T). To numerically evaluate the influence of different magnetic field strengths and spatial profiles on both male and female workers, we

have considered three realistic symmetric magnets: 1.5T Infinion (actively shielded, see ref [37]), 4T Siemens (actively shielded) and 7T EMI research magnet (unshielded). Table 2 details the geometries of these three magnets.

Table 2
Superconducting magnet geometry

B [T]	DSV size [5 ppm] r [cm] x z [cm]	Length [m]	Inner Radius [m]	Outer Radius [m]	5 Gauss Shielding r [m] x z [m]
1.5 T	40 x 50	1.27	0.48	0.87	~ 4.2 x 3.6
4.0 T	*	2.09	0.52	1.02	~ 4 x 6
7.0 T	52 x 52	2.60	0.49	0.77	~ 18 x 14

* not available

3.2 The computational method

The total electric field inside the biological sample is commonly split into primary vector field $\vec{E}_1$ and secondary field $\vec{E}_2$, according to:

$$\vec{E} = \vec{E}_1 + \vec{E}_2$$

$$\text{where } \vec{E}_1 = -\frac{\partial \vec{A}}{\partial t} \quad \text{and} \quad \vec{E}_2 = -\nabla\Phi \tag{1}$$

Here, $\vec{A}$ denotes the vector magnetic potential due to the source and Φ is the scalar electric potential. The primary electric field $\vec{E}_1$ causes a flow of current $\vec{J}_1 = \sigma\vec{E}_1$ in a conductive sample with the conductivity σ. Any conductivity differences along the path of the current, including the air-tissue interfaces cause non-uniformity of accumulating electric charges, giving rise to scalar potential Φ, the negative gradient of which is the secondary field $\vec{E}_2$, which causes a flow of current $\vec{J}_2 = \sigma\vec{E}_2$.

We first summarize the numerical method for the calculation of vector $\vec{A}$ generated by the superconducting main magnet. Since the coils producing the field are axially symmetric, only the azimuthal component A_θ of the vector magnetic potential $\vec{A}$ is non-zero. The vector magnetic potential components can be calculated as follows:

$$A_\theta(r,z) = \sum_{m=1}^{M} \frac{\mu J_0(m)}{2\pi} \int_{z'=z_1(m)}^{z_2(m)} \int_{r'=R_1(m)}^{R_2(m)} \Xi(r',z';r,z)\,dr'dz', \qquad A_r(r,z) = A_z(r,z) = 0, \tag{2}$$

$$\Xi(r',z';r,z) = \int_0^{\pi} \frac{\cos\beta\, d\beta}{\sqrt{(r')^2 + r^2 - 2r'r\cos\beta + (z'-z)^2}}$$

where $m = 1,2....,M$ is the number of the thick circular solenoids, μ is the permeability of the medium $J_0(A/m^2)$ is the current density within the coils, the primed variables refer to the source points within the solenoid, and the unprimed variables denote field points outside it. Thus, (r',z') is the position vector of a source point and (r,z) is a field point, and so on. For each

solenoid, R_1, R_2 are the inner and outer radii, and z_1, z_2 are the positions in the z-direction. The kernel function Ξ can be evaluated by complete elliptic integrals; however, for the expressions of the magnetic induction fields $B(r)$, a more rapid integral approach [31] is easily employed without introducing special functions. Based on our implementation of the quasi-static finite difference scheme (QSFD) [32], the computation of the electric fields is given by the governing surface integral equation:

$$\int_S (\sigma \frac{\partial A}{\partial t}) \cdot dS = \int_S (\sigma \nabla \Phi) \cdot dS \tag{3}$$

where S represents the surface of the integral region and σ is the conductivity of the sample. The governing equation (3) is subject to a boundary condition of the Neumann type:

$$\frac{\partial \Phi}{\partial n} = \hat{n} \cdot \left(- \frac{\partial A}{\partial t} \right) \tag{4}$$

which indicates that the normal component of the induced eddy current $J = \sigma E$ on the tissue-air boundary is zero inside the body. To calculate the scalar potential Φ, we divide the computational space into a large number of cubic cells and then equation (3) is approximated for each elementary cell. After discretization and rearrangement, the scalar potential for cell (i, j, k) can be expressed as:

$$\Phi_{i,j,k} = \frac{\Xi - f(A)h}{\sum_{q=0}^{1} (\sigma^a_{i+q,j,k} + \sigma^a_{i,j+q,k} + \sigma^a_{i,j,k+q})} \tag{5}$$

$$\Xi = \sum_{q=0}^{1} (\Phi_{i+q,j,k} \sigma^a_{i+q,j,k} + \Phi_{i,j+q,k} \sigma^a_{i,j+q,k} + \Phi_{i,j,k+q} \sigma^a_{i,j,k+q})$$

$$f(A) = \sum_{q=0}^{1} \left[\begin{array}{l} \left(\sigma^a_{(i+q,j,k)} \frac{\partial A}{\partial t}_{(i+q,j,k)} \right) \cdot s_x^q + \\ \left(\sigma^a_{(i,j+q,k)} \frac{\partial A}{\partial t}_{(i,j+q,k)} \right) \cdot s_y^q + \\ \left(\sigma^a_{(i,j,k+q)} \frac{\partial A}{\partial t}_{(i,j,k+q)} \right) \cdot sq \end{array} \right]$$

in which subscripts i, j and k indicate the cell indices, subscript q indicates two faces (0 or 1) in x, y, z directions, respectively, s is the unit vector normal to the cell faces, h is the cell size and σ^a is the local harmonic averaged conductivity. The governing equation in finite-difference form (5) can be solved using an iterative technique such as the Successive Over Relaxation (SOR) algorithm [32] with the advantage of rapid convergence. After the scalar potential has been calculated, the electric field components can be found using relationship (1). The current density is related to the electric field by multiplying by tissue conductivity. The computational method has been verified against other known solutions and the full validation details are given in [32-33].

3.3 Evaluation of E-fields/currents induced in the body models

This section describes the general methodology used in the computation of electric fields and current densities induced in the tissues due to body motion through non-uniform static magnetic

fields produced by the three selected superconducting magnets. Since the magnet coils are axially symmetric, it is sufficient to evaluate the azimuthal component of the vector magnetic potential in the *r*-*z*-plane and to transpose the vector entity from axial-symmetric two-dimensional cylindrical to three-dimensional Cartesian coordinates. It was assumed that all three main magnets are positioned *1.15 m* above ground relative to their central cylinder axis (z = 0). Also, it has been assumed that the superconducting coils of the 1.5 T and 4 T magnets were embedded in a cryostat vessel, which extended the magnets by *0.1 m* both radially and axially. In the case of 7 T, the cryostat vessel extended the magnet by *0.1 m* axially and *0.25 m* radially. The minimum distance between the phantom surface and the edge of the MRI scanner (including cryostat vessel) was assumed to be *0.01 m* for all simulations. Then, the time-varying magnetic flux is expressed by the difference *dA* of the vector potentials of two neighbouring cells divided by the time difference $dt = h/v_\gamma$, where γ is the motion direction, h is the cell size in meters and v is the body velocity in meters per second. The spatial precision of the displacement is therefore restricted to the cell size. We note that this formulation supports multi-directional translation using vector analyses of velocity. In all simulations carried out in this study, the velocity has been normalized to $1\ ms^{-1}$ and assumed to be constant throughout the body model. In that way the results obtained can be linearly extrapolated to other velocities of interest with ease. However, in an attempt to simulate a realistic human movement, the velocity of different parts of the body can be set to different values. Based on the computational method outlined in Section B, the electric field and current densities induced in the body can be computed. Several cases of body movement are considered in this study:

Motion I - walking along the magnet cylinder in the direction from the positive towards the negative z-axis

Motion II - walking perpendicular the magnet cylinder in the direction from the positive towards the negative x-axis (r-axis)

Motion III - upward motion while facing the negative direction of the z-axis.

Motion IV - upward motion while facing the negative direction of the x-axis (r-axis).

Figure 1 illustrates all four cases of body motion considered, indicating the assumed computational region and the magnet position.

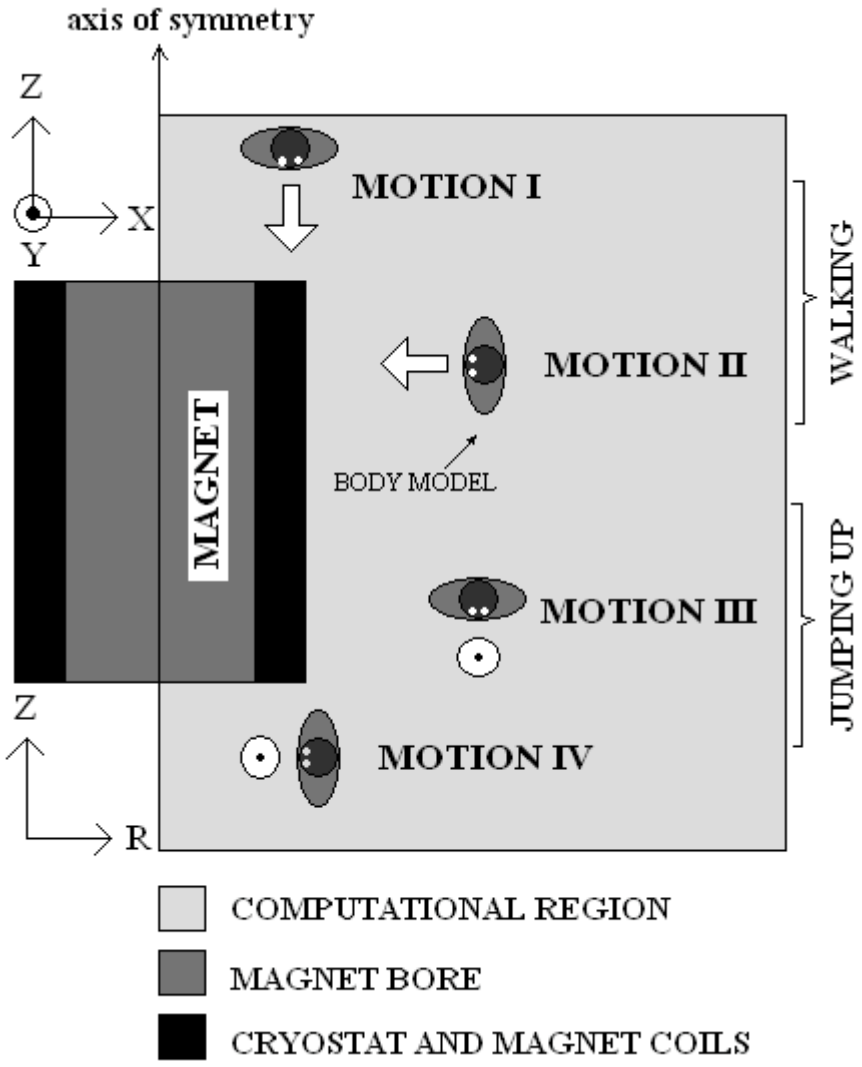

Figure 1 Sketch (top view) of four assumed body motions around the magnet of interest.

1. Region scanning computations at low model resolution

To evaluate the positions in the MRI room where peak current densities are induced in the body model, it is necessary to perform computations with the phantom movement beginning at numerous locations around the magnet of interest. Employing the high-resolution body models (*~2 mm)*, in this exercise would consume a considerable amount of computing time. To speed up the scanning process, we have employed male and female body models as the low-resolution first to register the peak values at various positions around the magnet, after which a higher resolution simulation at the position of interest was performed. Only the right side of the magnet region is considered (r > 0) and the typical scan area is assumed to be: $r = 0 \sim 2.2m$, $z = -2 \sim 2m$. The phantoms are then positioned in this region at spatial increments of *0.1 m* both radially and axially and the fields induced in the low-resolution body models as they undergo motions I-IV at 1m/s are evaluated.

Since the phantoms are voxel based, there are unrealistic sharp corners and edges defining the tissue boundaries. There can be also instances of large contrasts in conductivity between neighbouring voxels and where single isolated voxels occur embedded in another tissue. These

can introduce artificially high maximum values, associated with possible edge singularities in the induced fields. In the presence of such numerical staircase errors, 99% thresholded values (limits exceeded in only 1% of tissue voxels) serve, to a degree, as a more satisfactory estimate of maximum field levels [34]. Hence, for every position around the magnet, the 99% thresholded total electric field (denoted: *E99*) and current density (denoted: *J99*) are evaluated. This effectively removes any statistically insignificant numerical errors and singularities. The final results of these simulations are presented as field plots (around the magnet) of peak 99% thresholded electric field and eddy current densities induced in the body.

2. Detailed field evaluations at high model resolution

Once the position of peak electric field/ current density is determined during the region scan, we perform a detailed field computation with the high-resolution body models (Table 1). As the cell size decreases, the maximum value of current density increases for two reasons. The effect of averaging the conductivity in the rescaled cells (low-resolution) and its masking of high-conductivity voxels decreases with smaller cells. There is also a shape effect [35], whereby an indentation such as at the armpits and at the top of the legs or in a particular high-conductivity tissue will produce a tightening of the 'current lines' and an increase in the current density. If the indentation is very sharp the current density will increase significantly at the apex. Therefore there is a need to average over a finite area. The ICNIRP guidelines [23] state that the perpendicular current density components should be averaged over a square with $1\ cm$ edges centred on the voxel and parallel to the three principal Cartesian planes. According to Dawson *et. al*. [34], in the presence of complex heterogeneous models and non-uniform fields this definition is, at best, ill defined, as it can be estimated in two distinct ways. In one algorithm the averaging takes into account the current flowing in neighbouring, dissimilar tissues. The magnitude of the tissue-specific averaged current will therefore depend on the nature of the adjacent tissues. In that regard the algorithm treats the interfaces between dissimilar tissues as a *continuous zone* and can be classified as a *full averaging algorithm.* The other algorithm (*tissue specific*) works on the same principle as *full averaging algorithm*, but it zero-weights the neighbouring current values of dissimilar tissue type. By performing a simple analytical example, Dawson *et. al*. [34] were able to show that the tissue *specific algorithm* can easily underestimate the averaged values in both regions and in particular in organ/tissues of small spatial extent with local high conductivity ratios. However, the *full averaging algorithm* can overestimate the values in lower conductivity material and somewhat underestimate the values in the higher conductivity material.

During MRI imaging/segmentation and generation of the numerical voxel phantoms (here: NORMAN and NAOMI), it is generally difficult to ascertain the clear boundary between two different organs or tissue types. Furthermore, this study aims to determine the worst-case scenarios, and so the overestimates in averaged current densities, rather than underestimates, are preferred. In that regard, the *full averaging algorithm* is clearly a better candidate and thus has been used in all high-resolution evaluations of this study. The final results of the high-resolution simulations are presented in terms of electric field and eddy current distributions in the male and female voxel phantoms. In addition tables and graphs are used to illustrate the maximum and average tissue-specific E-fields/currents and peak $1\ cm^2$ averaged tissue-specific current densities, predominantly in tissues of the CNS and heart, as these are known to be affected by induced fields/currents. Table V also reports selected analogous results for other body tissues.

3.4 Estimation of 'safe distance from magnet'

In this investigation, we endeavor to estimate the distance away from the magnet at which the induced $1\ cm^2$ averaged current densities in the tissues of the CNS and heart are below the ICNIRP threshold of $40\ mAm^{-2}$ - rms. For this purpose, we have assumed that the high-resolution male voxel phantom is moving along the three MRI scanners (Motion I) and that the

body model is positioned at various axial distances away from the magnet end with a radial displacement of *0.3 m* from the magnet's central axis (e.g. location of largest induced current density). Then the induced electric field and current densities are computed for all tissues and only the results for the tissues of the CNS and heart are reported.

4.0 RESULTS

4.1 Magnetic field profiles of the three superconducting magnets

The total magnetic fields of the three main magnets (1.5T, 4T and 7T) are computed using equation (1), and the corresponding field profiles are illustrated in figure 2 (left column). In addition, figure 2 (right column) portrays the product of the total magnetic field $|B|$ and its spatial gradient $|\nabla B|$. The significantly larger $|B\nabla B|$ values in the physical magnets (including cryostat) have been blanked out in Figure 2 (right column) as in normal circumstances these fields would not come into direct contact with the worker. The plot illustrates the homogeneous static magnetic field in the working volume and the rapid field drop off near the magnet ends, which can potentially induce electric fields in the body, during motion around the magnet.

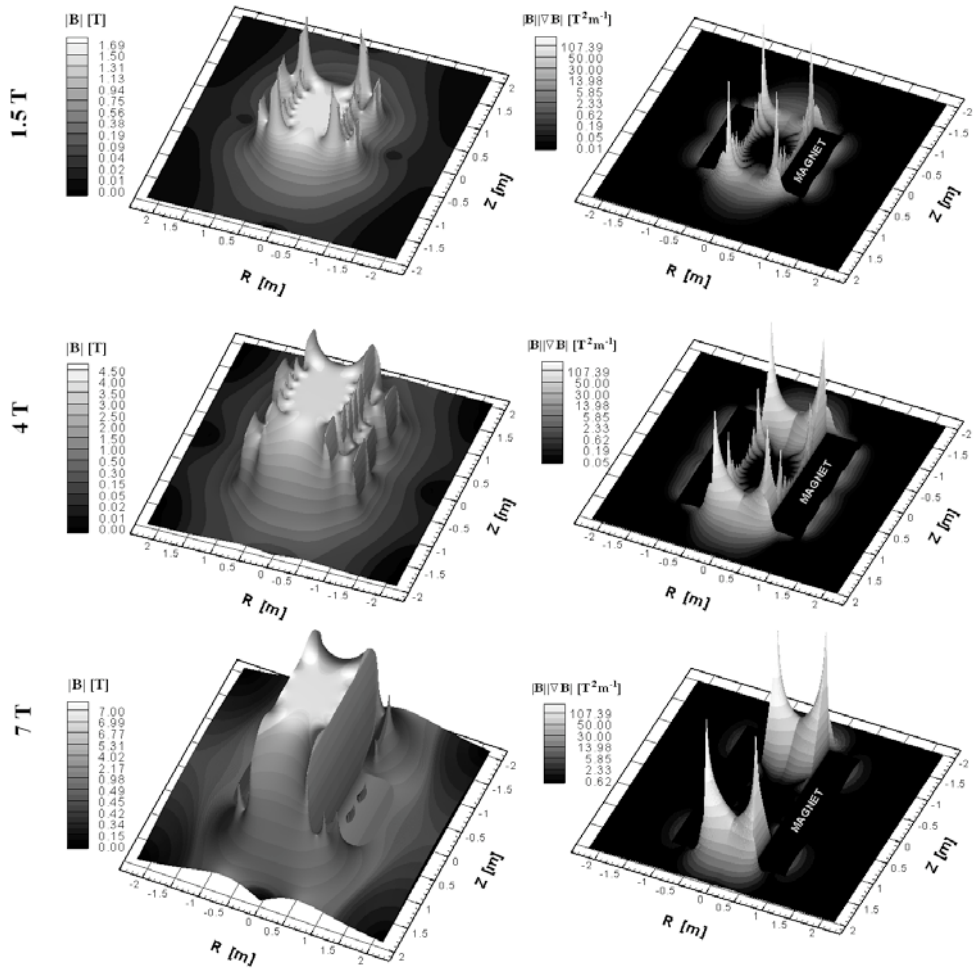

Figure 2 Left column: total magnetic field profile generated by the 1.5T (top), 4T (middle) and 7T (bottom) magnet. Right column: product of the total magnetic field and its spatial gradient for all three static magnets. The region occupied by the MRI magnet and its cryostat vessel is blanked out and labeled: 'Magnet'.

4.2 Results based on different body motions

1. Region scanning computations at low model resolution

Here, the lower resolution body models are engaged first to estimate the location(s) around the three magnets with peak thresholded current density *J99* and electric field *E99* induced in the male and female voxel phantoms during different body motions. The low-resolution region scans converge in about 4000 iterations and the typical computation time for one scan is around 8 hours on a dual XEON 3.6GHz / 4GB RAM PC platform. With all combinations of magnets, body models and motion types, a total of twenty-four low-resolution region scan simulations were performed. Figures 3 and 4 illustrate the peak *J99* magnitudes versus spatial position around the three magnets, recorded during four assumed body motions in case of the male and female voxel phantom, respectively. We note here that the field values at the physical location of the whole MRI scanner were not recorded and are zero (dark region labelled 'Magnet' in figures 3 and 4), as these spatial positions would be normally not accessible to the workers for the four body motions assumed. However, in a case that an worker is bending towards the magnet with the upper body partially inside the magnet bore, then the aforementioned region might show potentially larger magnitudes than those depicted in figures 3 and 4. Figures 5 and 6 show analogous plots to figures 3 and 4 in terms of the *E99* profiles.

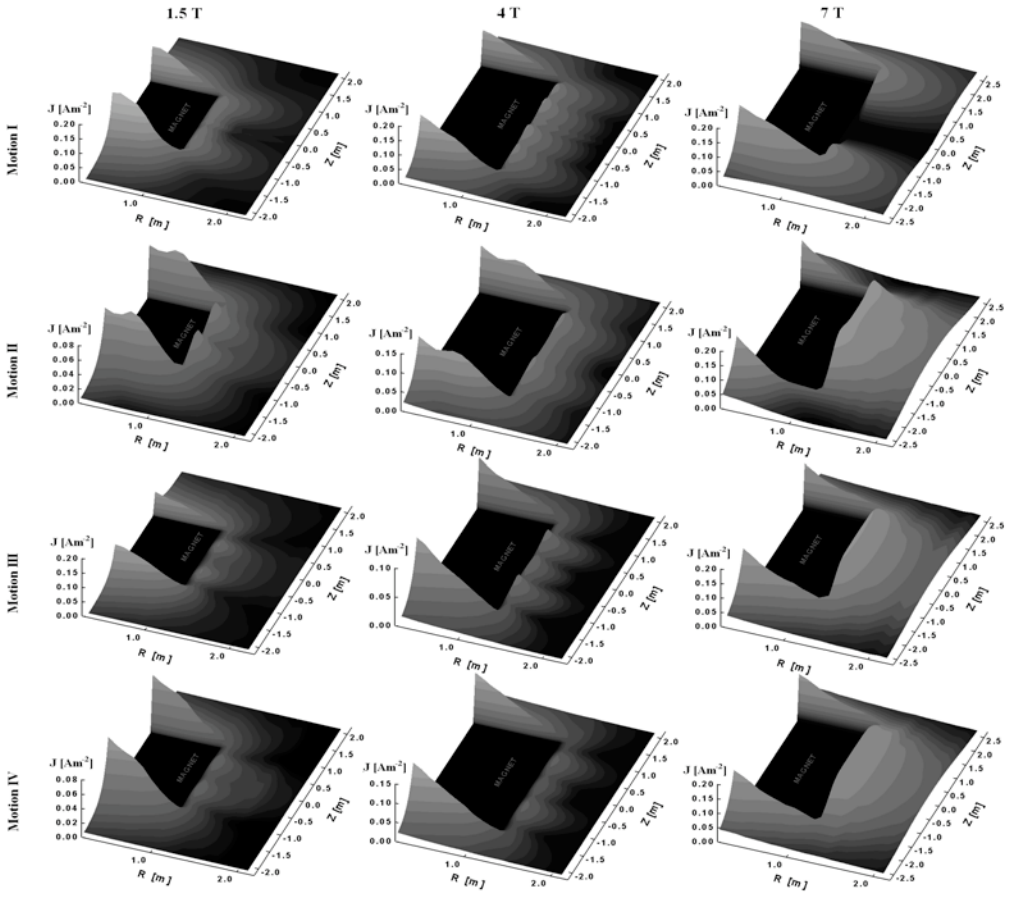

Figure 3 Peak *J99* field profiles around the 1.5T (left column), 4T (middle column) and 7T (right column) magnet during different body motions ('Motion I' – 'Motion IV') of the male voxel phantom.

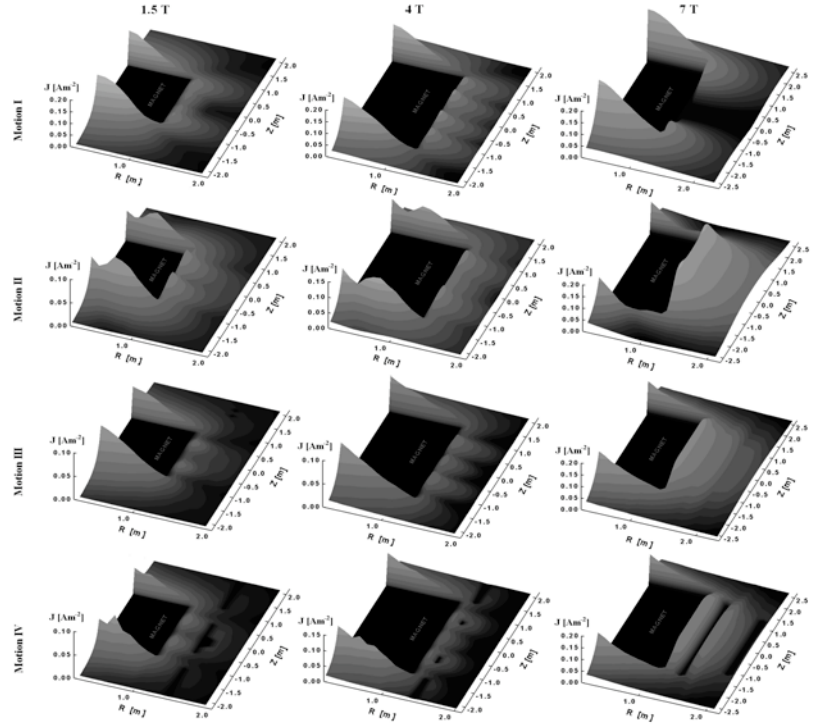

Figure 4 Peak *J99* field profiles around the 1.5T (left column), 4T (middle column) and 7T (right column) magnet during different body motions ('Motion I' – 'Motion IV') of the female voxel phantom.

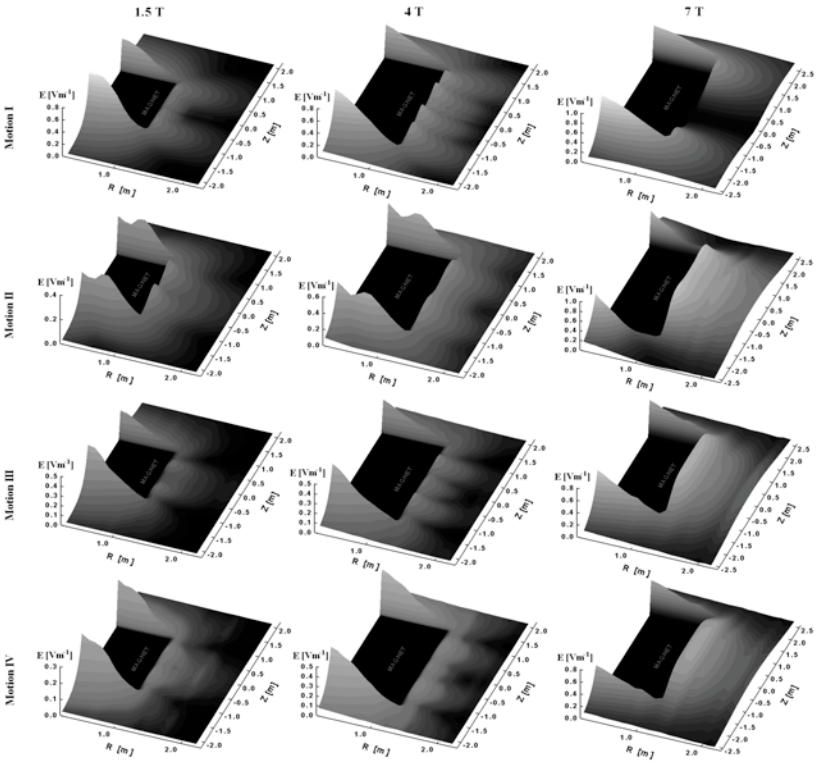

Figure 5 Peak *E99* field profiles around the 1.5T (left column), 4T (middle column) and 7T (right column) magnet during different body motions ('Motion I' – 'Motion IV') of the male voxel phantom.

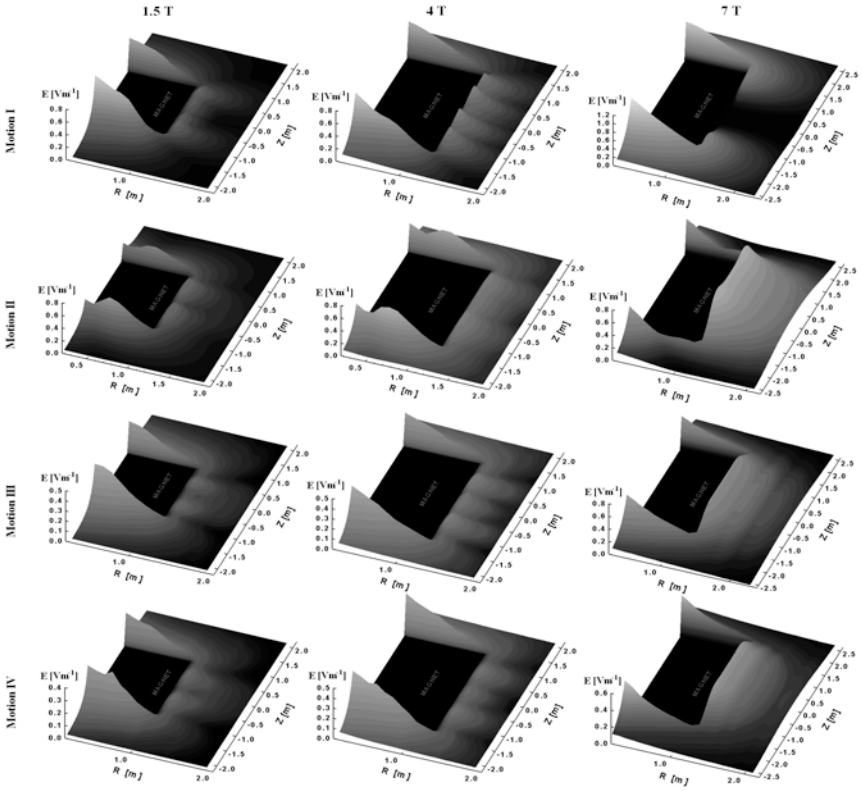

Figure 6 Peak *E99* field profiles around the 1.5T (left column), 4T (middle column) and 7T (right column) magnet during different body motions ('Motion I' – 'Motion IV') of the female voxel phantom.

Table 3 summarizes the largest recorded peak *J99* and *E99* values for all combinations of magnets, body models and motions considered. Table 4 lists the corresponding positions (in cylindrical coordinates) around the three magnets where the largest peak *J99* values are recorded during the four body motions for both voxel phantoms.

Table 3
Peak E99 and J99 in Norman and Naomi for different motions around the three magnets

FIELD	BODY MODEL	MOTION I		MOTION II		MOTION III		MOTION IV	
		E99	J99	E99	J99	E99	J99	E99	J99
		[Vm^{-1}]	[Am^{-2}]	[Vm^{-1}]	[Am^{-2}]	[Vm^{-1}]	[Am^{-2}]	[Vm^{-1}]	[Am^{-2}]
1.5T	**NORMAN**	0.821	0.165	0.332	0.081	0.450	0.103	0.306	0.083
	NAOMI	0.748	0.161	0.418	0.089	0.433	0.085	0.310	0.075
4 T	**NORMAN**	0.755	0.149	0.508	0.125	0.482	0.109	0.471	0.136
	NAOMI	0.731	0.166	0.518	0.123	0.493	0.094	0.477	0.110
7T	**NORMAN**	0.956	0.189	0.722	0.168	0.766	0.181	0.568	0.164
	NAOMI	1.099	0.242	0.704	0.187	0.605	0.159	0.508	0.133

Table 4
Worst-case voxel phantom positions (to the nearest 5 cm)

	MODEL	1.5 T		4 T		7 T	
		R [m]	Z [m]	R [m]	Z [m]	R [m]	Z [m]
I	NORMAN	0.30	-0.90	0.30	-1.30	0.30	-1.55
	NAOMI	0.30	-0.90	0.30	-1.30	0.30	-1.55
II	NORMAN	0.50	-1.00	0.20	-1.40	1.15	0.80
	NAOMI	0.50	-1.00	0.20	-1.40	1.15	0.80
III	NORMAN	0.40	-0.90	0.30	-1.30	0.30	-1.55
	NAOMI	0.30	-0.90	0.30	-1.30	0.30	-1.55
IV	NORMAN	0.20	-1.00	0.20	-1.40	0.20	-1.70
	NAOMI	0.50	-1.00	0.20	-1.40	0.20	-1.70

Table 5
Tissue-specific measures of electric field and current density induced in the male body model during Motion I around 4T magnet at the position of $r = 0.3m$ and $z = -1.3m$

TISSUE	E_{avg}	J_{avg}	$E_{\max}$	$J_{\max}$	$J^{\max}_{1cm^2,avg}$	$J^{avg}_{1cm^2,avg}$
	$[mVm^{-1}]$	$[mAm^{-2}]$	$[mVm^{-1}]$	$[mAm^{-2}]$	$[mAm^{-2}]$	$[mAm^{-2}]$
Bile	90.02	126.02	179.43	251.20	116.06	202.58
Gall Bladder	159.36	143.42	722.63	650.37	94.40	254.08
CSF	69.01	138.01	1039.38	2078.76	64.80	636.17
Blood	83.61	58.53	729.62	510.73	45.89	183.24
Spleen	561.02	57.78	1148.88	118.33	69.07	201.92
Prostate	172.14	72.99	1153.34	489.02	54.20	201.04
Small Intest.	151.49	80.59	1105.69	588.23	75.03	237.27
Testis	103.09	43.71	1419.66	601.94	31.48	215.72
Urine	51.93	77.89	318.11	477.16	67.35	189.62
Bladder	122.39	25.46	540.29	112.38	39.23	159.10
Thymus	107.83	56.50	294.06	154.09	46.06	86.74
Liver	423.98	17.55	1404.54	58.15	22.33	182.78
Breast	116.80	37.49	578.63	185.74	27.85	79.94
Muscle	179.83	57.74	3987.31	1279.93	50.98	455.24
Skin	210.27	0.04	6255.60	2.05	4.86	196.36
Fat	311.24	6.97	6482.13	145.20	15.97	424.85
Tendon	24.77	9.49	376.42	144.17	6.51	54.18
Trabec bone	97.70	7.96	1701.34	138.66	6.15	96.34
Pancreas	125.40	65.71	1152.92	604.13	51.24	306.07
Oeasophagus	124.93	65.46	864.10	452.79	40.31	152.37
Stomach food	188.88	60.63	523.80	168.14	63.76	213.58
Stomach	179.48	94.05	1290.19	676.06	72.25	291.82
Duodenum	139.50	74.22	590.22	314.00	65.03	188.68
Kidneys	316.80	35.80	798.27	90.20	35.96	122.02
Brain	87.60	10.42	570.40	67.88	15.58	213.49
Spinal cord	135.58	3.90	1628.63	46.90	33.15	332.03
Lower LI	240.95	55.90	1571.42	364.57	51.94	237.26
Upper LI	272.54	63.23	1071.14	248.51	60.28	177.29
Thyroid	101.35	53.11	202.26	105.99	46.62	84.63
Lens	29.11	9.52	68.38	22.36	22.22	29.22
Adrenals	172.18	90.22	489.70	256.60	57.66	115.54
Bone	221.53	4.47	3244.18	65.53	12.45	567.66
Humour	21.82	32.73	87.45	131.17	25.87	45.32
Retina	43.59	22.01	192.15	97.03	20.39	46.58
Heart	127.84	13.68	380.30	40.69	20.67	87.40
Lung air	138.84	11.04	800.41	63.63	14.98	121.14
Lung	229.93	49.66	1175.40	53.89	48.71	202.69

2. Detailed field evaluations at high model resolution

Based on the worst-case positions listed in Table 4 (i.e. positions with largest peak *J99* values), the high-resolution body models were employed to calculate the tissue-specific electric fields and current densities. On the same platform (dual XEON 3.6GHz / 4GB RAM PC), the high-resolution simulations converge in about 50,000 – 70,000 iterations and consume approximately 1.9GB RAM/10h CPU-time and 1.55GB RAM/9.5h CPU-time for the male and female phantom studies respectively. A total of twenty-four high-resolution simulations were performed. Table V details the average and maximum $1\ cm^2$ averaged current densities in the tissues of the central nervous system and heart of the male voxel phantom for all combinations of magnets and body motions.

Table 6

Worst-case selected $1\ cm^2$ - averaged current density induced in Norman in $[mA/m^2]$

	TISSUE	1.5 T		4 T		7 T	
		Avg	**Max**	**Avg**	**Max**	**Avg**	**Max**
I	**CSF**	50.90	360.51	64.80	636.17	83.60	875.89
	Brain	8.56	116.27	15.58	213.49	18.64	235.90
	Spine	40.99	227.38	33.15	332.03	44.19	457.15
	Retina	11.58	27.89	20.39	46.58	21.09	53.60
	Heart	12.37	59.11	20.67	87.40	30.33	142.63
II	**CSF**	23.04	194.01	37.62	280.24	52.66	397.94
	Brain	2.17	30.91	6.14	108.52	7.09	130.22
	Spine	24.83	165.69	32.62	193.65	17.46	261.42
	Retina	4.62	14.75	18.43	72.84	27.49	87.41
	Heart	8.77	52.58	14.37	88.00	18.68	123.22
III	**CSF**	35.82	242.72	54.16	431.35	59.70	585.14
	Brain	9.55	124.53	15.37	199.35	14.90	182.35
	Spine	11.10	123.99	16.65	173.14	23.86	237.20
	Retina	11.04	30.12	13.83	41.35	17.28	49.95
	Heart	6.33	3055	11.99	65.95	19.08	105.23
IV	**CSF**	20.28	173.96	37.11	303.92	30.74	206.64
	Brain	6.89	101.39	4.29	86.13	52.89	127.83
	Spine	6.83	46.94	38.09	247.11	15.22	96.92
	Retina	11.80	26.69	10.48	37.00	63.65	40.51
	Heart	3.65	16.17	13.23	82.67	39.46	32.21

Table 7

Worst-case selected 1 cm^2 - averaged current density induced in Naomi in [mA/m^2]

	TISSUE	1.5 T		4 T		7 T	
		Avg	**Max**	**Avg**	**Max**	**Avg**	**Max**
I	**CSF**	43.67	227.69	63.42	331.54	78.57	468.81
	White M	9.49	131.16	13.32	195.40	15.78	228.64
	Grey M	30.00	168.15	43.36	262.49	52.96	348.46
	Spine	30.25	213.87	45.74	313.48	60.53	445.21
	Retina	18.90	46.03	26.75	68.96	31.17	85.44
	Heart	7.19	37.29	10.92	56.28	15.75	77.09
II	**CSF**	19.24	119.22	35.72	241.55	53.11	359.91
	White M	3.59	113.16	6.97	119.01	9.89	173.75
	Grey M	10.92	93.57	21.54	208.67	33.38	297.44
	Spine	33.18	144.51	35.70	121.11	51.40	174.27
	Retina	11.32	30.24	28.52	88.21	37.98	112.24
	Heart	7.33	31.40	8.96	51.98	10.22	69.23
III	**CSF**	34.25	138.71	46.76	202.81	53.86	291.37
	White M	6.56	116.74	8.79	151.77	10.35	155.69
	Grey M	23.03	124.62	30.77	161.69	34.44	167.65
	Spine	16.26	124.93	25.31	198.50	37.48	284.98
	Retina	10.10	26.74	14.79	38.87	20.43	50.81
	Heart	4.69	25.22	7.75	42.51	12.57	70.73
IV	**CSF**	22.17	125.78	30.43	185.68	29.13	151.39
	White M	4.63	113.75	5.99	115.20	5.87	119.82
	Grey M	14.49	102.31	19.34	150.72	18.40	125.15
	Spine	7.64	28.19	14.30	70.44	18.12	96.80
	Retina	13.85	28.98	21.16	45.86	23.81	61.89

Table 7 lists analogous results to Table 6 for the female body model. The corresponding average and maximum tissue-specific electric fields have been tabulated in Tables 8 and 9, for the male and female body model respectively.

Table 8

Worst-case selected electric field induced in Norman in [mV/m]

	TISSUE	1.5 T		4 T		7 T	
		Avg	Max	Avg	Max	Avg	Max
I	CSF	52.66	687.46	69.01	1039.38	88.49	1418.30
	Brain	48.84	325.87	87.60	570.40	105.52	704.79
	Spine	139.12	871.41	135.58	1628.63	181.15	2219.38
	Retina	24.69	129.74	43.59	192.15	46.32	257.70
	Heart	72.62	245.51	127.84	380.30	189.32	536.21
II	CSF	23.13	377.47	38.72	407.47	51.32	488.96
	Brain	12.45	79.38	35.58	281.11	44.56	321.88
	Spine	82.46	429.84	114.88	624.90	59.45	776.54
	Retina	9.25	39.87	34.53	156.39	39.90	189.26
	Heart	55.46	230.67	86.01	373.20	101.29	455.21
III	CSF	62.72	486.77	85.95	863.61	93.10	911.28
	Brain	80.72	431.30	101.22	560.10	14.90	182.35
	Spine	61.28	415.70	107.34	477.29	23.86	237.20
	Retina	39.93	93.85	36.15	101.92	17.28	49.95
	Heart	40.94	175.21	104.59	417.94	19.08	105.23
IV	CSF	40.29	250.86	37.54	553.71	70.39	140.78
	Brain	42.92	314.25	24.62	184.62	53.61	444.48
	Spine	59.60	207.50	127.47	627.41	134.31	528.44
	Retina	24.85	94.65	20.89	94.49	41.03	126.03
	Heart	59.15	152.68	82.32	359.43	138.29	368.79

Table 9

Worst-case selected electric field induced in Naomi in [mV/m]

	TISSUE	1.5 T		4 T		7 T	
		Avg	Max	Avg	Max	Avg	Max
I	CSF	59.46	254.79	86.09	773.26	106.27	1074.17
	White M	92.56	569.70	129.60	830.79	154.09	1064.92
	Grey M	88.77	517.77	126.81	733.66	153.58	974.06
	Spine	75.75	421.49	114.72	615.00	151.27	879.02
	Retina	33.11	97.74	48.73	147.65	57.85	263.19
	Heart	50.53	155.01	76.66	233.03	110.30	336.97
II	CSF	26.43	293.37	46.47	243.24	66.79	345.33
	White M	35.43	250.29	69.84	507.54	26.55	790.42
	Grey M	32.64	193.72	63.04	564.33	89.92	667.02
	Spine	87.20	331.74	93.08	290.35	103.02	320.11
	Retina	18.94	52.84	45.26	137.26	56.97	213.48
	Heart	54.28	165.51	65.34	201.89	87.21	259.83
III	CSF	50.16	397.92	65.61	535.63	94.47	586.78
	White M	68.05	393.97	89.89	518.25	121.68	643.97
	Grey M	71.09	391.80	92.67	553.19	121.24	690.93
	Spine	60.46	246.67	99.22	387.95	162.34	618.17
	Retina	19.56	55.47	29.57	86.89	74.43	169.47
	Heart	47.34	175.82	79.95	286.54	134.36	475.43
IV	CSF	53.70	216.53	48.58	305.92	62.10	439.39
	White M	72.48	262.74	66.83	370.71	80.19	441.33
	Grey M	71.46	302.96	61.98	352.20	75.29	461.23
	Spine	24.57	30.55	104.93	275.73	143.03	383.89
	Retina	36.81	72.08	46.29	121.41	65.65	207.12

Figures 7 and 8 illustrate the selected electric field and eddy current density profiles in coronal, sagittal and axial slices of the male and female voxel phantoms during 'Motion I' around all three superconducting magnets. We note here that the conditions at which these results were obtained for different static field strengths were almost same (Table 4), i.e. both body models were situated 0.3 m radially away from the magnet's central z-axis and positioned axially so that the body surface is close, but not touching the first cryostat wall.

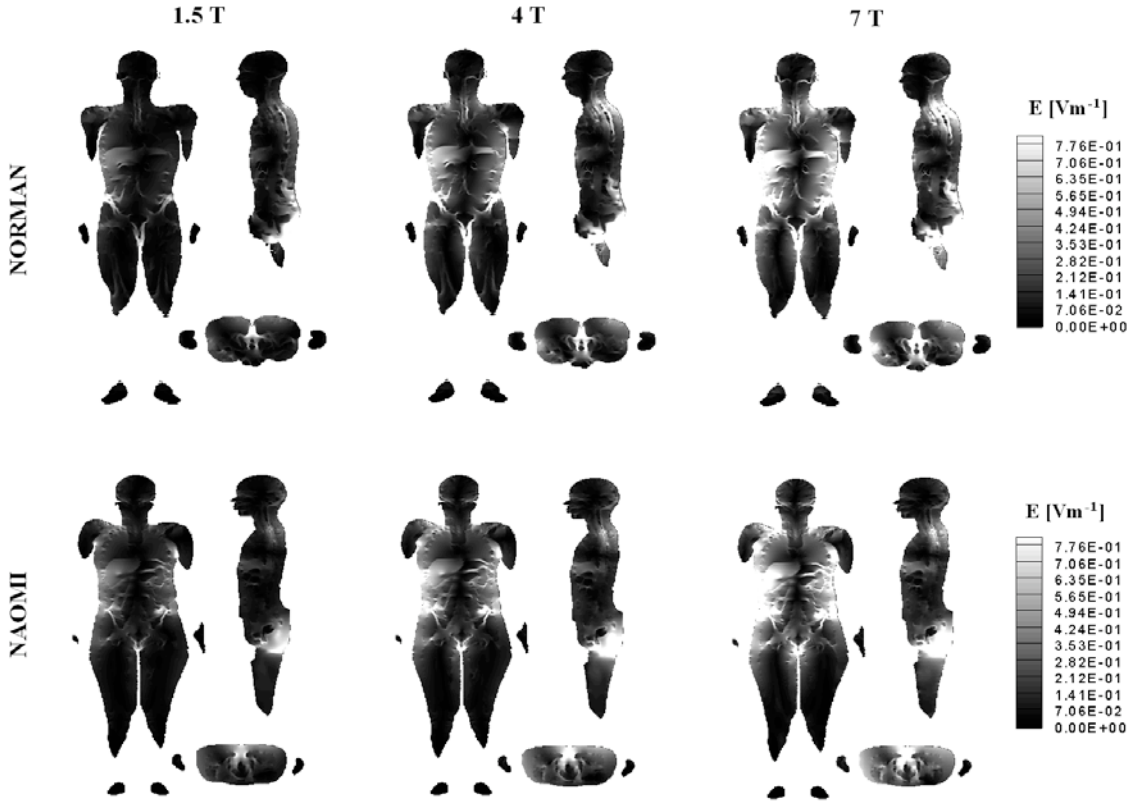

Figure 7 High-resolution coronal, sagittal and axial electric field distributions in the male (top row) and female (bottom row) voxel phantoms for normalized 'Motion I' around the 1.5T (left column), 4T (middle column) and 7T (right column) static superconducting magnet

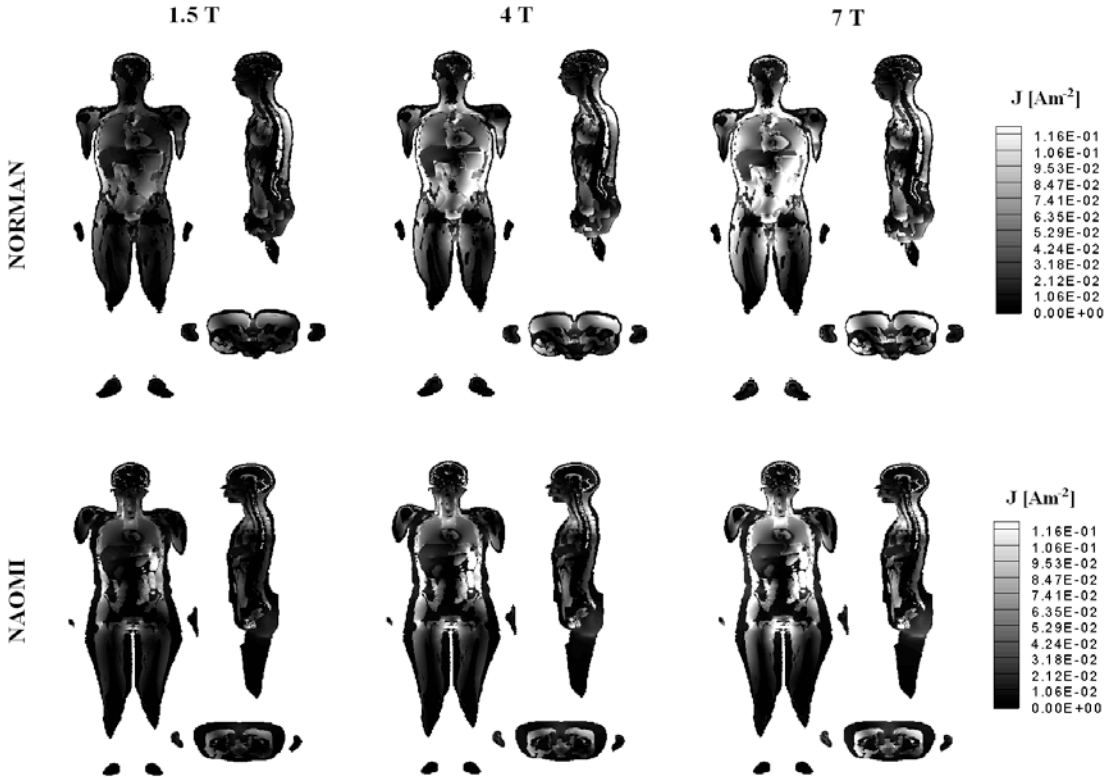

Figure 8 High-resolution coronal, sagittal and axial current density distributions in the male (top row) and female (bottom row) voxel phantoms for normalized 'Motion I' around the 1.5T (left column), 4T (middle column) and 7T (right column) static superconducting magnet.

The colour map in Figures 7 and 8 is a greyscale spectrum, where bright regions correspond to high and dark regions to low values. The current density values in figure 8 are related to the electric field by multiplying by tissue conductivity.

4.3 Estimation of the 'safe distance'

Figure 9 illustrates the maximum and mean $1\ cm^2$ averaged current densities and electric fields in the tissues of the central nervous system and heart of the male voxel phantom at different axial displacements from the particular magnet end with a radial displacement of 0.3 m from the central z-axis of the magnet. The results were obtained using the high-resolution male body model that is walking along the magnet bore from the positive towards the negative direction of the z-axis. The horizontal axes in figure 9 are absolute displacements from the MRI machine end as the body is moving away from it.

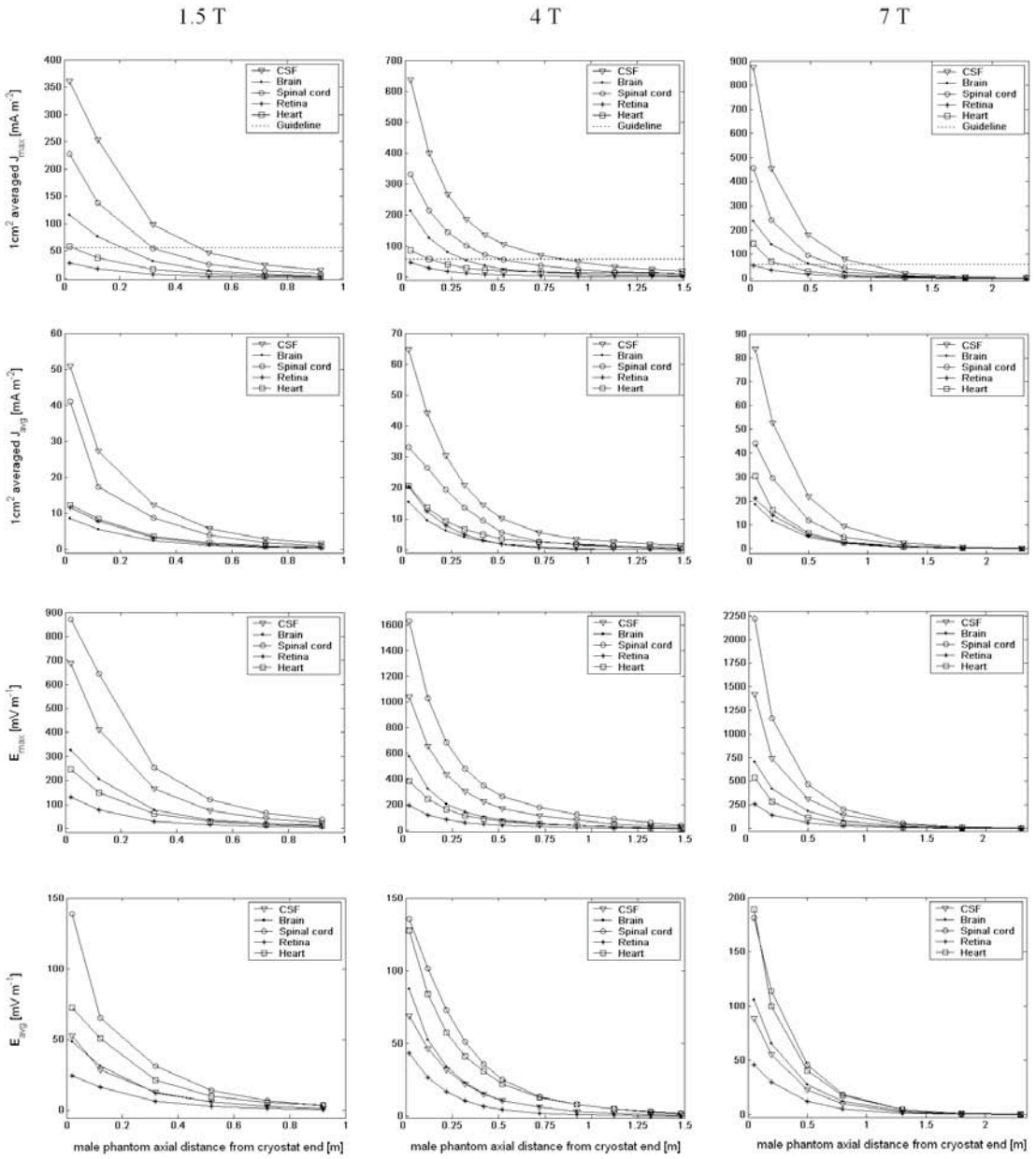

Figure 9 Maximum and average electric field and 1 cm^2 - averaged current densities induced in the central nervous system and heart tissues of male voxel phantom at different static field strengths versus axial distance away from particular magnet end (including cryostat vessel) (Table 2). In all cases, the phantom was positioned radially 0.3 m away from the magnets central z-axis.

5.0 DISCUSSION

Previous studies [2] indicate that the levels of the electric fields/ current densities induced in the body, during motion around a MRI magnet, relate to the strength of the total static magnetic field $|B|$ and the magnitude of the spatial gradient of this field $|\nabla B|$. In general, the MRI magnets generate strong static magnetic fields very close to the physical coil, while the strongest bending of magnetic flux lines occurs commonly between two (or more) superconducting coils where currents are flowing in opposing directions as well as close to the entrance edges of the magnet bore. The product of the total magnetic field and its gradient has been suggested as an indicator of locations around the magnet where largest *in situ* translational forces are produced [10]. However, during the four body motions studied herein, the locations of largest magnitudes of induced peak *J99* and *E99* fields (figures 3-6) correspond, to a degree, with the spatial positions of $|B\nabla B|$ peaks (Figure 2, right column), which is near the entrance edges of the magnet bore. In some instances (i.e. 7T - Motion II, Figures 3-6) however, the largest induced peak *J99* and *E99* fields are recorded near the sides rather than ends of the unshielded 7T magnet as predicted by the $|B\nabla B|$ distribution. It follows that the $|B\nabla B|$ factor might not be suitable in describing and predicting all outcomes of the motion induced fields, especially for unshielded cylindrical systems.

It is also interesting to observe, that approaching the unshielded 7T magnet from its side (Figure 3) can induce considerable electric field and current densities in tissues, which usually is not the case for actively shielded magnet systems (1.5T and 4T). In general, the levels in peak electric field and eddy currents (Table 3) increase for increasing static field strength and are larger when the body is aligned parallel to the z-axis (Motion I and Motion III) rather then perpendicular (Motion II and Motion IV) to it.

In Figures 7 and 8 the worst-case electric field and current density distributions are illustrated for male and female body model exposed to different field strengths during walking along the magnet bore. It is evident that both the electric field and eddy current magnitudes increase for increasing field strength. However, a strict relationship between the increase in the static magnetic field and the magnitudes of induced electric fields/ current densities recorded could not be established. It seems that the induced fields are also largely dependant on the static magnetic field pattern rather than on the static field strength alone. Since the body models are approaching the magnets from the positive z-axis, these largest field values are induced when the body models are moving away from the magnet (Table 6). This is clearly reflected in the larger field results induced in the back/bottom (sagittal views in Figures 7 and 8) and right side of the body (coronal views in Figures 7 and 8)). This also imposes larger values on the central nervous system and especially the synapses in spinal cord. In Tables 6 and 7, the worst case maximum and average tissue-specific 1 cm^2 - averaged current densities in the central nervous system and in heart are listed for the male and female body model respectively. In general, the current densities increase for the increasing field strength. Also, the 1 cm^2 - averaged current density magnitudes are on average larger when the body models are facing the magnet ends (e.g. Motion I) rather than magnet sides (e.g. Motion II). Similar behaviour can be observed for maximum and average electric field results recorded in the central nervous system and heart of the male and female voxel phantom (Tables 8 and 9).

More importantly, the maximum 1 cm^2 - averaged current densities (tables V and VI) for most combinations of magnets and motion type can be larger than the threshold of 40 mAm^{-2} -rms. (or 56.57 mAm^{-2} - peak) defined in the ICNIRP guidelines [23]. This clearly suggests that considerable current levels can be induced in the central nervous system and other body tissues, even during simple motion very close to the 1.5T MRI scanner. The worst-case maximum

electric fields induced in the brain exceed the IEEE standard of 25.03 mV/m-peak, while in some circumstances the electric fields exceed the value of 0.75 V/m-peak that is attributed to experimentally observed alternation of neural activity in hippocampal slices of the rat brain [20-21]. The pre-synaptic depolarization threshold of 74.95 mV/m-peak for retina [13-14] might be exceeded at very high and ultra-high field strengths for both male and female. However the magnitudes of maximum induced electric fields in the heart are below the IEEE threshold of 1.33 V/m-peak for all examined field strengths [12, 22]. The results detailed in Table V show that the electric field thresholds that result in peripheral nervous stimulation can be exceed in the tissues (mainly for the male) of fat and skin at very high and ultra high field strengths [12].
We have estimated the axial distances away from the three assumed magnets at which the induced maximum 1 cm^2 - averaged current density magnitudes would drop below the ICNIRP threshold of 56.57 mAm^{-2} - peak in the head and trunk. According to selected results demonstrated in figure 9 (for tissues of CNS and heart), the maximum 1 cm^2 - averaged current density magnitudes are below the 56.57 mAm^{-2} - peak threshold at distances from cryostat end of ~0.5-1.0 for the static magnetic fields between 1.5-7 T. The same holds true for all other tissues. This means, that for higher field strengths, workers moving at the same velocity should be further away from the magnet to be compliant . In order to be certain that 1 cm^2 - averaged current would not exceed the ICNIRP threshold, one should add contingencies to the aforementioned 'safety distances'. We note here, that these values are only representative of motion velocities normalized to 1 ms^{-1} and obviously, slower is better.

6.0 CONCLUSIONS

This paper describes the numerical evaluation of the induced electric fields and current densities in male and female models of workers exposed to static magnetic fields of 1.5T, 4T and 7T as they move around in the MRI room. The low-resolution body model results are presented as peak *J99* and *E99* values recorded around the assumed MRI magnets; the largest values occur close to the entrance edge of the magnet bore.

The high-resolution numerical results of this work indicate that the ICNIRP threshold of 40 mAm^{-2} - rms. in the head and trunk can be easily exceeded when the worker is moving close to any of the three MRI magnets used in this study. Since the motion velocity has been normalized to 1 ms^{-1} in all designated cases, the results can be scaled linearly for other velocity magnitudes. This implies, that walking faster than 1 ms^{-1} might trigger even larger currents in body tissues. It is shown that the levels of induced electric fields and current densities clearly increase for increasing static magnetic field strength. In order to limit the induced current densities to less than 40 mAm^{-2} - rms. in the tissues of the central nervous system when walking along the magnet bore, the simulation results suggest that the worker should be at least ~0.5-1.0 m axially away from the ends of 1.5-7 T magnet cryostats respectively, or should be moving at correspondingly lower velocities than 1 m/s. Further theoretical and experimental studies will need to be conducted to completely describe the regions around specific magnets where guidance should be given to occupationally exposed workers. It is hoped that these results will better inform the MRI community concerning compliant activity around MRI systems.

7.0 ACKNOWLEDGEMENTS SPECIFIC TO THIS SECTION

We thank Oxford Magnet Technology for providing the 4T magnet pattern.

8.0 REFERENCES

[1] Crozier,, S and Liu, F Numerical evaluation of the fields caused by body motion in or near high-field MRI scanners, *Progress in Biophysics and Molecular Biology*, **87**: 267-278, 2005

[2] Schenck, JF Safety of strong, static magnetic fields. *Journal of Magnetic Resonance Imaging*, **12**: 2–19, 2000

[3] Smith, MK, Stehling, and Turner, R Eds. *Echo-Planar Imaging Theory, Technique and Application*, Springer, 1998

[4] .Kangarlu, A and Robitaille, P-ML Biological effects and health implications in magnetic resonance imaging, *Concepts in Magnetic Resonance*, **12**: 321–359, 2000

[5] Purves, GJ Ausustine, D, Fitzpatrick, LC Katz, A–S LaMantia, and JO McNamara. *Neuroscience*. Sinauer, Sunderland, Massachusetts, 1997

[6] Jeheson, P, Duboc, D, Lavergne, T, Guize, L, Guerin, F, Degeorges, M, and Syrota, A Change in human cardiac rhythm induced by a 2-T static magnetic field, *Radiology*, **166**, 227-230, 1988

[7] Keltner, JR, Roos, MS, Brakeman, PR, and Budinger, TF Magnetohydrodynamics of blood flow, *Magnetic Resonance in Medicine*, **16**(1), 139-149, 1990

[8] Dorfman, YG Physical phenomena occurring in live objects under the effect of constant magnetic fields. In Kholodov, YA (ed.), *Influence of Magnetic Field on Biological Objects*, Springfield, VA, National Technical Information Service, Appendix JPRS63038, 11-19, 1971

[9] Schenck, JF, Dumoulin, CL, Redington, RW, Kressel, HY, Elliott, RT, and McDougall, IL. Human exposure to a 4-tesla magnetic field in a whole-body scanner, *Med. Phys.*, **19**(4), 1089-1098, 1992

[10] Schaefer, DJ, Bourland, JD, and Nyenhuis, JA, Review of patient safety in time-varying gradient fields, *Jl. Mag. Res. Imag.*, **12**, 20-29, 2000

[11] Reilly, JP *Applied Bioelectricity: from Electrical Stimulation to Electropathology*, New York, Springer, 1998b

[12] The **I**nstitute of **E**lectrical and **E**lectronics **E**ngineers (IEEE), C95.6: Standard for Safety Levels with Respect to Human Exposure to Electromagnetic Fields (0–3 kHz), New York, 2002

[13] Knighton, RW An electrically evoked slow potential of the frog's retina, I: Properties of response, *J. Neurophysiol*., **38**, 185-197, 1975a

[14] Knighton, RW An electrically evoked slow potential of the frog's retina, II: Identification with PII component of electroretinogram, *J. Neurophysiol.*, **38**, 198-209, 1975b

[15] Bergeron, J, Hart, MR, Mallick, JA, and String, LH Strength-duration curve for human electro- and magnetophosphenes, Proc. Bioelectromagnetics Soc. Ann. Meet., Boston, 1995

[16] Budinger, TF, Cullander, C, and Bordow, R Switched magnetic field thresholds for the induction of magnetophosphenes, Proc. Ann. Meet., Soc. Mag. Res. Med., New York, p. 118, 1984

[17] Carstensen, EL Sensitivity of the human eye to power frequency electric fields, *IEEE Trans.Biomed. Eng.*, BME-**32** (8), 561-565, 1985

[18] Lovsund, P, Oberg, PA, Nilsson, SE, and Reuter, T Magnetophosphenes: A quantitative analysis of thresholds, *Med. Biol. Eng. Comput.*, **18**, 326-334, 1980a.

[19] Lovsund, P, Oberg, PA, and Nilsson, SE Magneto- and electrophosphenes: A comparative study, *Med. Biol. Eng. Comput.*, **18**, 758-764, 1980b

[20] Bawin, SM, Sheppard, AR, Mahoney, MD, and Adey, WR, Influences of sinusoidal electric fields on excitability in the rat hippocampal slice, *Brain Res.*, **323**, 227-237, 1984

[21] Bawin, SM, Sheppard, AR, Mahoney, MD, Abu-Assal, M., and Adey, WR Comparison between the effects of extra cellular direct and sinusoidal currents on the excitability in hippocampal slices, *Brain Res.*, **362**, 350-354, 1986

[22] Reilly, JP Safety considerations concerning the minimum threshold for magnetic excitation of the heart, *Med. Biol. Eng. Comput.*, **31**, 651-654, 1993

[23] **I**nternational **C**ommission on **N**on-**I**onizing **R**adiation **P**rotection (ICNIRP), Guidelines for limiting exposure to time varying electric, magnetic and electromagnetic fields (up to 300 GHz) *Health Phys.* **74**: 494–522, 1998

[24] Directive 2004/40/EC of the European Parliament and of the Council, *Official Journal of the European Union*, L **159**, 2004

[25] Tzirtzilakis, EE A mathematical model for blood flow in magnetic field, Physics of fluids, **17**, 1-15, 2005

[26] Dimbylow, PJ Current densities in a 2 mm resolution anatomically realistic model of the body induced by low frequency electric fields, *Physics in Medicine and Biology*, **45**: 1013-1022, 2000

[27] Dimbylow, PJ Development of the female voxel phantom, NAOMI, and its application to calculations of induced current densities and electric fields from applied low frequency magnetic and electric fields, *Physics in Medicine and Biology*, **50**: 1047-070, 2005

[28] ICRP 2002 Basic anatomical and physiological data for use in radiological protection: reference values *ICRP, Publication* 89

[29] Andreuccetti, D, Fossi R, and Petrucci, C Dielectric properties of body tissues, Applied Physics – Italian National Research Council (Florence, Italy), available at:

http://niremf.ifac.cnr.it/tissprop/htmlclie/htmlclie.htm#atsftag, 2002

[30] Gabriel C, Gabriel, S and Corthout, E The dielectric properties of biological tissues: 1. Literature survey *Physics in Medicine and Biology*, **41:** 2231–49, 1996

[31] Forbes, LK, Crozier, S, and Doddrell, DM Rapid computation of static fields produced by thick circular solenoids, *IEEE Transactions on Magnetics*, **33**, 4405–4410, 1997

[32] Liu, HW, Zhao, H, and Crozier, S On the Induced Electric Field Gradients in the Human Body for Magnetic Stimulation by Gradient Coils in MRI *IEEE Transactions on Biomedical Engineering*, **50** (7): 804-815, 2003

[33] Liu, F and Crozier, S Electromagnetic Fields inside a lossy, multilayered spherical head phantom excited by MRI coils, *Physics in Medicine and Biology*, **49**: 1835-1851, 2004

[34] Dawson, TW, Caputa, K, and Stuchly, M A Magnetic field exposures for UK live-line workers, *Physics in Medicine and Biology*, **47**: 995-1012, 2002

[35] Baraton, P and Hutzler, B Magnetically induced currents in the human body *International Electrotechnical Commission Technology Trend Assessment* (IEC), 1995

[36] Cheng, Yu-C N, Eagan, TP, Brown, RW, Shvartsman SM, and Thompson, MR Design of actively shielded main magnets: an improved functional method, *MAGMA*, **16**:57-67, 2003.

SECTION 2

NUMERICAL EVALUATION OF HEALTHCARE WORKERS EXPOSURES TO PULSED MAGNETIC FIELD GRADIENT COILS IN MRI

1.0 ABSTRACT

In modern magnetic resonance imaging (MRI), workers are frequently exposed to gradient-pulsed magnetic fields outside of the scanner, which induce electric fields/ current densities in tissue. It is suspected that the largest electric fields could be stimulated when the worker is standing close to the coil windings near the MRI scanner ends and that these fields may well be above the defined international standards. This study presents numerical investigations into the magnitudes and spatial distributions of induced *in situ* electric fields and associated current densities in tissue-equivalent, whole-body, male and female models of workers when standing close to the ends of three cylindrical gradient coils. Note that bending, twisting or other actions taken by healthcare workers, particularly around the patient bed are acknowledged to be important but were beyond the modelling scope of this study. The results should therefore be reads in this light. Actively shielded, symmetric transverse (x- and y-axis) and longitudinal (z-axis) gradient coils with normalized gradient field strength of 1 mT/m in the working volume, were considered in this work. The results are then scaled to commonly used gradient strengths. The numerical calculations of induced E-fields are based on an efficient, quasi-static finite-difference (QSFD) scheme. The objectives of this research are to evaluate several worst-case exposure scenarios. Presented data include calculated electric fields and current densities induced in selected tissues, as well as current densities averaged over $1\ cm^2$ areas normal to the current flow. The results have been compared to the most recent IEEE, ICNIRP and EU-Directive 2004/40/EC standards for magnetic and electric field exposure in controlled environments. The simulations indicate that it is possible to induce electric fields/ current densities above the current regulatory guidelines, especially when the body models are located very close to the gradient coils and when two or three gradient coils are switched simultaneously, as is often the case. Furthermore, it is estimated that both male and female workers should be at least approximately 1 m axially away from the gradient coil ends to bring the exposures within regulatory limits when maximum, currently taken to be 40mT/m, gradients are operational. Note that the gradient coil ends are normally inset from the end of the magnet itself and the degree of inset varies across different MRI platforms. The methodology presented in this paper can be extrapolated to other dynamic field strengths for the evaluation of the effects at various positions. It is hoped that these results will better inform the MRI community concerning compliant practices around MRI systems.

2.0 INTRODUCTION

Magnetic resonance technology employs a wide range of electromagnetic frequencies and field strength for rapid generation of high-resolution anatomical images [1]. These electromagnetic fields are known to interact with the living tissue in different ways and mechanisms causing potentially detrimental physiological effects. For instance, body motion through a strong static magnetic field can induce electric fields and associated current densities in the low-conducting tissues, causing uncomfortable sensations and various biological side effects [2]. During the operation of a transmission radio frequency (RF) coil, RF waves interact with living tissue, causing some thermal heating and possibly tissue/cell injury [3].

Magnetic field gradient coils are commonly switched at low frequencies of around 1 kHz or so, which can lead to depolarization of voltage sensitive ion-channels/ membranes and subsequent nerve excitation [4]. Studies have shown that patients who are situated inside an MRI bore and are subjected to time-varying magnetic fields can experience physiological reactions predominantly associated with the excitation of peripheral nerves of skin and subcutaneous fat [5-7]. Peripheral nervous stimulation (PNS) can range from harmless tingling feelings in the skin, to burning sensations and even pain. Pulsed gradient fields can bring about other types of biological interactions, as recent studies have shown [8-9]. Symptoms such as muscle twitching and spasms, headaches, changes in heart activity and vertigo have been reported. It seems that some of these reactions could be linked to the excitation of central nervous system (CNS) synapses, common to the tissues of brain, spinal cord, and retina of the eye. Occupationally exposed workers, when positioned or moving close to the end the scanner, as is common in several clinical scenarios, are similarly exposed. To date, however, there has not been an in depth study of the potential exposure to workers due to the pulsed field gradients of MRI.

The mechanism of unwelcome stimulation of peripheral and central nervous systems through pulsed gradient fields is an active area of research [4-11]. Several theoretical and experimental studies indicate that a long, straight nerve may be activated by the first spatial derivative of the component of the induced electric field [12]. For short or bent axons, however, the electric field appears to be more influential in the excitation process yielding a relatively low threshold of excitation [13]. The reported stimulation points on the body often, but not always, correlate well with the positions of large electric field magnitudes [1]. Faber *et al* [14] have investigated the relationship of PNS with different patient positions inside whole-body gradient coils and claim that the knowledge of the dependency of the stimulation threshold on patient positioning would make faster imaging possible at some significant body locations such as the head, heart and pelvis. In a numerical study, So and associates [15] have employed three tissue-equivalent human models to compute the electric fields in skin and subcutaneous fat of patients lying inside the MRI scanner while subject to different pulsed gradient coils. They were able to show that the stimulation thresholds during MRI imaging depends on the coil type, the coil position relative to the body, and on the resolution and anatomy of the human body model. Their results were in good agreement with those of Liu *et al* [16], who studied the induction of electric fields in a 4 mm heterogeneous human model due to pulsed y-gradient coils.

Regulatory agencies such as the IEEE and the ICNIRP have defined limits on the time-varying electric, magnetic and electromagnetic field exposures to the general public and in controlled environments. According to the IEEE standard [17], the *in situ* electric field stimulation thresholds for most CNS and PNS neurons are around 12.3 V/m and 6.15 V/m for exposure durations of 0.128 ms, respectively. However, heart and other tissues are limited to electric field exposures of 7.98 V/m and 0.86 V/m respectively, at a frequency of 1 kHz (for controlled environments). The ICNIRP guideline [18] and the Directive 2004/40/EC of the European Parliament and Council [19] on the other hand, state that the current density averaged over a $1\ cm^2$ surface must not exceed a threshold of $10\ mA/m^2$ - rms. in the head and trunk at a frequency of 1 kHz.

In these theoretical investigations, we have computed the electric fields and current densities induced in whole-body male and female models of workers near the entrance of longitudinal and transverse actively shielded symmetric gradient coils. The objectives of the research Reported here are to evaluate several worst-case exposure scenarios and to estimate the axial distance from the coil end where the maximum induced current densities are below the defined safety limits. Various measures of electric field and $1\ cm^2$ - averaged current densities are reporteded for the tissues of CNS, heart, muscle, skin and fat and the results are compared to

international thresholds. It is hoped that this study will help in the evaluation of the regulatory compliance involved with workers and patients when standing close to the ends of gradient coil systems.

3.0 MATERIALS AND METHODS

3.1 Human body models

According to ICRP 89 guidelines for the reference male and female human [20], the anatomically accurate, whole-body voxel phantoms NORMAN (1.75*m*, 73*kg*) and NAOMI (1.65*m*, 58*kg*) [21-22] were used in this research study to numerically model the workers standing near the MRI gradient coils. The number of voxels in x, y and z-dimension for the male body model were 277x148x871, while the horizontal and vertical voxel dimensions were *2.021 mm* and *2.077 mm*, respectively. The female model had 294x124x791 cells along the Cartesian dimensions with horizontal and vertical voxel sizes of *1.948 mm* and *2.061 mm*. The recently measured conductivity values [23-24] of some forty body-identified tissue types were appropriately scaled to the frequency of interest and assigned to the appropriate body voxels.

Due to the large computational burden associated with the simulations involved, the models were initially decreased in resolution to about *8 mm.* These lower resolution body models were then employed first to efficiently estimate the locations around the gradient coils where largest electric fields and current densities are induced in the phantoms, after which the high-resolution body models were engaged for more detailed field evaluations at the determined spatial positions. The low-resolution male and female body models had 70x37x218 and 74x31x198 voxels along the Cartesian coordinates, respectively. The conductivities of the downscaled cells in the low-resolution models were taken as the volume average of the component voxels.

3.2 Gradient coils

Longitudinal (z-axis) and transverse (x- and y-axis) actively-shielded, whole-body, symmetric gradient coils are engaged in this investigation to compute the electric fields and current densities induced in the described body models during gradient switching. It is assumed throughout all computations that each coil generates normalized gradient field strength of 1 mT/m in the working volume. In that way the simulations results can be linearly extrapolated to field strengths of interest with ease. In order to evaluate the induced fields due to each gradient individually under similar conditions, all three gradient coils have been designed to have approximately same axial length of ~ 1.4 m, yet to remain radially separated, i.e. the six coil layers (primary and secondary) are allocated to different radii assuming a layer thickness (including former, etc) of 5 mm. The axial length of ~ 1.4 m has been chosen so that the gradient coils would fit inside most conventional 1.5T MRI magnets (see for example [32]) (or larger scanners) and yet be able to provide maximum (i.e. worst-case) exposure to the worker. Table 1 lists some important parameters while figure 1 (first column) illustrates the geometries of the three gradient coils. We note that the distance from the end of the gradient coil set to the end of the magnet varies between MRI systems and, for cylindrical systems, is typically smallest in short 1.5T magnets and larger in higher field systems. We therefore use the end of the gradient set as a reference point for model positioning.

Table I
Geometrical properties of gradient coils

PARAMETER	X-gradient	Y-gradient	Z-gradient
1st layer - Z [m]	1.18	1.20	1.29
2nd layer - Z [m]	1.37	1.40	1.40
1st layer - R [m]	0.31	0.32	0.33
2nd layer - R [m]	0.36	0.37	0.39
DSV: r [m] x z [m]	0.42 x 0.42	0.42 x 0.42	0.50 x 0.56

Note: Z denotes axial length and **R** denotes the radius of the primary and secondary gradient coil layers. The DSV size is given as the region where the gradient field is uniform to 5% peak-peak and is expressed as diameter by length in meters.

It is also assumed that the gradient coil current is pulsed trapezoidally at the frequency of 1 kHz and 100 μs rise-time. Harmonic analysis of the trapezoidal excitation has been performed assuming Fourier integration via the following equation:

$$F(t) = \sum_{n=1}^{\infty} \underbrace{\frac{4A\sin((2n-1)w\tau)}{(2n-1)^2 w\pi\tau}}_{C_n} \sin((2n-1)wt)$$

where A is the amplitude of the gradient coil current in [Amps], t is transient time in [s], τ is rise-time in [s], w is the angular frequency in [rad/s] and n is the order of the Fourier harmonic. Based on this decomposition, the induced electromagnetic fields are calculated at each frequency and summed accordingly. At least $n = 7$ Fourier harmonics have been employed in the synthesis of the trapezoidal gradient waveform.

3.3 The computational method

In the time-harmonic analysis, the total electric field inside the body model can be split into primary field E_1 and secondary field E_2, according to [16]:

$$\vec{E} = \vec{E}_1 + \vec{E}_2 \tag{1}$$

$$\vec{E}_1 = -\frac{\partial \vec{A}}{\partial t} = -w\vec{A} = 2\pi f\vec{A} \tag{2}$$

$$\vec{E}_2 = -\nabla\Phi = \left(\frac{\partial}{\partial x}\hat{x} + \frac{\partial}{\partial y}\hat{y} + \frac{\partial}{\partial z}\hat{z}\right)\Phi \tag{3}$$

Here, $\vec{A}$ denotes the vector magnetic potential due to the source, Φ is the scalar electric potential, ∇ is the gradient operator and f is the frequency of the Fourier component. The primary electric field $\vec{E}_1$ causes a flow of current $\vec{J}_1 = \sigma\vec{E}_1$ in a conductive sample with the conductivity σ. Any conductivity differences along the path of the current, including the air-tissue interfaces cause non-uniformity of accumulating electric charges, giving rise to scalar potential Φ, the negative gradient of which is the secondary field $\vec{E}_2$, which causes a flow of current $\vec{J}_2 = \sigma\vec{E}_2$.

The vector potential $\vec{A}$ can be evaluated using the Biot-Savart's method in Cartesian coordinates within the body and boundary air region:

$$A(r') = \frac{\mu}{4\pi}\iiint \frac{J_0(r)}{|r'-r|} d^3 r \qquad (4)$$

where μ is magnetic permeability of the air; r is the position vector of the gradient coil wire segment, r' is the position vector of the field point and J_0 is the current flowing in the wire segment. Once the vector potential is obtained, the primary electric field can be deduced from (2).

However, the computation of the scalar electric potential and thus the secondary electric field is performed with the previously developed quasi-static finite-difference (QSFD) scheme, full details can be found in [16, 25]. The complete computational method outlined herein has been verified against other known solutions and the full validation details are given in [26]. The total *in situ* electric field is then obtained based on relationship (1), whereby the current density is related to the total electric field by multiplying by tissue conductivity. The entire computational scheme was coded in C.

3.4 Evaluation of E-fields/currents induced in the body models

This section describes the general methodology used in deriving the electric fields and current densities induced in the body models during pulsing of gradient coils. It is assumed that all three gradient coils are positioned 1.15 m above ground relative to their central cylinder axis (z = 0 m), as this is the vertical elevation common to most clinical MRI scanners. The minimum distance between the phantom surface and the edge of the gradient coil end was assumed to be 10 mm for all simulations, i.e. the body model is not allowed to physically touch/coincide with the gradient coils, as this could unrealistically induce numerical singularities in evaluated *in situ* field results. Naturally, in many situations, the distances will be considerably greater than this and a variety of distance are modeled.

All three gradient coils are symmetric and therefore create same magnetic field profiles and strengths at both ends of the coil. In addition, the walls of the cryostat vessel and companion thermal radiation shields, shield the superconducting magnets inside the helium tank by attenuating the residual fields of the pulsed gradients in the radial direction. Therefore the gradient fields to the sides of the MRI scanner are expected to be quite small in magnitude. The magnetic fields generated by the three gradients near the coil end represent the major risk areas due to worker access. In all simulations the voxel phantoms are positioned so that they are facing the gradient coil end of interest. Both the male and female phantoms are assumed stationary for the purposes of these studies.

1. Region scanning computations at low model resolution

To determine the positions in front of the gradient coil(s) where peak current densities are induced in the body model, it is necessary to perform computations at numerous locations of the phantom around the coil(s) of interest. Due to the large computational burden associated with the use of high-resolution models (~2 mm) during the region probing operation, we have employed male and female body models as the low-resolution first to register the peak values at various positions in front of the gradient coils, after which a more detailed simulation at the position of interest was performed at the higher resolution.

The typical scan area is assumed to be: $r = -1 \sim 1.m$, $z = 0.71 \sim 2.5m$ relative to the diameter spherical volume (DSV) center. The phantoms are then positioned in this region at spatial

increments of 0.2 m both radially and axially and the fields induced in the low-resolution body models are evaluated. Finer radial increments were employed very close to the coil to estimate the location of worst-case magnetic field exposure more precisely.

Akin to other voxel-based model, the body geometries of NORMAN and NAOMI contain sharp corners and edges, especially near the armpits and in the groin region where the legs meet. In addition, large contrasts in conductivity can exist between neighbouring cells and where isolated voxels appear embedded inside another tissue. Numerical singularities can be introduced at these body locations leading to unrealistically large induced in situ electric field magnitudes. In the presence of such numerical staircase errors, Dawson and authors [27] have proposed 1-percentile thresholds (limits exceeded in only 1% of tissue voxels) that serve, to a degree, as a more satisfactory estimate of maximum field levels. Hence, for every position near the coil end, the 1% - thresholded total electric field and current density are evaluated. This can effectively remove any statistically insignificant numerical errors and singularities. The final results of these simulations are presented as field plots (around the gradient coils) of peak 1% - thresholded electric field and eddy current densities induced in the body.

2. Detailed field evaluations at high model resolution

Once the position of peak electric field/ current density is determined during the region scan, we perform a detailed field computation with the high-resolution body models. A host of numerical studies suggests that there is a notable influence of voxel size on the evaluated maximum *in situ* electric field and current density [21, 28-30]. For instance, as the cell size decreases, the maximum value of current density increases. One explanation is that the averaging of conductivity in rescaled cells of lower resolution models and the associated masking of high-conductivity voxels decreases with smaller voxel size. Also, the geometrical indentations in the apex of armpits and top of the legs, where tissue-air and air-tissue boundaries with large conductivity contrasts meet in a small localized space, can lead to tightening of 'current lines' and thus to an unrealistically large induced electric field/ current density. It is therefore common to average the current density over a finite area. In fact, the ICNIRP guidelines [18] state that the perpendicular current density components should be averaged over a square with $1\ cm$ edges centred on the voxel and parallel to the three principal Cartesian planes. The averaging of current density at the interfaces between two dissimilar tissue types is not always straightforward and has attracted some debate [27]. One way to average over the defined area of $1\ cm^2$ is to account for the current densities induced in the neighbouring voxels of the dissimilar tissue type, which predominantly leads to overestimates in the averaged current density depending on the nature of the adjacent tissues. The other averaging algorithm works on the same principle, whereby it zero-weights the contribution of current densities in neighbouring voxels of dissimilar tissue type, thus always leading to underestimates in averaged results.

Since in this investigation we are interested in worst-case exposure scenarios, the contingencies introduced by overestimates are favourable and so the former algorithm that takes into account the currents flowing in adjacent dissimilar tissues has been engaged in the averaging of tissue-specific current densities induced in the high-resolution body model. The final results of these high-resolution simulations are presented in terms of electric field and eddy current distributions in the male and female voxel phantoms. Tables and graphs are used to detail the maximum and average tissue-specific electric fields/ current densities and peak $1\ cm^2$ averaged current densities, predominantly in tissues of the CNS, heart, muscle, skin and subcutaneous fat.

3.5 Estimation of 'safe distance' from gradient coils

The purpose of this series of simulations is to estimate the distance away from the gradient set at which the induced $1\ cm^2$ averaged current densities in significant tissues are below the ICNIRP standard of $10\ mAm^{-2}$ - rms. Both the male and female high-resolution body models were

positioned at intervals of 0.3 m axially away from the coil end of interest, while standing and facing the gradient coil that is aligned with the z-axis. A total of five simulations were performed for each gradient coil individually and for the combination of all three coils, and the electric field and current densities were recorded for all tissues. The results of these simulations are illustrated as graphs of $1\ cm^2$ averaged current densities in tissues of CNS, heart, muscle, skin and fat.

4.0 RESULTS AND DISCUSSION

4.1 Gradient coil magnetic field profiles

Figure 1 (second and third column) illustrates the total magnetic flux density profiles generated by the three cylindrical gradient coils. From the field distributions we note a rapid spatial drop in the magnetic flux at the coil ends, which implies that these are the most likely positions to induce substantial fields in the body. The shielding performances of the secondary coils are good, i.e. the fields drop off rapidly with distance away from the coil and are minimal at the first eddy current source (inner wall of the cryostat).

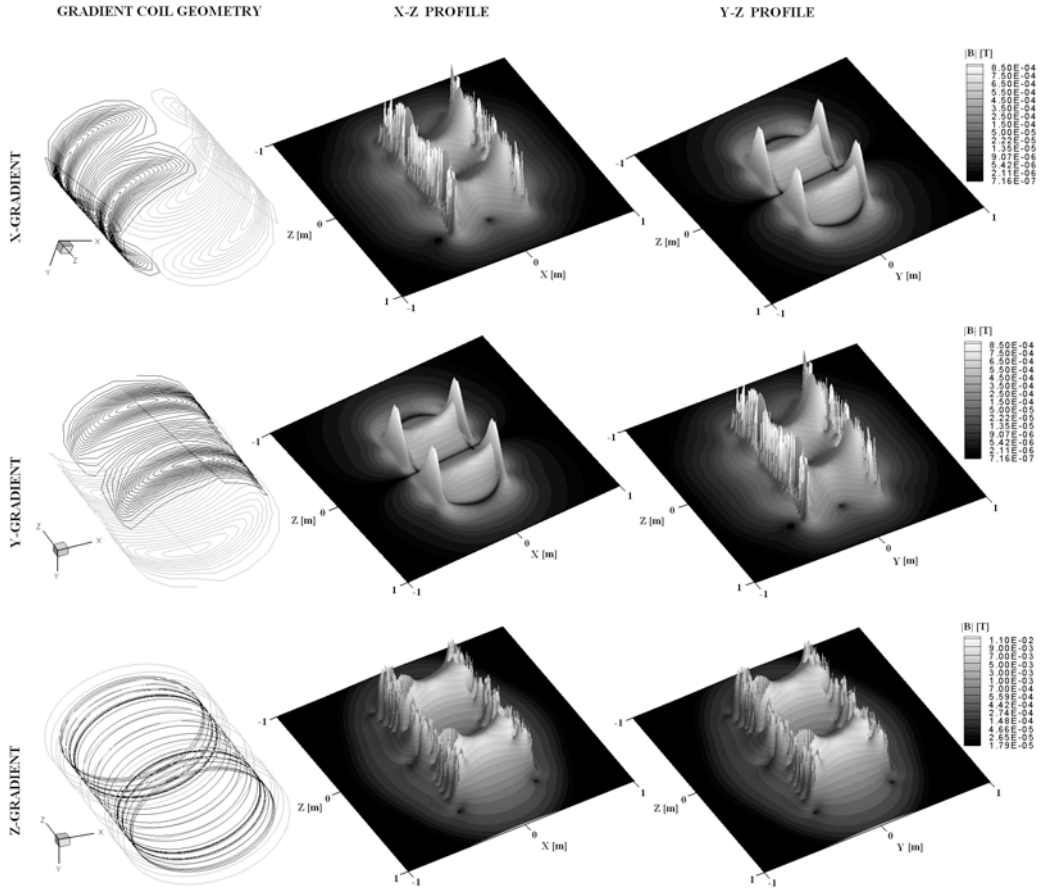

Figure 1 Left column: three-dimensional plot of transverse and longitudinal gradient coil geometry (for transverse coils only one primary and one secondary layer is illustrated, while all coil loops are plotted for the longitudinal gradient coil). The primary and secondary windings are indicated in black and grey respectively. Middle and right column: x-z and y-z profiles of the total magnetic flux density generated by the three gradient coils.

4.2 Induced electric field and current densities

1. Region scanning computations at low model resolution

Here, the lower resolution body models are engaged first to estimate the location(s) in front of the three gradient coils of recorded maximum and peak 1%-thresholded current density and electric field induced in the male and female voxel phantoms. Figure 2 illustrates a sketch of the typical position and orientation of the body model outside the gradient coil. This is a worst case scenario.

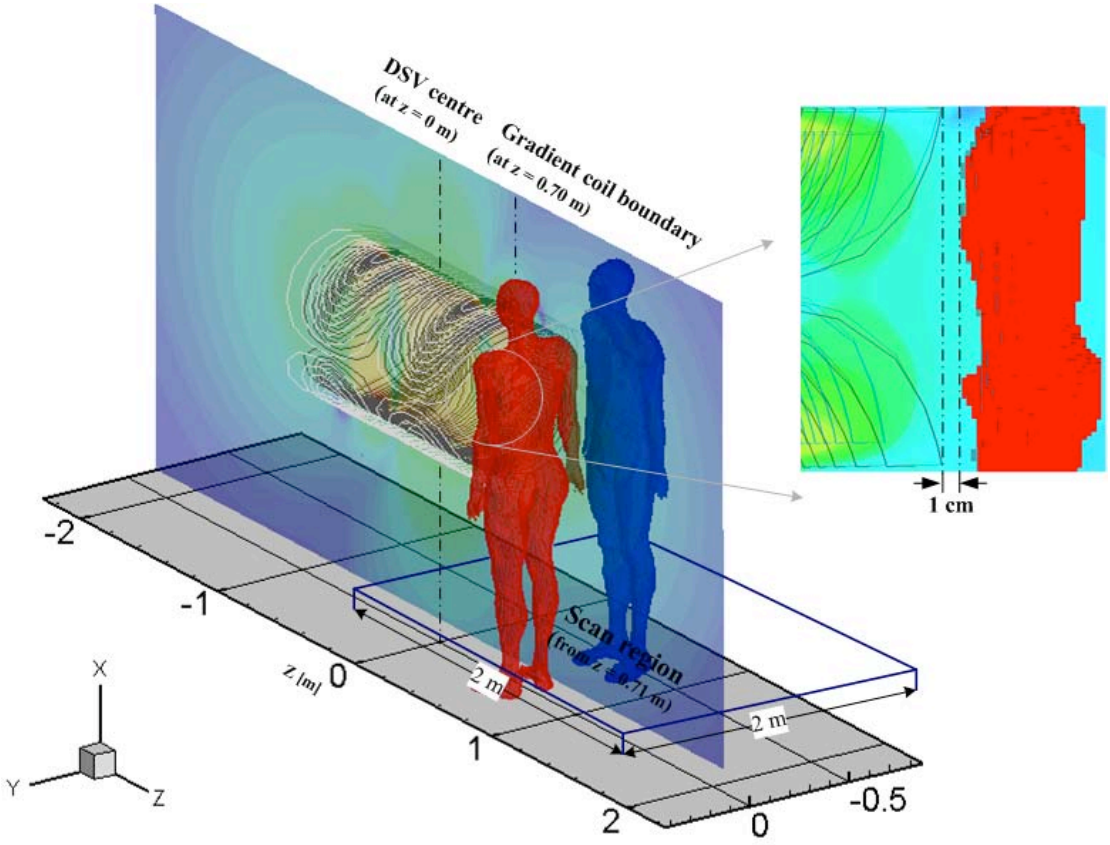

Figure 2 Sketch of the male body model in a typical upright standing position and orientation near the x-gradient coil end and (in blue) rotated to be beside a patient bed.

.

The low-resolution region scans converge on average in about 4,000 iterations and the typical computation time for one scan is around 3 hours on a dual Intel Xeon 3.6GHz, 4GB RAM PC workstation. Figure 3 illustrates the scan profiles (in front of coil) of recorded maximum and 1%-thresholded electric field induced somewhere in the male voxel phantom during switching of x, y and z-gradient coils, as well as the combination of all three gradients. The corresponding current density region scans are illustrated in Figure 4.

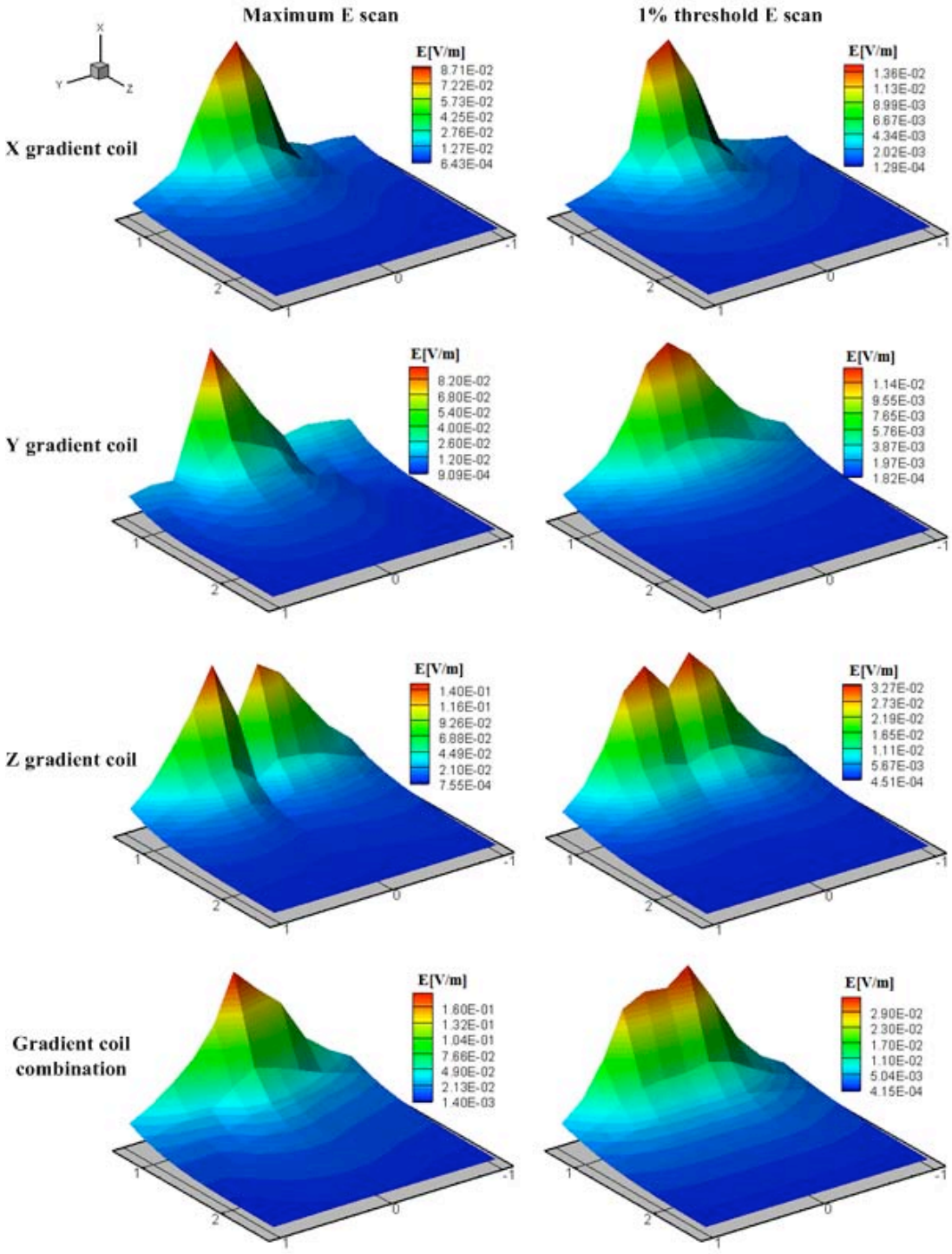

Figure 3 Records of maximum (left column) and 1%-thresholded (right column) electric fields induced somewhere in Norman versus spatial position around the three gradient coils when considered individually (first three rows) and for the combination of all three gradient coils (last row). All dimensions are in metres

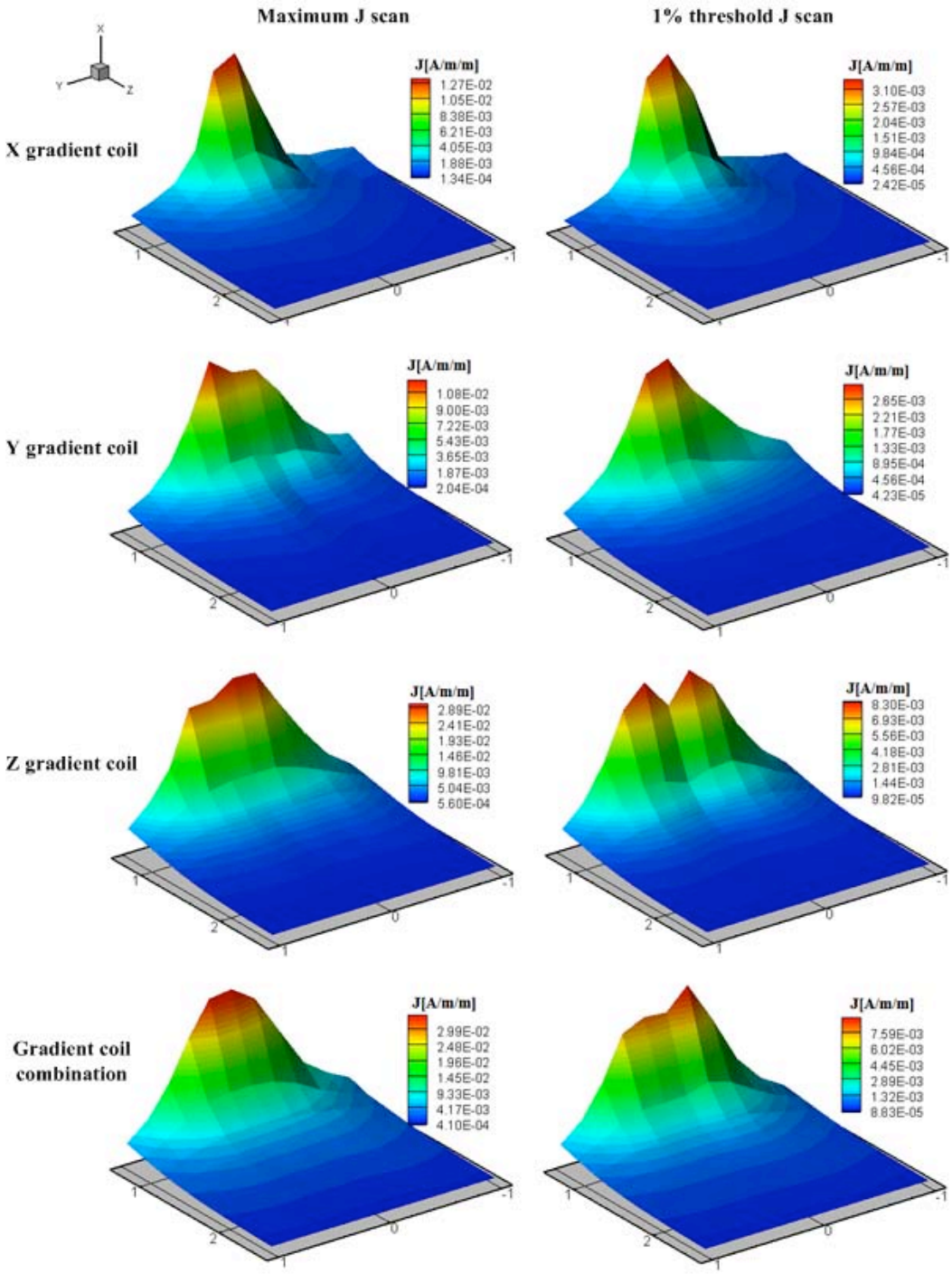

Figure 4 Records of maximum (left column) and 1%-thresholded (right column) current density induced somewhere in Norman versus spatial position around the three gradient coils when considered individually (first three rows) and for the combination of all three gradient coils (last row). All dimensions are in metres.

Figures 5 and 6 show the scan profiles for the female body model analogous to figures 3 and 4, respectively. From these results we note that, in case of the transverse gradient coils, the largest induced fields appear in the central region of the coil entrance. However, for the z-gradient coil,

the largest induced fields are close to the coil edges as two distinct peaks in E and J for z-coil are evident at ~r = 0.2 m.

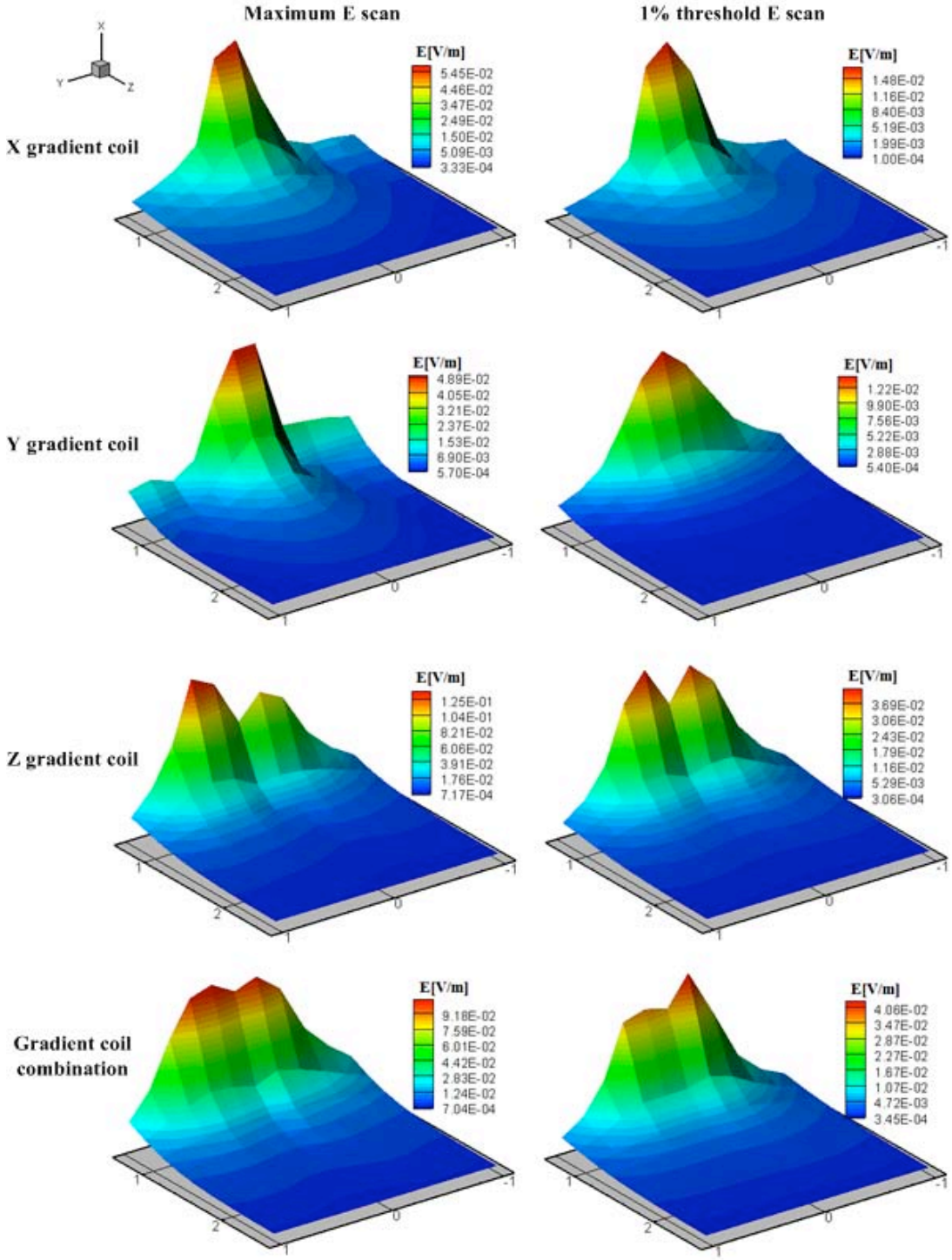

Figure 5 Records of maximum (left column) and 1%-thresholded (right column) electric fields induced somewhere in Naomi versus spatial position around the three gradient coils when considered individually (first three rows) and for the combination of all three gradient coils (last row). All dimensions are in metres.

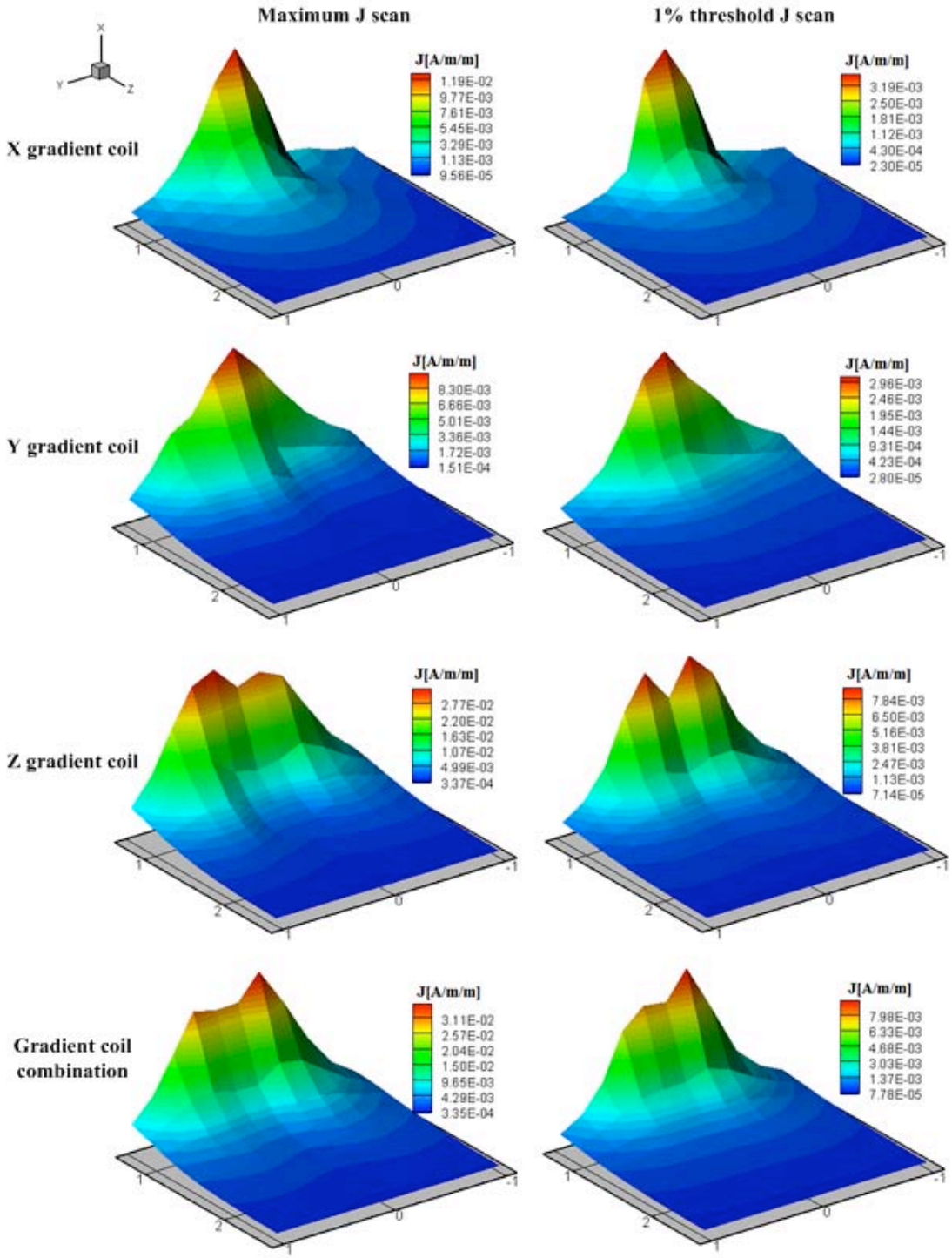

Figure 6 Records of maximum (left column) and 1%-thresholded (right column) current density induced somewhere in Naomi versus spatial position around the three gradient coils when considered individually (first three rows) and for the combination of all three gradient coils (last row).

Figure 7 illustrates the particular locations of the recorded peak 1%-thresholded electric fields and current densities for the three gradient coils near the coil end.

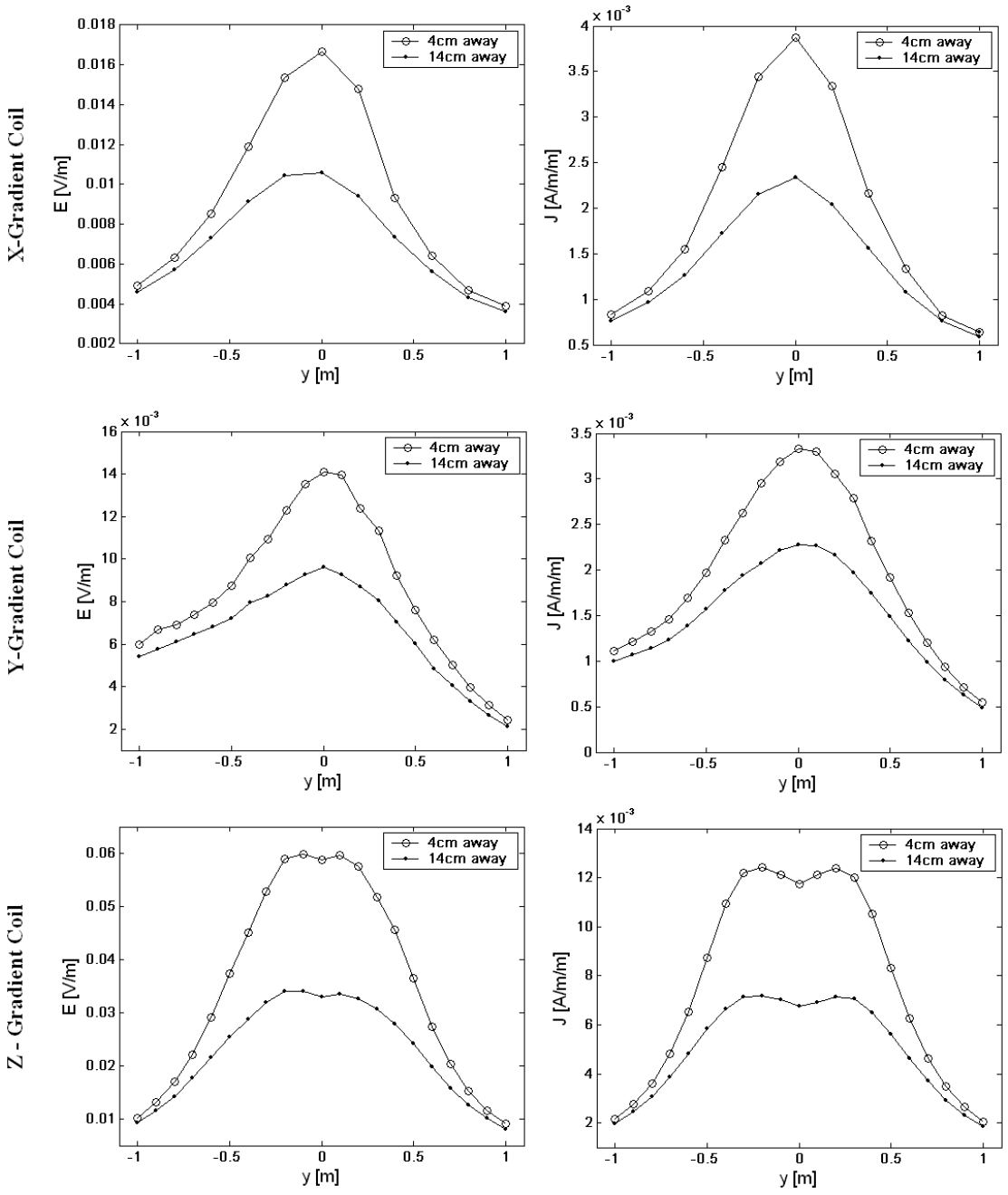

Figure 7 Peak 1% thresholded electric field (left column) and current density (right column) in male recorded at 40mm and 140mm axial distances away from the coil along the y-direction (body positioning) for the x (top row), y (middle row) and z (bottom row) gradient coil. The field lines are extracted from figures 3-5 and show the peak field spatial occurrences more clearly.

It is also noteworthy to observe that the z-gradient coil could potentially induce larger electric fields and current densities (by a factor of ~ 2) in both male and female workers than either of the two transverse gradient coils used in this study. This is different from patient exposure; when patients are positioned inside the MRI machine, typically the y-gradient will induce larger fields/currents in the patient [16]. This is probably due to clustering of loops close to the coil ends common to the z-gradients, whereby this superimposition of current sources might potentially increase the level of magnetic field exposure to the worker, who is standing close to one end of that z-gradient coil. The other explanation is that the z-gradient currents are generating magnetic flux gradients spatially different from the transverse gradients near the coil ends. Furthermore, when all three gradient coils are considered in a combination (i.e. operated simultaneously), the resulting exposure on the body is larger than if each gradient coil is switched independently (figures 3-6, last row). We note, however, that the maximum levels of electric field and current densities illustrated in figures 3-6 for each coil alone do not always add constructively and linearly to produce the combined effect. In fact, the induced field results suggest that the magnetic fields produced by each coil separately can add destructively in certain locations when all three coils are operated simultaneously. All Cartesian field components are necessarily included in the simulations, not simply those that provide spatial location in MRI (the B_z derivatives).

According to Figures 3-6, the fields induced in the female body model are on average larger than the fields induced in the male. This is most probably due to the dissimilar anatomy of the two models. Finally, Table 2 lists the worst-case exposure locations and the maximum induced electric field and current density levels, when the subject is standing in front of all three gradient coils.

Table 2

Maximum and average $1\ cm^2$ - averaged current densities in selected tissues of Norman at various axial distances from the ends of longitudinal and transverse gradient coils in $[mA/m^2]$

Body Positions Y = 0 [m]	TISSUE	X gradient		Y gradient		Z gradient		X+Y+Z	
		Avg	Max	Avg	Max	Avg	Max	Avg	Max
Z = 0.01 [m]	**CSF**	1.12	5.20	1.14	6.85	3.39	16.77	4.87	22.15
	Brain	0.25	2.94	0.11	1.23	0.57	6.91	0.85	10.20
	Spine	0.62	3.44	1.10	6.19	2.60	14.99	3.57	20.37
	Retina	0.47	1.33	0.17	0.39	1.24	3.35	1.64	4.68
	Heart	0.87	4.68	0.82	3.12	2.43	11.61	3.29	14.22
	Skin	0.08	2.68	0.07	3.02	0.18	6.11	0.24	8.43
	Fat	0.28	6.96	0.27	3.82	0.59	15.08	0.78	20.62
	Muscle	0.85	5.55	0.79	5.92	1.83	13.86	2.55	18.06
Z = 0.31 [m]	**CSF**	0.37	1.94	0.34	1.38	0.99	5.00	1.41	6.11
	Brain	0.10	1.16	0.08	1.05	0.17	2.23	0.27	3.38
	Spine	0.15	0.83	0.22	1.28	0.76	4.39	0.95	5.50
	Retina	0.18	0.52	0.18	0.46	0.34	0.79	0.45	1.04
	Heart	0.22	1.03	0.15	0.63	0.53	2.38	0.74	3.15
	Skin	0.02	0.54	0.02	0.60	0.05	1.30	0.06	1.94
	Fat	0.08	1.56	0.07	1.00	0.16	3.42	0.20	4.64
	Muscle	0.23	1.30	0.19	1.29	0.49	2.91	0.65	4.05
Z = 0.61 [m]	**CSF**	0.15	0.83	0.13	0.44	0.39	2.00	0.55	2.30
	Brain	0.04	0.51	0.04	0.48	0.07	0.92	0.12	1.48
	Spine	0.05	0.30	0.06	0.38	0.30	1.76	0.36	2.05
	Retina	0.08	0.21	0.08	0.19	0.15	0.36	0.20	0.52
	Heart	0.08	0.35	0.04	0.19	0.18	0.85	0.25	1.04
	Skin	0.01	0.17	0.01	0.21	0.02	0.47	0.02	0.67
	Fat	0.03	0.52	0.03	0.37	0.06	1.18	0.08	1.58
	Muscle	0.09	0.50	0.07	0.52	0.20	1.04	0.25	1.34
Z = 0.91 [m]	**CSF**	0.07	0.39	0.05	0.21	0.19	0.95	0.26	1.06
	Brain	0.02	0.25	0.02	0.21	0.04	0.43	0.06	0.72
	Spine	0.02	0.14	0.03	0.15	0.14	0.84	0.17	0.94
	Retina	0.04	0.09	0.03	0.08	0.08	0.21	0.11	0.29
	Heart	0.04	0.16	0.02	0.07	0.08	0.41	0.11	0.44
	Skin	0.01	0.08	0.01	0.10	0.01	0.21	0.01	0.30
	Fat	0.01	0.23	0.01	0.18	0.03	0.52	0.04	0.69
	Muscle	0.04	0.23	0.03	0.25	0.09	0.48	0.11	0.60
Z = 1.21 [m]	**CSF**	0.04	0.20	0.03	0.11	0.11	0.51	0.14	0.56
	Brain	0.01	0.13	0.01	0.10	0.02	0.23	0.03	0.39
	Spine	0.01	0.07	0.01	0.08	0.08	0.45	0.09	0.49
	Retina	0.02	0.04	0.01	0.03	0.05	0.12	0.07	0.17
	Heart	0.02	0.08	0.01	0.03	0.04	0.22	0.06	0.22
	Skin	0.01	0.05	0.01	0.05	0.01	0.12	0.01	0.15
	Fat	0.01	0.12	0.01	0.10	0.02	0.26	0.02	0.35
	Muscle	0.02	0.14	0.02	0.14	0.05	0.27	0.06	0.33

2. Detailed field evaluations at high model resolution

Based on the worst-case positions listed in Table 2, (i.e. the positions with largest recorded peak 1%-thresholded current density), the high-resolution body models were employed to calculate the tissue-specific electric fields and current densities. On the previously described computer platform, the high-resolution simulations converge in about 300,000 iterations and consume approximately 1.9GB RAM/50h CPU-time and 1.55GB RAM/45h CPU-time for the male and female phantom studies respectively. By parallelising the problem, however, we were able to speed up the computational process by factors of around 5-6. Figures 8 and 9 illustrate the

electric field and current density profiles in coronal, sagittal and axial views of male and female respectively, for different gradient coil field exposures. Body regions of large and small field magnitudes are illustrated in colour gradation from red to blue respectively. From Faraday's law, it follows that the largest values of circumferentially induced electric field normal to the direction of applied magnetic field will localize in the outermost body surfaces. Since the body models are inhomogeneous in conductivity distribution due to different tissues, current flow will be modified by the boundary conditions at these tissue interfaces. Therefore, high values of induced electric field are notable on the front and lower back surfaces of the trunk (figures 8 and 9, sagittal views) with low electric field values in the middle of the body. It follows that the induction of electric fields in the heart (located close to the middle of the torso) compared to other tissues close to the body surface are reasonably small. On the other hand, the peripheral nerves in the skin and subcutaneous fat of the frontal and rear end torso are exposed to strongest electric fields. As the current density relates to the electric field by multiplying by tissue conductivity, high values of current density occur when high values of conductivity combine with enhanced electric field values such as in the muscle, cerebral spinal fluid and reproductive organs.

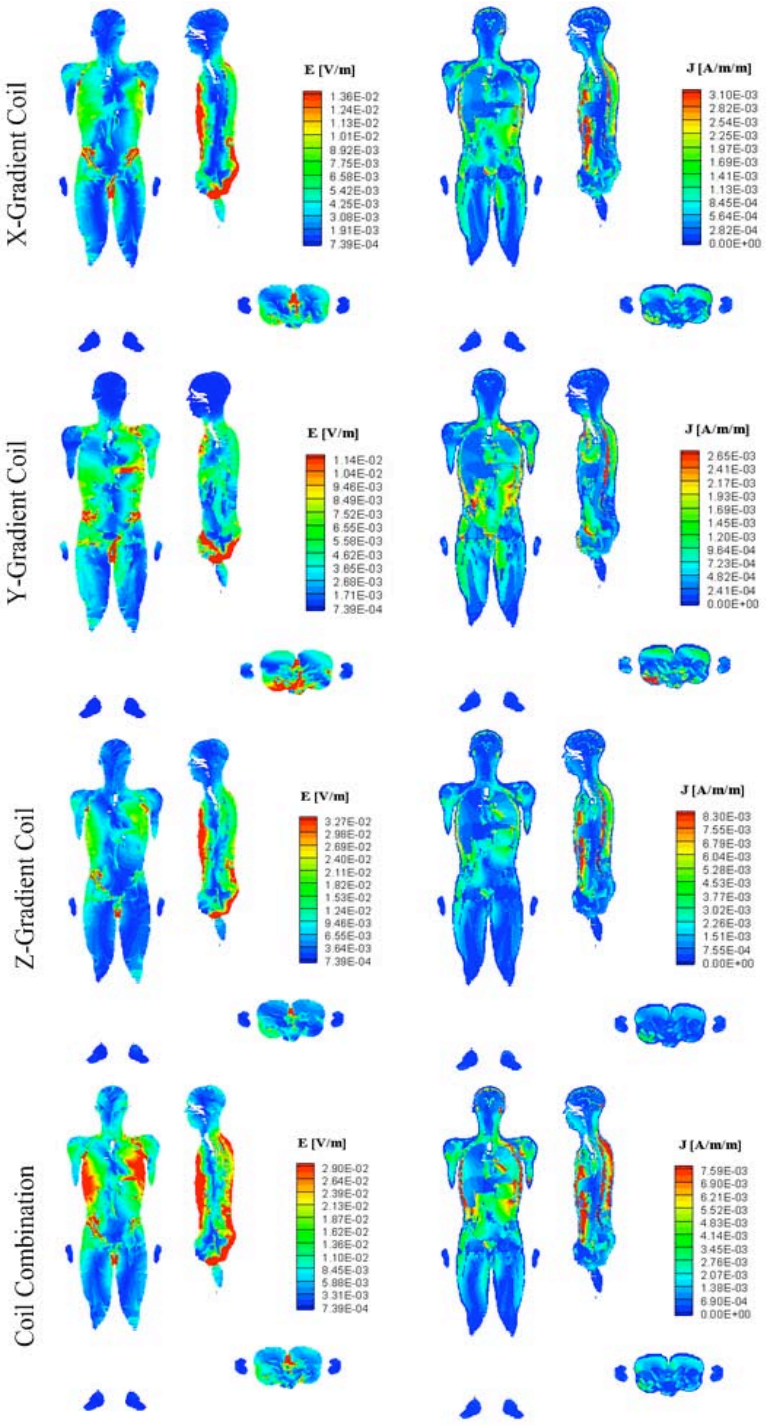

Figure 8 High-resolution coronal, sagittal and axial electric field (left column) and current density (right column) distributions in the male voxel phantom for different gradient field exposures

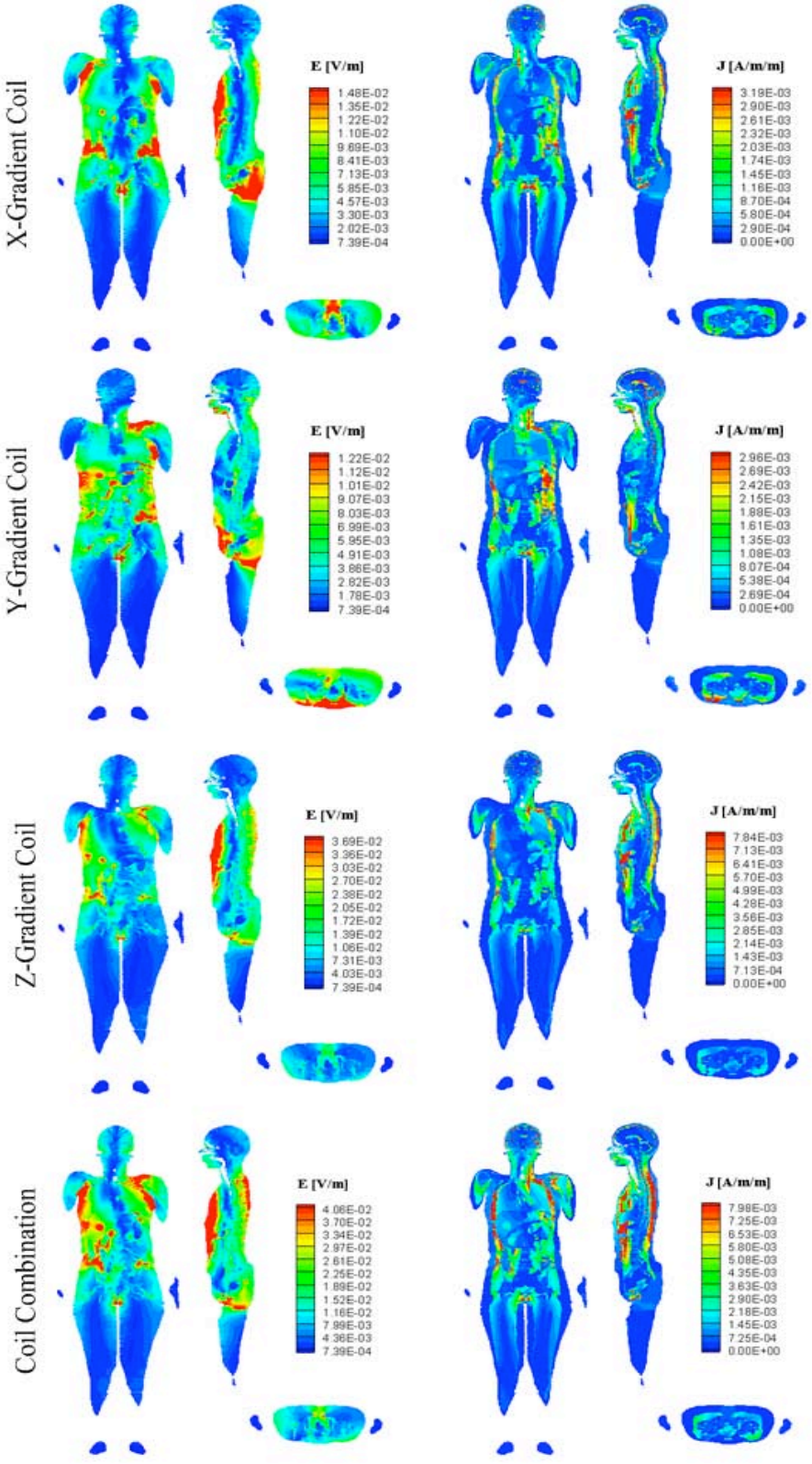

Figure 9 High-resolution coronal, sagittal and axial electric field (left column) and current density (right column) distributions in the female voxel phantom for different gradient field exposures

Table 2 lists the average and maximum $1\ cm^2$ averaged current densities in the tissues of CNS, heart, muscle, skin and fat for the male voxel phantom due to each gradient coil and their combined effect for various locations in front of the coils. The corresponding electric field results are detailed in Table 3.

Table 3

Maximum and average electric fields in selected tissues of Norman at various axial distances from the ends of longitudinal and transverse gradient coils in [mV/m]

Body Positions Y = 0 [m]	**TISSUE**	**X gradient**		**Y gradient**		**Z gradient**		**X + Y + Z**	
		Avg	**Max**	**Avg**	**Max**	**Avg**	**Max**	**Avg**	**Max**
Z = 0.01 [m]	**CSF**	1.12	8.89	1.07	8.99	3.36	27.13	4.81	37.47
	Brain	1.59	7.64	0.74	3.16	3.60	16.26	5.36	23.02
	Spine	2.59	13.18	3.61	12.93	8.72	39.89	12.20	55.34
	Retina	0.89	2.98	0.32	0.93	2.42	8.55	3.19	11.59
	Heart	5.94	20.39	5.52	18.26	16.89	67.38	22.65	77.42
	Skin	3.86	166.53	3.44	118.17	8.27	250.10	11.22	358.85
	Fat	5.16	104.43	4.91	76.58	10.31	141.43	13.48	217.48
	Muscle	2.99	64.26	2.77	47.53	6.47	99.87	9.00	131.42
Z = 0.31 [m]	**CSF**	0.37	2.99	0.35	1.89	0.97	7.50	1.39	9.79
	Brain	0.62	2.89	0.52	2.31	1.07	4.98	1.71	7.38
	Spine	0.65	3.00	0.76	2.47	2.36	10.94	3.10	14.38
	Retina	0.35	1.27	0.35	1.15	0.68	2.17	0.88	3.05
	Heart	1.54	5.35	1.02	3.73	3.63	13.97	5.14	17.92
	Skin	1.09	38.45	0.91	35.00	2.28	58.66	2.96	90.72
	Fat	1.41	23.26	1.22	22.81	2.82	44.84	3.50	51.72
	Muscle	0.81	14.23	0.68	14.11	1.74	27.27	2.29	31.66
Z = 0.61 [m]	**CSF**	0.15	1.22	0.13	0.76	0.38	2.86	0.55	3.57
	Brain	0.26	1.15	0.22	1.01	0.43	1.75	0.72	3.29
	Spine	0.23	0.98	0.24	0.72	0.90	4.15	1.13	5.23
	Retina	0.15	0.54	0.15	0.50	0.29	1.28	0.40	1.80
	Heart	0.55	1.90	0.30	1.11	1.24	4.69	1.75	5.98
	Skin	0.43	12.43	0.35	14.31	0.90	18.20	1.13	30.24
	Fat	0.55	7.58	0.46	9.33	1.11	17.97	1.35	21.45
	Muscle	0.31	4.42	0.25	5.77	0.69	10.91	0.86	13.10
Z = 0.91 [m]	**CSF**	0.07	0.56	0.06	0.36	0.19	1.32	0.26	1.61
	Brain	0.12	0.57	0.10	0.45	0.23	0.93	0.36	1.69
	Spine	0.10	0.47	0.10	0.37	0.43	1.91	0.51	2.36
	Retina	0.07	0.24	0.06	0.20	0.16	0.71	0.22	0.98
	Heart	0.25	0.84	0.11	0.40	0.54	1.99	0.76	2.53
	Skin	0.21	4.97	0.17	6.96	0.43	6.99	0.53	12.52
	Fat	0.27	3.51	0.22	4.53	0.53	8.46	0.63	10.30
	Muscle	0.15	1.70	0.12	2.80	0.33	5.13	0.40	6.28
Z = 1.21 [m]	**CSF**	0.04	0.28	0.03	0.19	0.11	0.27	0.14	0.84
	Brain	0.06	0.30	0.05	0.22	0.13	0.58	0.20	0.93
	Spine	0.05	0.25	0.05	0.21	0.23	1.00	0.27	1.22
	Retina	0.04	0.12	0.02	0.08	0.10	0.40	0.13	0.56
	Heart	0.13	0.45	0.05	0.16	0.28	0.99	0.38	1.26
	Skin	0.12	2.61	0.09	3.80	0.23	3.29	0.28	6.04
	Fat	0.15	1.87	0.13	2.47	0.29	4.48	0.34	5.51
	Muscle	0.08	0.89	0.07	1.53	0.18	2.71	0.21	3.36

Analogous to Tables 2 and 3, Table 4 and 5 list results for the female body model.

Table 4

Maximum and average $1\ cm^2$ - averaged current densities in selected tissues of Naomi at various axial distances from the ends of longitudinal and transverse gradient coils in $[mA/m^2]$

Body Positions Y = 0 [m]	TISSUE	X gradient		Y gradient		Z gradient		X+Y+Z	
		Avg	Max	Avg	Max	Avg	Max	Avg	Max
Z = 0.01 [m]	CSF	0.70	3.95	0.56	1.67	1.03	5.95	1.54	8.74
	White M	0.30	4.44	0.30	5.38	0.59	6.98	0.91	12.10
	Grey M	1.01	7.13	0.85	5.41	1.89	7.70	2.98	11.94
	Spine	0.89	4.33	1.15	4.11	4.46	15.80	5.52	17.46
	Retina	1.14	2.84	1.30	3.53	1.84	3.83	2.87	5.70
	Heart	0.78	4.22	0.50	2.00	1.97	9.59	2.52	13.16
	Skin	0.10	2.96	0.08	3.25	0.21	6.06	0.28	8.21
	Fat	0.23	6.32	0.20	5.08	0.45	15.41	0.62	21.25
	Muscle	0.89	6.12	0.77	7.40	2.00	18.27	2.75	24.30
Z = 0.31 [m]	CSF	0.17	0.97	0.12	0.47	0.22	1.36	0.31	2.06
	White M	0.09	1.20	0.08	1.40	0.17	2.29	0.27	3.76
	Grey M	0.30	1.79	0.25	1.58	0.57	2.45	0.92	4.36
	Spine	0.21	1.10	0.22	0.81	1.02	3.93	1.24	4.27
	Retina	0.33	0.76	0.34	0.72	0.64	1.54	0.96	2.43
	Heart	0.18	0.96	0.08	0.37	0.37	1.64	0.50	2.39
	Skin	0.03	0.72	0.02	0.65	0.05	1.51	0.07	1.84
	Fat	0.06	1.36	0.05	1.15	0.10	3.02	0.14	4.18
	Muscle	0.23	1.48	0.19	1.39	0.46	4.11	0.61	5.34
Z = 0.61 [m]	CSF	0.06	0.35	0.05	0.19	0.08	0.42	0.10	0.69
	White M	0.03	0.44	0.02	0.45	0.07	0.88	0.11	1.39
	Grey M	0.11	0.52	0.08	0.56	0.23	1.26	0.36	1.75
	Spine	0.07	0.39	0.06	0.27	0.36	1.43	0.43	1.51
	Retina	0.12	0.25	0.10	0.22	0.28	0.68	0.38	1.00
	Heart	0.06	0.31	0.02	0.10	0.12	0.48	0.16	0.69
	Skin	0.01	0.25	0.01	0.23	0.02	0.60	0.03	0.64
	Fat	0.02	0.51	0.02	0.41	0.04	0.96	0.05	1.27
	Muscle	0.09	0.57	0.07	0.45	0.17	1.42	0.22	1.78
Z = 0.91 [m]	CSF	0.03	0.16	0.02	0.09	0.03	0.16	0.05	0.28
	White M	0.01	0.20	0.01	0.18	0.03	0.49	0.05	0.64
	Grey M	0.05	0.19	0.03	0.22	0.11	0.75	0.16	0.82
	Spine	0.03	0.17	0.03	0.13	0.16	0.64	0.19	0.68
	Retina	0.05	0.10	0.03	0.07	0.14	0.33	0.18	0.47
	Heart	0.02	0.13	0.01	0.03	0.05	0.21	0.07	0.27
	Skin	0.01	0.11	0.01	0.11	0.01	0.28	0.01	0.29
	Fat	0.01	0.24	0.01	0.20	0.02	0.41	0.02	0.52
	Muscle	0.04	0.27	0.03	0.21	0.08	0.63	0.10	0.77
Z = 1.21 [m]	CSF	0.01	0.08	0.01	0.05	0.02	0.07	0.02	0.14
	White M	0.01	0.10	0.01	0.09	0.02	0.29	0.03	0.36
	Grey M	0.03	0.10	0.02	0.10	0.06	0.44	0.09	0.44
	Spine	0.02	0.09	0.01	0.07	0.08	0.33	0.10	0.35
	Retina	0.03	0.05	0.01	0.03	0.08	0.18	0.10	0.24
	Heart	0.01	0.07	0.01	0.02	0.03	0.11	0.03	0.13
	Skin	0.01	0.06	0.01	0.06	0.01	0.15	0.01	0.15
	Fat	0.01	0.13	0.01	0.11	0.01	0.21	0.01	0.26
	Muscle	0.02	0.15	0.02	0.12	0.04	0.32	0.05	0.39

Table 5

Maximum and average electric fields in selected tissues of Naomi at various axial distances from the ends of longitudinal and transverse gradient coils in [mV/m]

Body Positions Y = 0 [m]	TISSUE	X gradient		Y gradient		Z gradient		X+Y+Z	
		Avg	Max	Avg	Max	Avg	Max	Avg	Max
Z = 0.01 [m]	**CSF**	1.90	10.48	1.72	9.92	4.10	26.52	6.16	39.14
	White M	2.89	14.54	2.97	17.21	5.55	22.29	8.60	34.84
	Grey M	2.87	12.80	2.52	13.54	5.48	26.14	8.57	40.80
	Spine	2.16	9.68	3.09	9.14	11.11	33.96	13.75	42.41
	Retina	2.00	6.23	2.30	7.61	3.19	7.91	5.01	12.05
	Heart	6.02	19.14	4.06	12.77	15.38	55.97	19.69	75.44
	Skin	5.00	176.43	4.21	97.25	10.55	213.52	14.46	317.58
	Fat	5.94	142.58	5.11	80.02	10.86	172.63	15.19	294.72
	Muscle	3.28	42.47	2.80	49.65	7.35	90.85	10.08	115.88
Z = 0.31 [m]	**CSF**	0.55	2.88	0.48	3.31	1.19	6.43	1.81	8.50
	White M	0.83	3.95	0.75	4.84	1.62	7.40	2.54	10.38
	Grey M	0.85	3.54	0.70	4.61	1.64	7.26	2.62	12.24
	Spine	0.50	2.22	0.60	1.61	2.54	8.56	3.06	9.80
	Retina	0.58	1.60	0.61	1.65	1.12	3.19	1.67	5.06
	Heart	1.36	4.65	0.68	2.34	2.95	10.02	3.95	14.55
	Skin	1.34	44.32	1.06	30.43	2.56	36.51	3.41	61.37
	Fat	1.55	35.88	1.26	24.94	2.59	30.08	3.45	56.62
	Muscle	0.85	9.90	0.69	9.41	1.68	19.91	2.25	25.25
Z = 0.61 [m]	**CSF**	0.20	0.95	0.16	1.07	0.47	2.33	0.69	3.01
	White M	0.31	1.29	0.24	1.44	0.67	3.84	0.99	4.86
	Grey M	0.32	1.26	0.23	1.46	0.65	2.76	1.01	4.39
	Spine	0.17	0.74	0.17	0.55	0.90	3.13	1.05	3.41
	Retina	0.21	0.53	0.17	0.51	0.49	1.41	0.67	2.08
	Heart	0.45	1.55	0.20	0.67	0.95	2.98	1.26	4.38
	Skin	0.51	14.92	0.40	12.71	0.96	10.24	1.24	19.45
	Fat	0.58	12.08	0.47	10.39	0.99	9.23	1.27	17.85
	Muscle	0.31	3.79	0.26	2.88	0.62	6.69	0.80	8.61
Z = 0.91 [m]	**CSF**	0.09	0.40	0.06	0.39	0.23	1.05	0.32	0.41
	White M	0.14	0.51	0.09	0.50	0.33	2.01	0.46	2.43
	Grey M	0.14	0.58	0.09	0.52	0.32	1.55	0.46	1.89
	Spine	0.08	0.32	0.06	0.26	0.40	1.42	0.46	1.53
	Retina	0.09	0.21	0.06	0.19	0.26	0.68	0.32	0.97
	Heart	0.19	0.68	0.08	0.24	0.40	1.19	0.52	1.76
	Skin	0.24	6.18	0.19	6.20	0.45	4.40	0.57	8.21
	Fat	0.27	5.00	0.22	5.05	0.47	3.98	0.59	7.48
	Muscle	0.15	1.79	0.12	1.32	0.29	3.01	0.36	4.16
Z = 1.21 [m]	**CSF**	0.05	0.22	0.03	0.15	0.12	0.61	0.17	0.77
	White M	0.07	0.27	0.04	0.21	0.18	1.14	0.24	1.32
	Grey M	0.08	0.30	0.04	0.21	0.17	0.90	0.24	0.98
	Spine	0.04	0.16	0.03	0.14	0.21	0.74	0.24	0.79
	Retina	0.05	0.10	0.02	0.07	0.14	0.36	0.17	0.51
	Heart	0.10	0.35	0.04	0.11	0.20	0.56	0.26	0.85
	Skin	0.13	2.95	0.10	3.37	0.24	2.33	0.30	4.08
	Fat	0.14	2.39	0.12	2.74	0.25	2.01	0.31	3.70
	Muscle	0.08	0.98	0.06	0.71	0.16	1.68	0.19	2.22

It is important to mention that all results detailed in Tables 2 - 5 are based on central gradient field strengths of 1 mT/m. By extrapolating the normalized tissue-specific results to gradient field strength of (say) 40 mT/m, as a common maximum used in clinical MRI, the maximum induced electric fields of this study are in the range 1.2 - 3 times smaller in magnitude than the fields induced in the patients inside the MRI scanner [9-10]. It follows that the results obtained *herein* are in the same order of magnitude as those induced in patients during imaging and therefore should not be ignored. Note that in order to scale the results as presented for 1 mT/m and 100 μs rise-time, the amplitudes scale linearly, but change to both the waveform and rise-time requires a recalculation of the Fourier components. For example, in the 1 kHz waveform, a change in rise-time from 100 μs to 250 μs causes the results for induced fields and currents to be reduced by a factor of approximately 1.25. So then a combination of a central gradient strength of 40 mT/m and a 250 μs rise-time would mean that the induced fields and currents should be scaled by a factor of approximately 32.

The maximum stimulated *in situ* 1 cm^2 - averaged current densities (Tables 2 and 4) at 40 mT/m gradient field strengths are larger than the ICNIRP threshold of 10 mAm^{-2} - rms. (or ~14.14 mAm^{-2} - peak) for the head and trunk [18] under all designated gradient field exposures when the worker, whether male or female, are standing near the gradient coil end. Note that in ascertaining the limits, the harmonic content of the input waveform is relevant, as higher frequencies have higher thresholds. With the waveform used herein the difference in the limits from a pure sinusoid was relatively small; approximately 13.1 mA/m^2-rms for the trapezoidal pulse compared with 10 mA/m^2-rms for a pure sinusoid, but the effect of waveform shape is important to note for completeness.

The worst-case maximum *in situ* electric fields induced in the brain can exceed the IEEE standard of 1.25 V/m - peak [17] only in the case of female, provided the body is subjected to all three pulsed gradient coils simultaneously, while each gradient coil has a central field strength of 40 mT/m and the worker is standing 1 cm away from the end of that gradient system. Such positioning is not entirely uncommon in short magnets when workers are attending to anxious, sedated or intubated patients, although the model would likely be bending and angled.

The case where the healthcare worker is ninety degrees to the position in Figure 2 and moved sideways as so to approximate an upright position beside the patient bed, results in a different distribution to the situation in Figure 2 but almost identical maximum values.

For gradient field strengths marginally larger than 40 mT/m, the z-gradient coil and possibly the transverse gradient coils could potentially exceed the brain excitation threshold as well. On the other hand, heart tissue requires a 7.98 V/m *in situ* electric field to trigger nerve excitation [17]. In order to match this stimulation threshold, all three gradient coils would need to be operated simultaneously at 1 kHz (with 100 μs rise-time in the trapezoid) with central gradient field strengths of ~106 mT/m and the worker (either male or female) would have to stand 1 cm away from the gradient system end. All of these conditions accruing together is unlikely. Therefore, according to the simulation results herein, the excitation of heart synapses is unlikely at 40 mT/m. The median electrical stimulation threshold of peripheral nerves (with assumed maximum nerve diameter of 20 microns) is around 6.15 V/m. In order to trigger peripheral nervous stimulation, all three gradient coils would need to be operated simultaneously at gradient strengths of around 23 mT/m (tables II-V), and provided that the body models are positioned close to the gradient set end. Otherwise it is sufficient to operate the x, y and z-gradient coil independently at gradient field strengths of around 34.8 mT/m, 33.8 mT/m and 24.6 mT/m respectively, to be near the threshold for PNS. The threshold for induced current to result in PNS is estimated to be around 0.48 A/m^2 for dynamic fields [31]. According to worst-

case current density results listed in tables II-V, simultaneous switching of all three gradient coils at gradient field strengths of around 22.6mT/m could potentially result in PNS.

We have estimated the axial distances away from the three assumed magnets at which the induced maximum 1 cm^2 - averaged current density magnitudes would drop below the ICNIRP threshold of 14.14 mAm^{-2} - peak in the head and trunk at central gradient field strengths of 40 mT/m. According to selected results shown in figure 10 (for tissues of CNS, heart, skin, fat and muscle), the maximum 1 cm^2 - averaged current density magnitudes are below the 14.14 mAm^{-2} - peak threshold at distances from gradient end of approximately 1 m. The same holds true for all other tissues. This means, that for higher gradient field strengths, workers should be even further away from the gradient set to be compliant. In order to be certain that 1 cm^2 - averaged current would not exceed the ICNIRP threshold, one should add contingencies to the aforementioned 'safety distances'.

As the physiology and dielectric properties of each and every person is different to a degree, and since the body is a highly non-linear medium, it is quite difficult to predict the exact mechanisms of induced fields and their effects on the physiology. It still remains unknown to what degree the low-frequency electromagnetic fields can be harmful to the humans. Nevertheless, it is possible to gain useful information by evaluating the peak fields relative to different positions of the radiologist/technician within the MRI room and to define the regions in the this room, which should be avoided for long exposures.

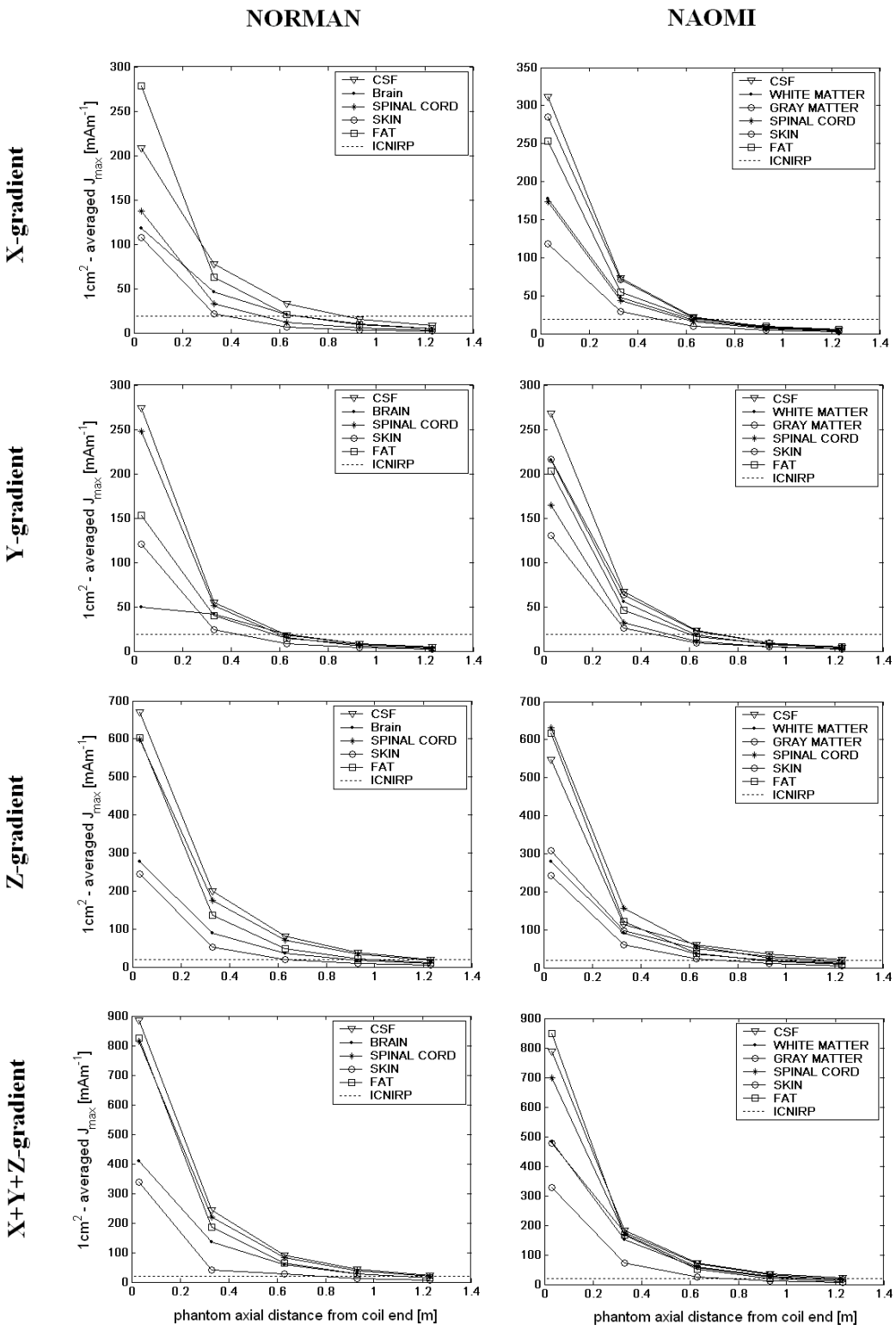

Figure 10 Maximum 1 cm^2 - averaged current densities induced in selected tissues of the male (left column) and female (right column) body models versus axial distance from the ends of three gradient coils (first three rows) and the combination of all three gradient coils (last row). Results have been scaled to the commonly operated central field strength of 40 mT/m.

5.0 CONCLUSION

In this work we have modelled the exposures of male and female workers to pulsed field gradient gradients typically used in MRI. These gradients are intended to be typical of currently available cylindrical MRI systems, but do not cover all gradient sets on the market and therefore provide indicative results only. The simulations show that the induced fields and currents can be in the same order of magnitude as those induced in the patients during MRI imaging and therefore should not be ignored. The normalized simulation results obtained can be extrapolated to evaluate the potential safety issues at different gradient strengths and distances away from transverse and longitudinal coils. The longitudinal gradient tend to induce more fields in workers than the transverse coils. The strongest levels of field exposure are observed when all three gradient coils are operated simultaneously. As suspected, the induced current densities and electric fields, when the worker is standing near the gradient coil entrance, can be well above the relevant EU, ICNIRP and IEEE standards. The calculations show that to be within regulatory limits the workers need to be approximately 1 metre away from the gradient coils when they are all pulsed simultaneously so as to generate 40mT/m each in the dsv. Experimental work into the typical gradient field exposures used in routine scanning is underway and will further inform these results. We note that the distance from the end of the gradient coil set to the end of the magnet varies between MRI systems and, for cylindrical systems, is typically smallest in short 1.5T magnets and larger in higher field systems. The methodology described in this work is able to be used to calculate regions of compliance for specific magnet/gradient coil combinations. Further modeling work is required to better understand exposures in a variety of occupational postures, such as leaning into the magnet. It is hoped that simulations such as these will help inform compliant clinical practices and work procedures.

6.0 ACKNOWLEDGEMENTS SPECIFIC TO THIS SECTION

We thank Gary Cowin of The Centre for Magnetic Resonance for assistance in gradient measurement.

7.0 REFERENCES

[1] Stehling, SMK, and Turner, R Echo-planar imaging theory, technique and application, Springer, 1998.

[2] Crozier, S and Liu, F Numerical evaluation of the fields caused by body motion in or near high-field MRI scanners, *Progress in Biophysics and Molecular Biology*, **87**: 267-278, 2005

[3] Trakic, A, Crozier, S and Liu, F Numerical modelling of thermal effects in rats due to high-field magnetic resonance imaging (0.5-1GHz) *Physics in Medicine and Biology*, **49:** 5547-5558, 2004

[4] Purves, GJ, Ausustine, D, Fitzpatrick, LC, Katz, A.–S, LaMantia, and McNamara, JO *Neuroscience*. Sinauer, Sunderland, Massachusetts, 1997

[5] Budinger, TF, Fischer, H, Hentschel, D, Reinfelder, H, and Schmitt, F Physiological effects of fast oscillating magnetic field gradients, *J. Computer Assisted Tomography*, **15**(6): 909-914, 1991

[6] Cohen, MS, Weisshoff, RM, Rzedzian, RR, and Kantor, HC Sensory stimulation by timevarying magnetic fields, *Magnetic Res. Med*., **14**: 409-414, 1990.

[7] Hebrank, FX SAFE model—a new method for predicting peripheral nerve stimulation in MRI, *Proc. Intl. Soc. Mag. Res. Med*., **8**, p. 2007, 2000.

[8] Mansfield, P and Harvey, PR Limits to neural stimulation in echo-planar imaging, *Magnetic Res. Med.*, **29**: 746-758, 1993.

[9] Schaefer, DJ, Bourland, JD, and Nyenhuis, JA Review of patient safety in time-varying gradient fields, *Jl. Mag. Res. Imag.*, **12**: 20-29, 2000.

[10] Yamagata, HS, Kuhara, S, Seo, Y, Hiwaki, O, and Ueno, S Evaluation of dB/dt thresholds for nerve stimulation elicited by trapezoidal and sinusoidal gradient fields in echo-planar imaging, *Soc. Mag. Res. Med., Proc. 10th Ann. Meet.*, Berkeley, San Francisco, p.1277, 1991.

[11] Schaefer, DJ, Bourland, JD, and Nyenhuis, JA, *et al.* Determination of gradient-induced, human peripheral nerve stimulation thresholds for trapezoidal pulse trains (abstract). *Proceedings of the Society of Magnetic Resonance 2nd Annual Meeting*, San Francisco, p.101, 1994

[12] Liu, R and Ueno, S Calculating the activating function of nerve excitation in inhomogeneous volume conductor during magnetic stimulation using finite element method, *IEEE Transactions on Magnetics*, **36**(4): 1796-1799, 2000.

[13] Abdeen, MA and. Stuchly, MA Modeling of magnetic fields stimulation of bent neurones. *IEEE Transactions on Biomedical Engineering*, **41**: 1092-1095, 1993

[14] . Faber, SC, Hoffman, A, Ruedig, C, and Reiser, M MRI-induced stimulation of peripheral nerves: dependency of stimulation threshold on patient positioning. *Magnetic Resonance Imaging*, **21**: 715-724, 2003

[15] So, PPM, Stuchly, MA, and. Nyenhuis. JA Peripheral Nerve Stimulation by Gradient Switching Fields in Magnetic Resonance Imaging, *IEEE Transactions on Biomedical Engineering*, **51**(11): 1907-1914, 2004

[16] Liu, HW, Zhao, H, and Crozier, S On the Induced Electric Field Gradients in the Human Body for Magnetic Stimulation by Gradient Coils in MRI *IEEE Transactions on Biomedical Engineering*, **50** (7): 804-815, 2003

[17] The **I**nstitute of **E**lectrical and **E**lectronics **E**ngineers (IEEE), C95.6: Standard for Safety Levels with Respect to Human Exposure to Electromagnetic Fields (0–3 kHz), New York, 2002

[18] **I**nternational **C**ommission on **N**on-**I**onizing **R**adiation **P**rotection (ICNIRP), Guidelines for limiting exposure to time varying electric, magnetic and electromagnetic fields (up to 300 GHz) *Health Phys.* **74**: 494–522, 1998

[19] Directive 2004/40/EC of the European Parliament and of the Council, *Official Journal of the European Union*, L **159**, 2004

[20] ICRP 2002 Basic anatomical and physiological data for use in radiological protection: reference values *ICRP, Publication* 89

[21] Dimbylow, PJ Current densities in a 2 mm resolution anatomically realistic model of the body induced by low frequency electric fields, *Physics in Medicine and Biology*, **45**: 1013-1022, 2000

[22] Dimbylow, PJ Development of the female voxel phantom, NAOMI, and its application to calculations of induced current densities and electric fields from applied low frequency magnetic and electric fields, *Physics in Medicine and Biology*, **50**: 1047-070, 2005

[23] Andreuccetti, D, Fossi, R and Petrucci, C Dielectric properties of body tissues, Applied Physics – Italian National Research Council (Florence, Italy), available at: http://niremf.ifac.cnr.it/tissprop/htmlclie/htmlclie.htm#atsftag, 2002

[24] Gabriel C, Gabriel S and Corthout E The dielectric properties of biological tissues: 1. Literature survey *Physics in Medicine and Biology*, **41:** 2231–49, 1996

[25] Liu, F, Crozier, S, Zhao, H, Lawrence, B Finite-difference time-domain-based studies of MRI pulsed field gradient-induced eddy currents inside the human body. Concepts in Magnetic Resonance, **15**(1): 26-36, 2002

[26] Liu, F, and Crozier, S Electromagnetic Fields inside a lossy, multilayered spherical head phantom excited by MRI coils, *Physics in Medicine and Biology*, **49**: 1835-1851, 2004

[27] . Dawson, TW, Caputa, K, and Stuchly, MA Magnetic field exposures for UK live-line workers, *Physics in Medicine and Biology*, **47**: 995-1012, 2002

[28] Mason, PA, Ziriax, JM, Hurt, WD, and Gajcek, P "Averaging Mass Used for SAR-Based Standards: One gram or 10 grams? That is the question," US Air Force Workshop: A Forum on EMF Safety Standards and Science, Munich, Germany, 2000

[29] Dawson, TW and Stuchly, MA "High-resolution organ dosimetry for human exposure to low-frequency magnetic fields," *IEEE Trans. Mag.*, **34**(3): 708-71, 1998

[30] Gandhi, OP Personal communication of data and tables to J. P. Reilly, 2000.

[31] Kangarlu, A, and Robitaille, P-.ML Biological effects and health implications in magnetic resonance imaging, *Concepts in Magnetic Resonance*, **12**: 321–359, 2000

[32] Cheng, Yu-C N, Eagan, TP, Brown, RW, Shvartsman, SM, and. Thompson, MR Design of actively shielded main magnets: an improved functional method, *MAGMA*, **16**:57-67, 2003.

SECTION 3
THE MEASUREMENTS OF MAGNETIC FIELD EXPOSURES FOR HEALTHCARE WORKERS IN SELECTED MR ENVIRONMENTS

1.0 ABSTRACT

This study presents results of tri-axial measurements of static and dynamic magnetic fields using a portable magnetic field dosimeter worn by workers during normal working shifts. We recorded and analysed magnetic field exposures in and around 1.5T, 2T, and 4T magnets during routine patient procedures. The data was integrated and averaged over time to ensure that recommended time-weighted exposure limits were not exceeded during the working shift.
Time varying magnetic fields occur when individuals move through spatially non-uniform static magnetic fields or during gradient-pulsed magnetic fields or a combination of both situations. Such dynamic fields induce electric fields and currents in tissue. Our previous numerical analysis shows that at certain positions surrounding the MRI scanner ends, large current densities and electric fields are induced that may exceed the relevant EU, ICNIRP and IEEE standards.

The root-mean-square (RMS) values of the dynamic magnetic fields were evaluated and compared against the numerical simulations and the most recent IEEE, ICNIRP and EU-Directive 2004/40/EC standards. Our measurements confirm that workers can be exposed to magnetic fields exceeding the guidelines at positions near the gradient coil ends during clinical imaging and a high degree of correlation exists with the numerical results. While the time weighted average magnetic field exposures in 1.5T, 2T, and 4T were all within the regulatory limits during static magnetic field measurements, the peak limits for the head were exceeded in some circumstances. The small number of routine shifts acquired provide indicative results only and more extensive studies are needed. We have shown that magnetic field dosimetry can be achieved in a practical manner and will be useful in providing workers with instantaneous warnings about over-exposure to magnetic fields.

2.0 INTRODUCTION

The potential epidemiological and biological interactions between living tissue and the broadband electromagnetic fields utilized to form MR images and the mechanisms of these interactions have been widely documented [1-8].

A major concern for workers in MRI is the repetitive and lengthy exposure to large magnetic fields up to 4T clinically and up to 7T in research. Whilst static magnetic field exposures seemingly pose less short-term threats than the time varying magnetic fields, long-term effects including possible carcinogenic effects have not been conclusively correlated to these chronic exposures. Nevertheless, based on evidence from animal and cellular studies, the National Radiation Protection Board (NRPB) recommends limiting the time-weighted exposure to 200mT per working day with instantaneous maxima of 5T for extremities and 2T for the head or trunk. The guidelines conclude that static magnetic fields greater than 2T can induce vertigo, nausea, a metallic taste and phosphenes [11].

Though the MRI magnet generates strong and uniform magnetic fields within the imaging volume, there are strong, long-term spatial magnetic field gradients outside this central region and persons moving in and around the MRI magnet experience time varying magnetic fields.

Time varying magnetic fields are also produced when the magnetic field gradient coils are switched at low frequencies of around 1 kHz. These dynamic magnetic fields can produce uncomfortable sensations and various biological side effects due to the electric fields and currents that are induced in tissue [2] and furthermore, can also lead to depolarization of voltage sensitive ion-channels in cell membranes and subsequent nerve excitation [4] causing tingling feelings in the skin, burning sensations and pain.

Pulsed gradient fields during high speed imaging techniques can cause symptoms such as muscle twitching and spasms, headaches, changes in heart activity and vertigo [8-9]. Workers in MRI can be exposed to these magnetic field gradients, and are at particular risk when positioned or moving close to the end the scanner, near the gradient coil ends, as is common in clinical practice.

Due to these health hazards agencies such as the IEEE and the ICNIRP have defined exposure limits on the static and time-varying electric, magnetic and electromagnetic field exposures for workers in controlled environments.

The IEEE Standard (C95.6) [10] prescribes the maximum permissible exposure (MPE) levels for magnetic fields in terms of the RMS of the magnetic flux density. The MPE is expressed as a function of frequency of the field and the limit is stricter for the head and torso than for the extremities. For the head and torso the MPE for RMS magnetic flux density is 353mT at DC and 0.6867mT at 3 kHz, and for the extremities the MPE is 353mT at DC and 1.263mT at 3 kHz. The ICNIRP guideline [11] however recommends much tighter exposure limits of 200mT at DC and 0.0307mT up to 65 kHz. Furthermore, the standard stipulates that the peak environmental magnetic field shall be limited according to the peak and phase duration of any excursion of dB/dt.

With the Directive 2004/40/EC [12] of the European Parliament and Council being enforced by April 30, 2008, the need arises to be able to measure, monitor, and ensure that workers are not being exposed to static and gradient magnetic fields above the limits set out in the directive. We have developed a magnetic field dosimeter that measures the static and dynamic magnetic fields that a worker is exposed to during their routine working shift. The dosimeter is an ambulatory device that measures the magnetic field tri-axially in order to measure the absolute isotropic magnitude of the magnetic field over a $1cm^3$ volume.

In this investigation we have measured the magnetic flux densities and time varying gradients associated with the static magnetic field B_0 that workers were exposed to during the course of their normal working day. These measurements were taken in clinical 1.5T , 2T and 4T systems. Overall, 30 working shifts of data were generated and analyzed. The analysis involved calculating the time weighted average isotropic exposure for each shift to compare with the regulatory guidelines. We extended the bandwidth of the device to measure the pulsed magnetic field gradients during high-speed clinical imaging. The measurements were made in the ZX plane at Y = 0m to produce a map of the B_{rms} magnitudes and then compared these values against our numerical data and the regulatory safety limits. The purpose of this research was to measure magnetic field exposures for workers in MRI and to validate the outcomes of the numerical research presented in Appendices 1&2 and thus confirming that maximum induced current densities can exceed safety limits in clinical MRI. It is hoped that this study will help in the evaluation of the regulatory compliance involved with occupational workers.

3.0 MATERIALS AND METHODS

3.1 The dosimeter

The patented magnetic field dosimeter [13] measures exposure to magnetic fields, rate of change of magnetic fields, and enables ambulatory monitoring of instantaneous and cumulative exposure to a wide range of static magnetic fields. It also monitors and measures the cumulative amount of static field gradient that the monitored person is exposed to, thus providing field gradient dosimetry.

The dosimeter provides accurate measurements over a wide range of magnetic field strengths between 0 to 7T bipolar whilst maintaining high resolution of 0.25mT at low field strengths and achieving a broad dynamic range with a bandwidth ranging from 0Hz to tens of kilohertz.

The dosimeter uses a three-axis system orientated in three orthogonal directions, allowing isotropic measurements over a $1cm^3$ volume. The dosimeter has on board interfaces to a PC though a USB interface. The software application on the PC uploads the data and presents the data showing cumulative exposure to magnetic fields, rate of change in magnetic fields, peak values, and time-weighted average exposures, and periods of exposures over a preset value.

3.2 Static magnetic field measurements

For static field dosimetry measurements we must consider the time varying magnetic fields caused by body movements though the long term spatial magnetic field gradients produced by the MRI magnet outside its central imaging region. Previous simulations [15] have shown that electric field magnitudes induced by typical body movements are less than, but of a similar magnitude, as those induced by switched gradient.

1. Measurement procedure

In this study we have considered mass body movements with the dosimeter typically being worn around the waist area on a belt clip or inside pant or shirt pocket. A bandwidth from 0Hz to 7Hz was chosen for these dosimetry measurements according to kinematics of normal human gait and lateral motion such as leaning forward and bending over [16-19]. In this configuration the dosimeter has a total active battery life of more than 50 hours and is able to retain 75 hours worth of data. This is suitable for magnetic field dosimetry over a week of 8-hour shifts.

The device was used at various installation sites in Brisbane, Australia and overall 240 hours of measurements were collated. Workers used the dosimeter during their normal working shifts in a 1.5T Siemens Magnetom Sonata clinical system at UQ research facility at the Wesley Hospital, a 1.5T Siemens Vision clinical system in a private radiology firm at the Wesley hospital, a 1.5T Siemens Vision Plus system at the Royal Brisbane Hospital, a Bruker S200/Oxford Magnet Technology 2T research system at UQ, and a Bruker 4T Siemens clinical imaging system at the Wesley Hospital. All studies conformed to the ethical standards set down by The University of Queensland ethics board.

Figure 1 illustrates calculations of the absolute value of the total magnetic flux density produced by the 1.5T Infinion and 4T Siemens super conducting magnets during our previous numerical study [15]. Of particular interest for the static field exposure for workers are the peaks in the magnetic fields near the inner bore edges of the magnet end were the flux densities approach and exceed the 2T instantaneous limit for the head and torso. Furthermore, because the peak |B|-fields and spatial gradients of |B| are observed near the inner edges of the magnet ends, this location is where maximum dB/dt values occur as the radiologist is undergoing a fast translational or bending motion near the magnet bore inner edges. We have measured therefore, field exposures at these specific locations and applied the kinematics of bending motions at these locations.

For each study the isotropic magnetic flux density was calculated as:

$$B_{norm} = \sqrt{\vec{B}_x^2 + \vec{B}_y^2 + \vec{B}_z^2} \quad (1)$$

And then the B_{norm} was integrated over time to produce the overall cumulative exposure (Tesla-seconds) during the shift. The cumulative exposure was then averaged over the duration of the shift to yield the time weighted average exposure that the worker was exposed to and assessed against the ICNIRP guidelines.

2. Calibration of the measuring device

Calibration of the dosimeter involves low magnetic field strength calibration for the Hall sensor linear region and high magnetic field strength calibration for the coils.

For low magnetic field strength calibration, a powerful 0.5T permanent magnet was used in conjunction with a Hirst Magnetic Instruments GM04 handheld portable Gauss meter using a zero flux chamber. The Gauss meter was used to measure magnetic field strength at four defined calibration points for each axis around the 0.5T magnet. Measuring the Hall sensor outputs at each defined position and calculating a best-fit function for these calibration points to produce an overall calibration factor for each axis calibrated each dosimeter. The post calibration error curves the units used in this study are shown in Figure 2.

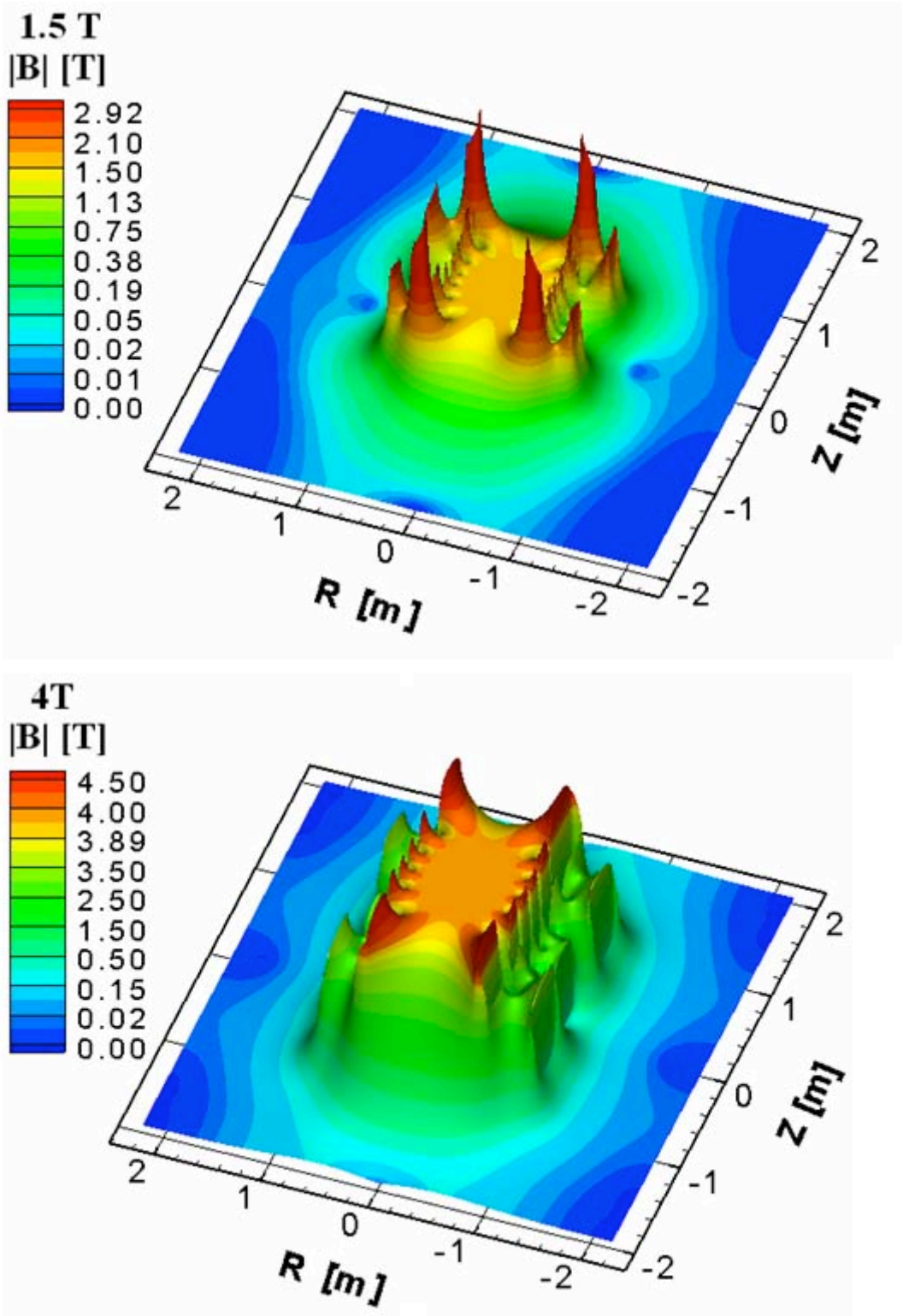

Figure 1 Absolute value of total magnetic field produced by 1.5T and 2T theoretical main superconducting magnets

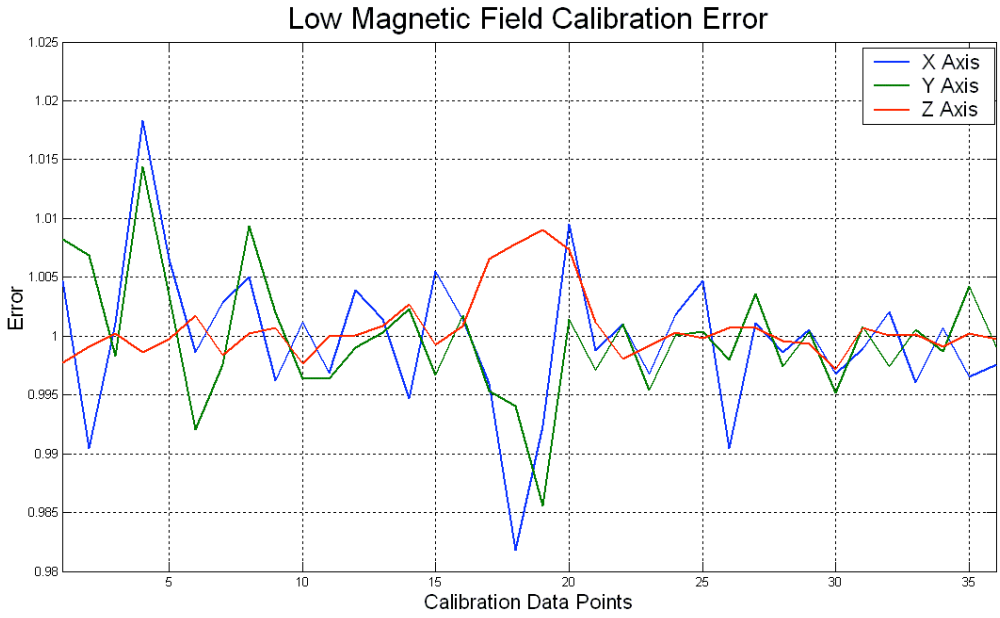

Figure 2 Low Magnetic Field Calibration Error Curves

The high magnetic field calibration was performed after the low field Hall sensor calibration was performed to correlate and correct any errors between the rate of change integration and the Hall effect sensor. Three units were also tested at high field strengths to ensure linearity at higher field strengths following the calibration routine. Each unit was inserted into the DSV of the 2T magnet with each measurement axis aligned perpendicular to the B_0 field to ensure that each measurement axis registered the magnetic field strength according to the centre frequency of the magnet within the specifications of the device.

3.3 Gradient pulsed magnetic field measurements

1. Measurement procedure

For gradient switching magnetic field measurements the bandwidth of the dosimeter was extended up to a sampling frequency of 40 kHz per channel using only the coil loops to perform the measurements. This bandwidth increase was selected to allow the dosimeter to fully capture the minimum static gradient field durations (75 µsec) and gradient rise time durations (200 µsec) experienced during the imaging sequence in compliance with digital sampling theory. In this configuration the active battery life of the dosimeter was reduced down to 1.5 hours and it was able to retain 2 hours worth of information.

The regulations stipulate that the peak environmental magnetic field shall be limited according to the peak and phase duration of any excursion of dB/dt. Based on the timing diagram for this sequence (figure 3) we can calculate that the phase duration of the dB/dt's for the phase encoding is 200 µsec, the readout gradient is 270 µsec whilst for the slice selection gradient it is 250 µsec. Following the procedure prescribed in IEEE standard we determine the peak allowable limits for each of the gradient coils for the head and torso and for extremities. Under the ICNIRP guidelines the maximum peak field exposure for any of the three gradient coils is fixed at 0.0434mT for any part of the body. Table 1 describes the full set of MPEs according to IEEE and ICNIRP for each of the gradient coils. We note that the ICNIRP guidelines impose much tighter restrictions ascertaining to incident environmental fields than the IEEE Standard

(about 100 times larger MPEs) and that the limits in the 2004/40/EC directive is based upon the recommendations of the ICNIRP.

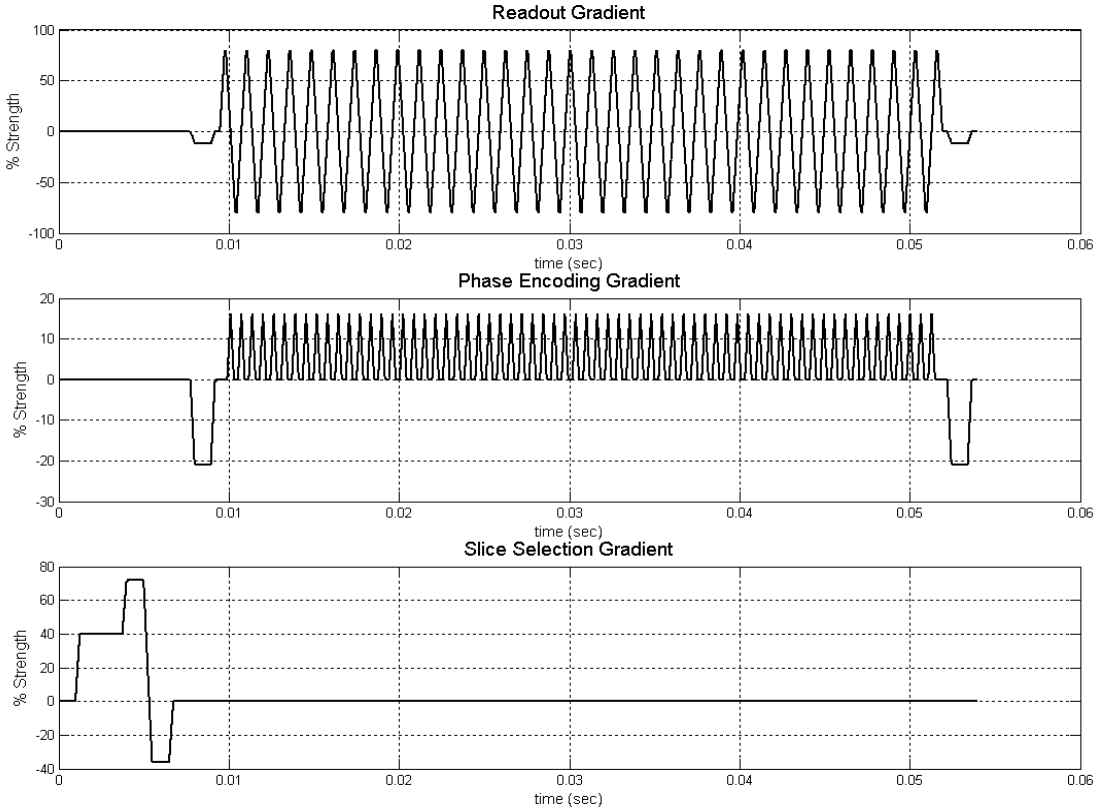

Figure 3 The Echo Planar Imaging sequence

Table 1 IEEE and ICNIRP MPE for the EPI sequence

PARAMETER		**Read-out Gradient**		**Slice Select Gradient**		**Phase Encode Gradient**	
		IEEE MPE	**ICNIRP MPE**	**IEEE MPE**	**ICNIRP MPE**	**IEEE MPE**	**ICNIRP MPE**
B_{rms}	***Extremities***	2.048mT	30.7 μT	1.895mT	30.7 μT	1.516mT	30.7 μT
	Head/Torso	1.113mT		1.03mT		0.824mT	
Peak B	***Extremities***	2.896mT	43.4 μT	2.68mT	43.4 μT	2.144mT	43.4 μT
	Head/Torso	1.574mT		1.457mT		1.165mT	
Peak dB/dt	***Extremities***	$10.726Ts^{-1}$	$0.16Ts^{-1}$	$10.719Ts^{-1}$	$0.1736Ts^{-1}$	$10.720Ts^{-1}$	$0.217Ts^{-1}$
	Head/Torso	$5.83Ts^{-1}$		$5.826Ts^{-1}$		$5.825Ts^{-1}$	
Frequency $f = 0.5t_p$		1852Hz		2000Hz		2500Hz	

Table 2 Dimensions of theoretical gradient coils

PARAMETER	X-gradient	Y-gradient	Z-gradient
1st layer - Z [m]	2.07	2.06	2.21
2nd layer - Z [m]	2.40	2.40	2.40
1st layer - R [m]	0.31	0.32	0.33
2nd layer - R [m]	0.36	0.37	0.39

Note: Z denotes axial length and R denotes the radius of the primary and secondary gradient coil layers.

We measured gradient switching during EPI sequences (see figure 3) at the Siemens Magnetom Sonata whole-body MRI clinical system, and at the Bruker S200/Oxford Magnet Technology 2T research system. The Siemens system was fitted with Sonata gradients capable of 40mT/m, with a slew rate of 200T/m/s and measurements were taken during imaging at a position of X = 15cm, Z = 110cm, and Y = 20cm.

The Bruker system was fitted with 63 cm Bruker gradients, capable of 30mT/m, with a minimum rise-time of 200 μsec. In this system we were able to perform a more detailed investigations and comparisons to numerically evaluated field profiles because the length of the gradient set was known. Measurements were taken on the XZ plane at Y = 0cm, from X = 0 to 60cm and Z = 120cm to 175cm. Figure 4 shows the region of interest (ROI) at which the measurements were taken.

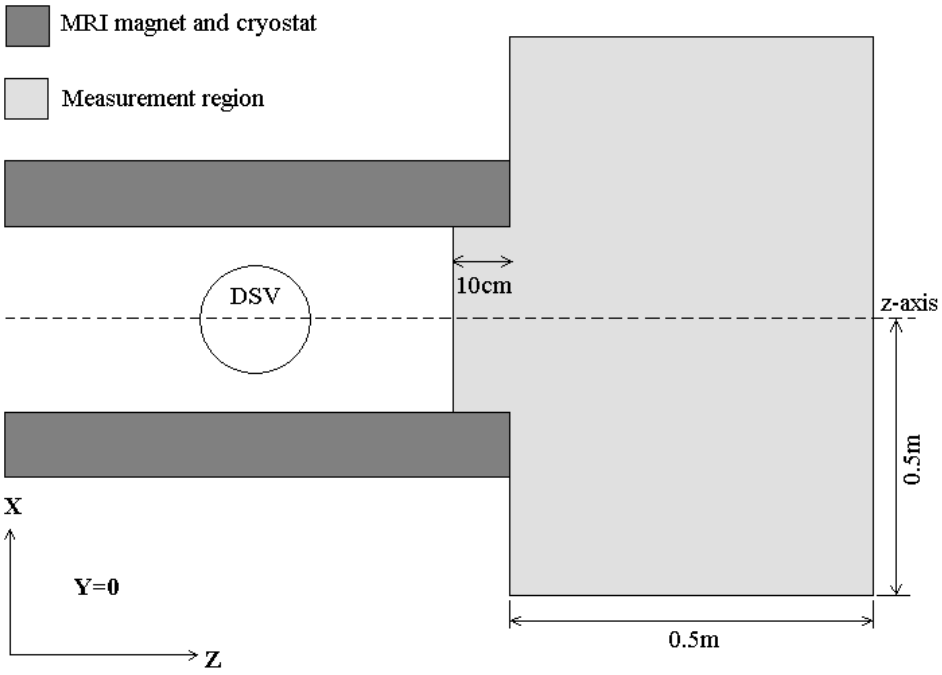

Figure 4 The measurement regions for the switched gradients.

The dB/dt measurement from each loop was then integrated over time using a cumulative sum digital integration routine with drift error compensation for digitization noise to yield the B_x, B_z, and B_y components of the gradient switching.

The isotropic magnetic flux density was calculated using equation (1) and the RMS value of the isotropic magnetic flux density strength was calculated for each TR period and averaged at each measurement point. The RMS averages were mirrored along the Z-axis because the transverse gradients are symmetrical and then used to map the magnetic field strength across the XZ plane by 2D interpolation using a cubic spline technique.

2. Calibration of the measuring device

Since the Hall effect sensors were not used for the gradient switching measurements, low magnetic field strength calibration was not necessary and a high magnetic field strength calibration was performed instead, whereby the following procedure was performed for each axis. The measurement axis was first aligned perpendicular to the B_0 field of the MRI magnet and was inserted into the DSV from the 5 Gauss line and back out. The loop measurement was then integrated and scaled such that the minimum value was set at 5 Gauss and the maximum value matched the magnetic field strength according to the centre frequency of the magnet. The calibration curves are shown in Figure 5.

Figure 5 Magnetic Field Calibrations at 2T for High Speed sampling unit

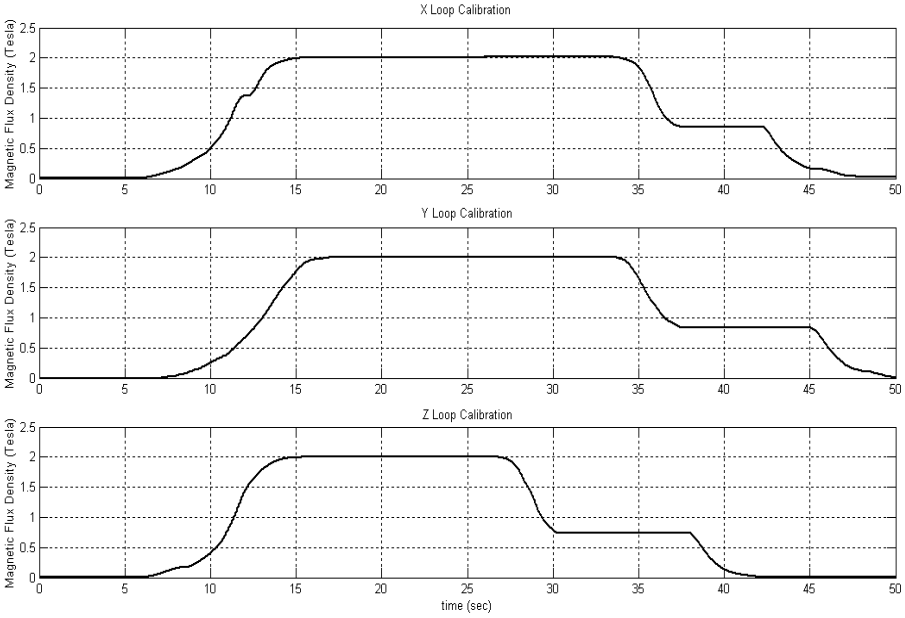

3.4 Gradient field simulations

In a recent study [21] we have numerically evaluated male and female occupational worker exposures to magnetic fields produced by trapezoidally switched gradient coils. The region where the body models were placed was at the outside end of the imager bore. The total magnetic field profile produced by all three gradients within the designated region depends on the coil geometries and current magnitudes employed in driving the coil. In this section we compare measured magnetic fields produced by the gradient set of the Bruker 2T system with the magnetic fields generated by the gradient coils from the theoretical study [21]. The motive

behind this comparison is to corroborate experimentally measured and theoretically evaluated magnetic fields.

1. Gradient coils for simulation

The gradient coil set within the Bruker 2T machine has an approximate length of 2.2m and an inner diameter of 0.6m; however, the exact current pattern that generates the field is not provided by the manufacturer and is therefore unknown. In this preliminary comparative study, the dimensions of the theoretic, actively shielded, symmetric gradient coils [21] were appropriately scaled to conform to the actual size of the gradient set in the Bruker system. Therefore, the three theoretical coils (both longitudinal and transverse) feature approximately the same length (~ 2.4m), yet they remain radially separated, i.e. the six coil layers (primary and secondary) are allocated to different radii assuming a layer thickness (including former, etc) of 5 mm. Table 2 details the gradient coil dimensions. We note here that the theoretical gradient coils might not have the same current distribution as the gradients of the Bruker machine, and therefore provide only indicative results on magnetic field magnitude and spatial distribution.

2. Computation of the magnetic fields (direct current)

To facilitate the computation of the magnetic field profiles, the gradient coils were segmented into current carrying wire elements. Each of these segments is represented as a line that connects two points (the nodes) in three-dimensional Cartesian space. The transverse and longitudinal gradient coils were modelled with a total of 22,384 and 4,400 nodes, respectively. The three Cartesian components of the magnetic field due to each gradient coil were computed with the Biot-Savart method in the same X-Z plane and region of interest as performed during measurement (see figure 4). The magnitudes of the driving direct currents are adjusted so that each coil generates gradient field strength of 30 mT/m in the working volume.

3. Field simulation with the Echo Planar Imaging (EPI) sequence

Figure 3 illustrates the EPI sequence that was applied to the gradient set of the Bruker 2T system. The vertical axis of the plot in figure 3 expresses the percentage of maximum gradient field strength in the working volume. The gradients in the Bruker machine were switched at 30mT/m each and therefore the central field strength for all three theoretical gradients was adjusted to 30mT/m. Then the EPI timing sequence (figure 3) was engaged to amplitude modulate the gradient field of the theoretical gradient coils and thus to fully mimic the experimentally observed field behavior in the laboratory.

a) |dB/dt| evaluation

Considering the EPI sequence, the gradient rise times of the x, y and z-gradient coils were 270, 200 and 250 μsec, respectively. Each gradient coil produced central gradient field strength of 30mT/m and this field strength was percentage weighted by the EPI sequence. The dB/dt value was calculated as the difference of the total magnetic flux density when the gradient field was turned on and when it was turned off, and this value was divided by the specific gradient rise time between these two field magnitude points. The dB/dt values were computed at all designated spatial locations near one end of the gradient coil set.

b) $|B_{rms}|$ evaluation

At every time point of the EPI sequence, the individual Cartesian magnetic flux components due to each gradient coil were added first, and then the absolute value of the total magnetic flux density produced by all three coils was computed using equation (1). Hence the resulting simulation results are in terms of the total magnetic flux density profile produced by the theoretical gradient set over time and is governed by the EPI sequence. Similar to the experimental study and based on the numerical space-time data, the RMS values of the total

magnetic flux density were calculated for each TR period similar to the experimental study to yield a spatial distribution of B_{rms}.

4.0 RESULTS AND DISCUSSION

4.1 Static magnetic field measurements

Figures 6-13 illustrate example magnetic field exposure plots during working shifts in clinical MRI measured at 1.5T, 2T, and 4T. The figures show plots of the absolute value of the total magnetic flux density as calculated using equation 1 as well as the absolute value of the dB/dt of the magnetic field exposure. From this data, the cumulative exposure and the time weighted average exposure were calculated for each of the thirty working shifts as well as peak dB/dt and peak B field. This information was tabulated (table 3) together with information about the number of patients attended to during the shift and the site in which the measurements were taken.

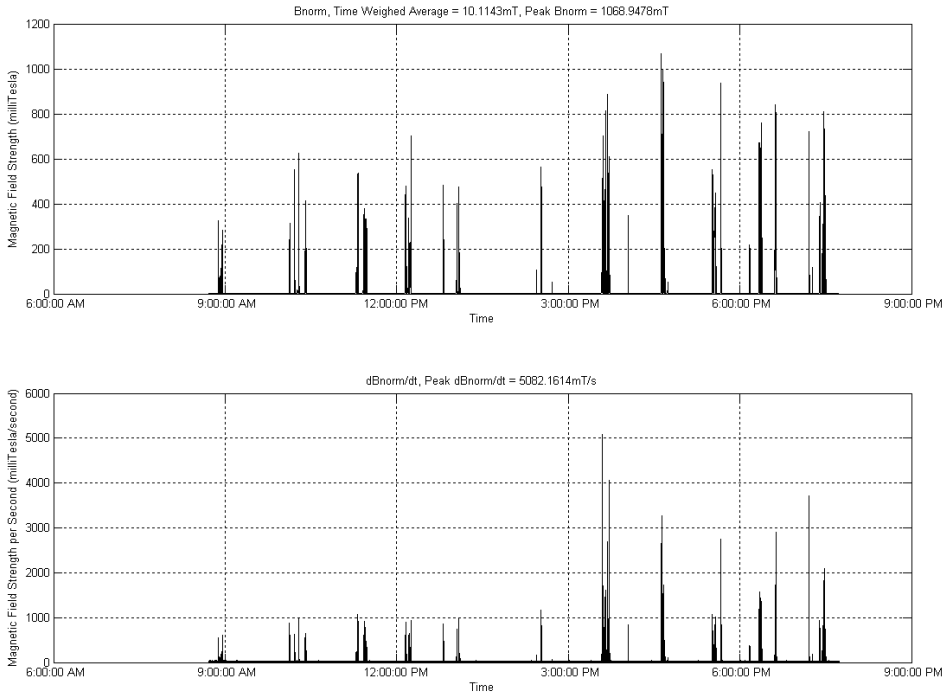

Figure 6 The Maximum Cumulative Exposure was measured during Shift 30

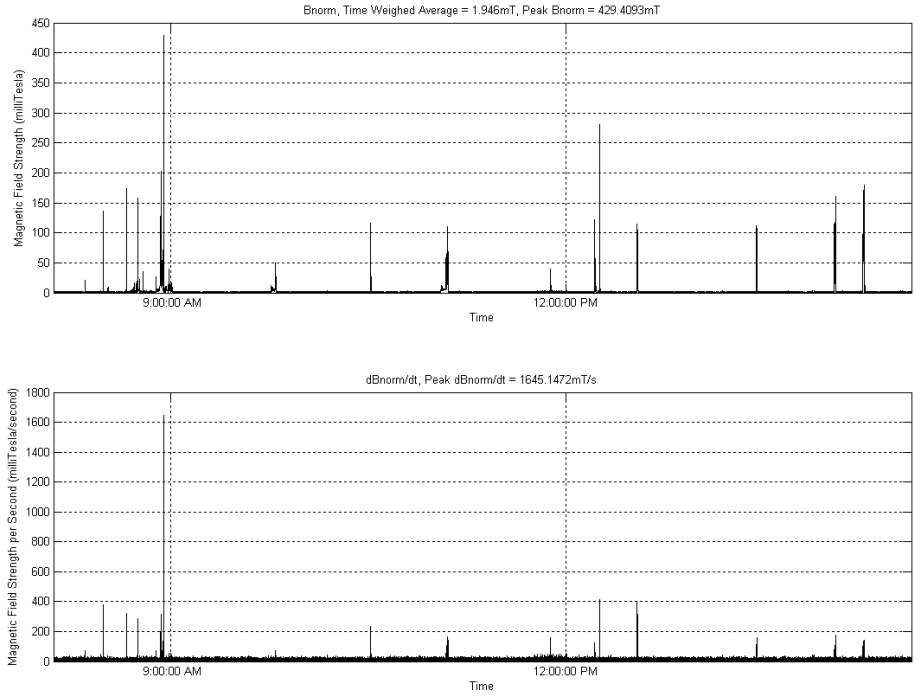

Figure 7 The Minimum Cumulative Exposure was measured during Shift 2

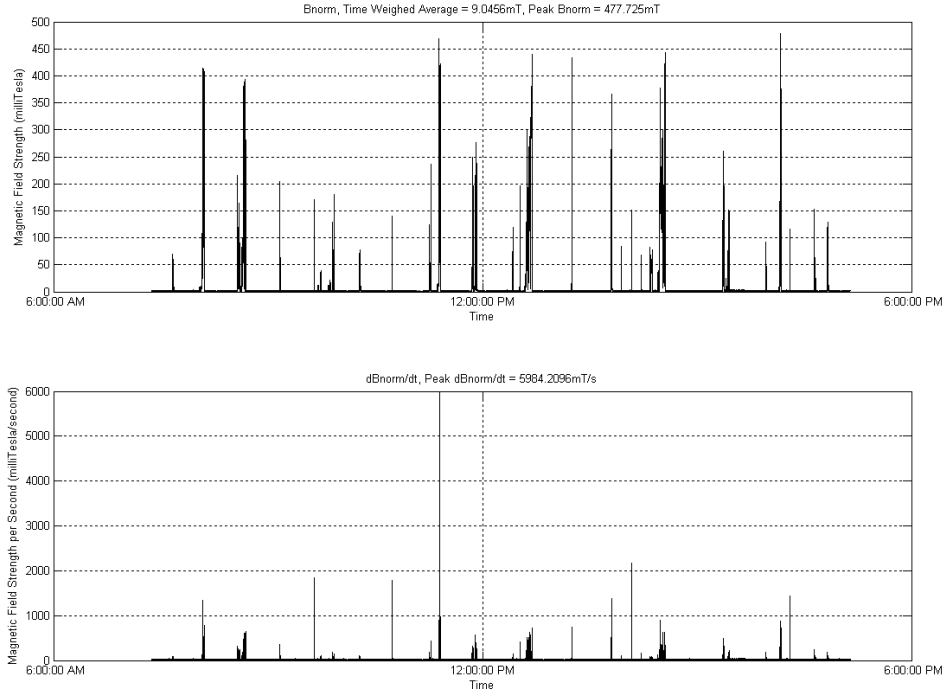

Figure 8 The Maximum Peak |dB/dt| was measured during Shift 3

Figure 9 The Minimum Peak |dB/dt| was measured during Shift 4

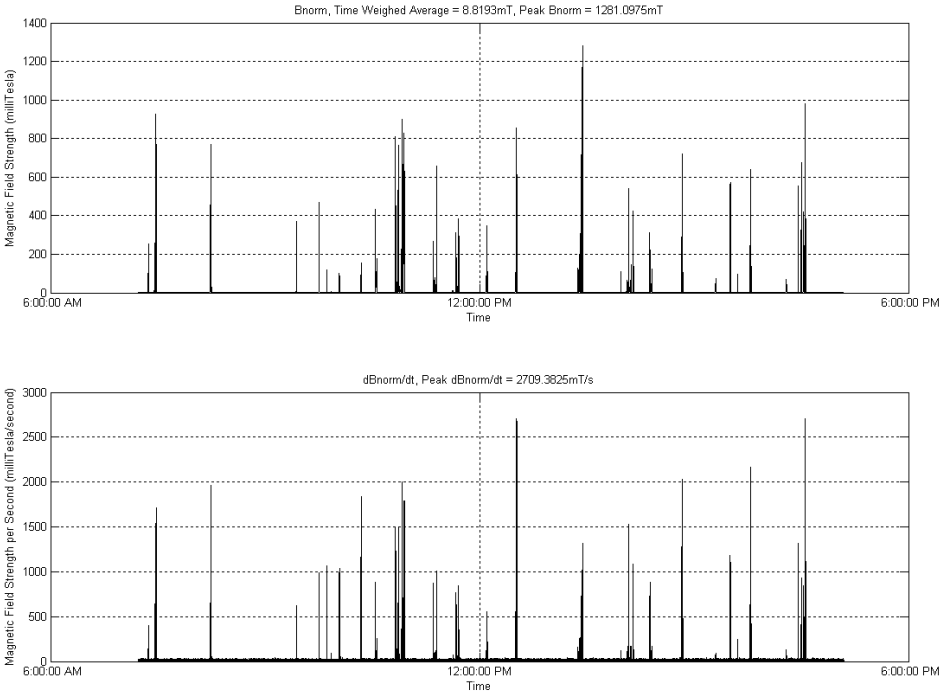

Figure 10 The Maximum Peak |B| was measured during Shift 11

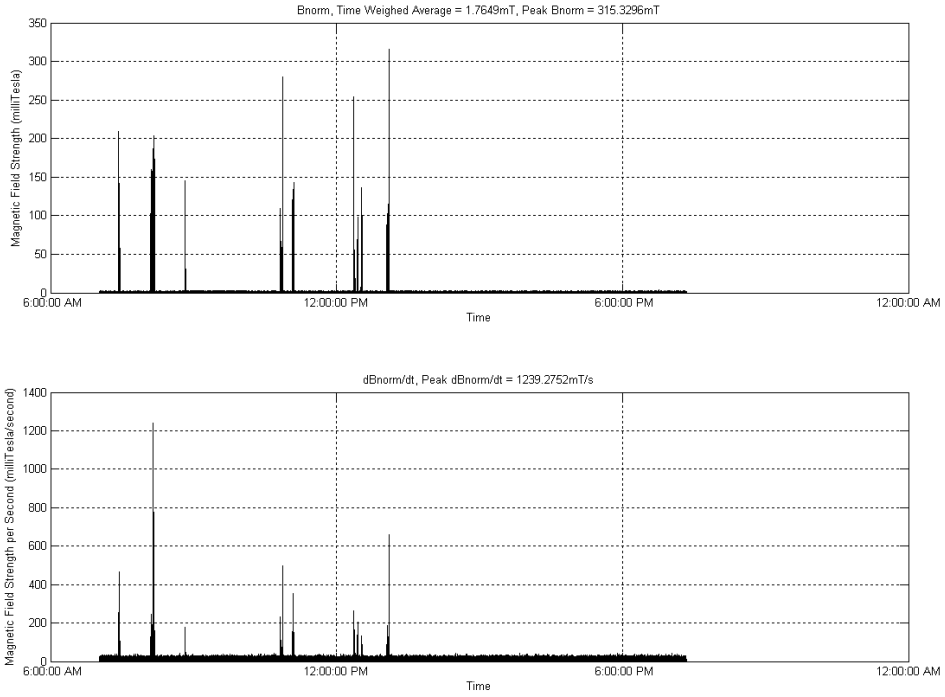

Figure 11 The Minimum Peak |B| was measured during Shift 10

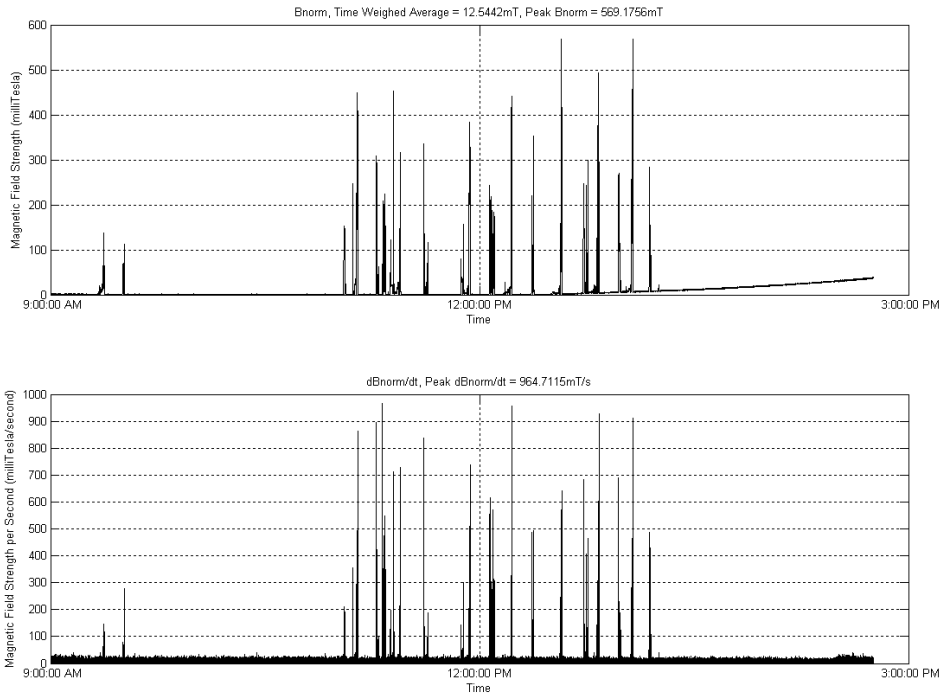

Figure 12 The Maximum Time Weighted Average was measured during Shift 5

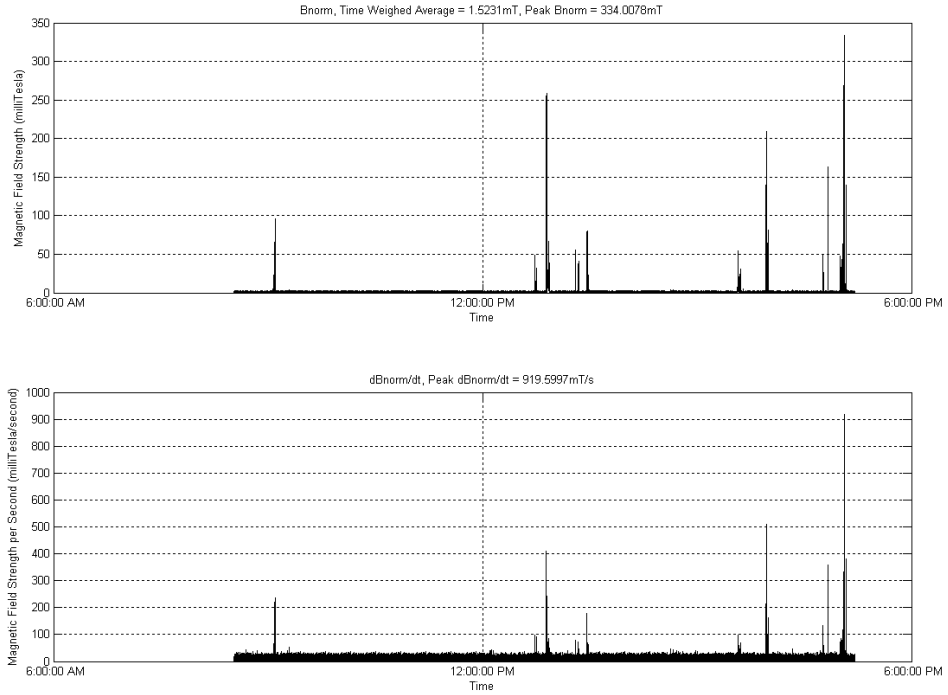

Figure 13 The Minimum Time Weighted Average was measured during Shift 15

We identified that the average worker at these sites attended to 9.9 patients per shift in average in this study and worked an average of 9.3 hours per shift. However workloads experienced by medical personnel can range between two and three patients an hour and working shifts can be as long as 14 hours. During this investigation, however, it was found that the time-weighted averages ranged between 1.52mT and 12.54mT. This represents only 6.25% of the total allowable time-weighted average of 200mT. The maximum and minimum cumulative exposure values were 401.22Ts and 45.67Ts,and were not dependant on the magnet strength but rather on the amount of time spent at high fields, the number of patients attended to, and the nature and position of movements inside the magnet room. These results correlate well with the measurements taken during a previous investigation [20]. The peak |B| and |dB/dt| values were 1.281 T/s and 5.08 T/s respectively and were also independent of the magnet strength because these values largely depend on the positioning of the person within the magnet room and the nature of the body movements whilst in the magnet room, although higher field magnets do have the potential to cause higher peaks in both |B| and |dB/dt|, due to their higher field profile outside the bore (Fig 2). The peak |B| values were all within the instantaneous maximum magnetic field limits for both the head and torso and the extremities as defined in the standards. However, 28 out of the 30 peak |db/dt| recorded exceeded the maximum allowable dB/dt of 767.9mT/s within the measurement bandwidth.

Table 3 Statistics of Shifts during Static Magnetic Field Dosimetry

SHIFT	Location	Magnet Strength (T)	|B| Peak (T)	|dB/dt| Peak (T/s)	|B| Time Weighted Average (mT)	Cumulative |B| (Ts)	Number of Patients	Duration of Shift (HH: MM)
1	Wesley-UQ	4	0.616	1.2	9.92	305.29	8	08:33
2	Wesley-UQ	4	0.429	1.65	1.95	45.67	6	06:31
3	Wesley-UQ	1.5	0.478	5.98	9.05	318.32	12	09:46
4	Wesley-UQ	1.5	0.321	0.56	2.78	80.26	8	08:02
5	Wesley-UQ	1.5	0.569	0.96	12.54	259.51	9	05.44
6	Wesley-UQ	1.5	0.494	1.17	4.28	123.12	6	08:00
7	RBH	1.5	0.446	1.27	7.38	192.41	9	07:14
8	RBH	1.5	0.713	2.77	2.90	96.22	6	09:12
9	Wesley	1.5	0.575	1.56	2.88	127.58	11	12:19
10	Wesley	1.5	0.315	1.24	1.77	78.19	7	12:18
11	RBH	1.5	1.281	2.71	8.82	313.45	10	9:52
12	RBH	1.5	0.592	2.14	3.44	99.75	6	8:03
13	RBH	1.5	0.982	3.85	9.69	392.71	12	11:15
14	RBH	1.5	0.526	4.59	2.50	117.49	9	13:03
15	RBH	1.5	0.334	0.92	1.52	47.62	7	8:41
16	RBH	1.5	0.743	1.96	1.52	54.50	8	9:56
17	Wesley	1.5	0.542	0.85	3.02	86.83	12	7:59
18	Wesley	1.5	0.694	1.37	4.93	159.05	9	8:58
19	Wesley-UQ	4	0.516	2.04	6.63	195.62	10	8:11
20	Wesley-UQ	4	0.493	2.50	7.15	208.83	11	8:06
21	Wesley-UQ	4	0.511	1.27	6.24	183.00	8	8:08
22	UQ-CMR	2	0.584	1.15	6.03	184.56	8	8:30
23	UQ-CMR	2	0.538	1.75	7.67	234.38	8	8:29
24	Wesley	1.5	0.570	1.95	4.49	114.64	9	7:05
25	Wesley	1.5	0.366	1.11	4.20	199.69	20	13:13
26	Wesley	1.5	0.474	0.68	3.61	153.27	18	11:47
27	Wesley	1.5	0.589	2.12	5.23	194.55	14	10:19
28	Wesley	1.5	0.704	2.00	7.73	273.29	11	9:49
29	Wesley	1.5	0.439	3.20	3.61	117.46	11	9:01
30	RBH	1.5	1.070	5.08	10.11	401.22	15	11:01

The instantaneous peak magnetic fields measured during the head exposure studies during bending movements at the inner edges of the magnet ends are presented in figures 14 to 16.

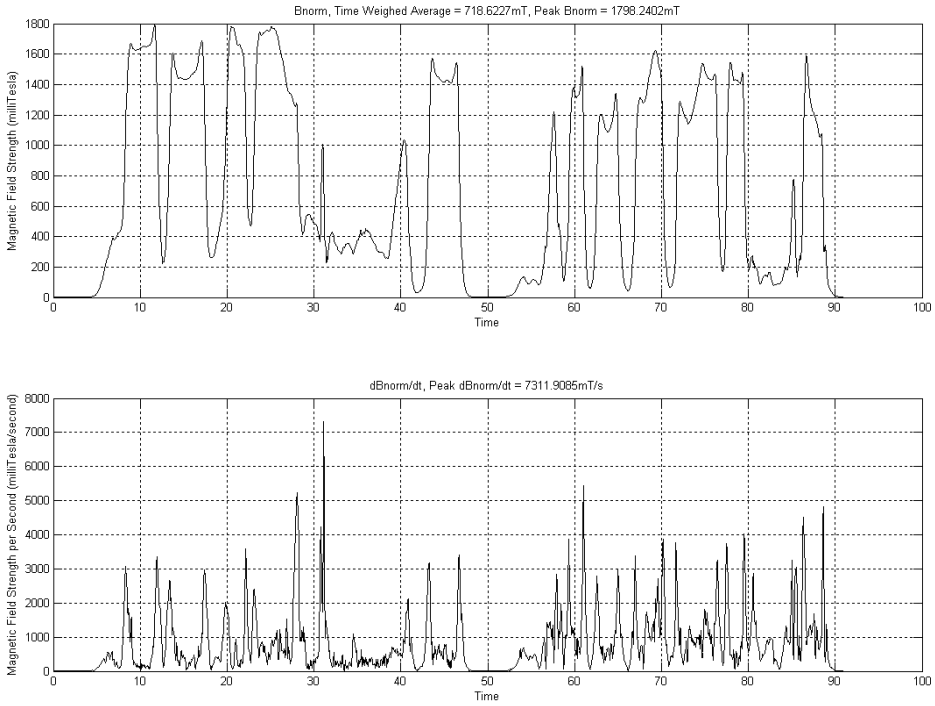

Figure 14 Peak Instantaneous B Field at inner bore at scanner end, 1.5T magnet

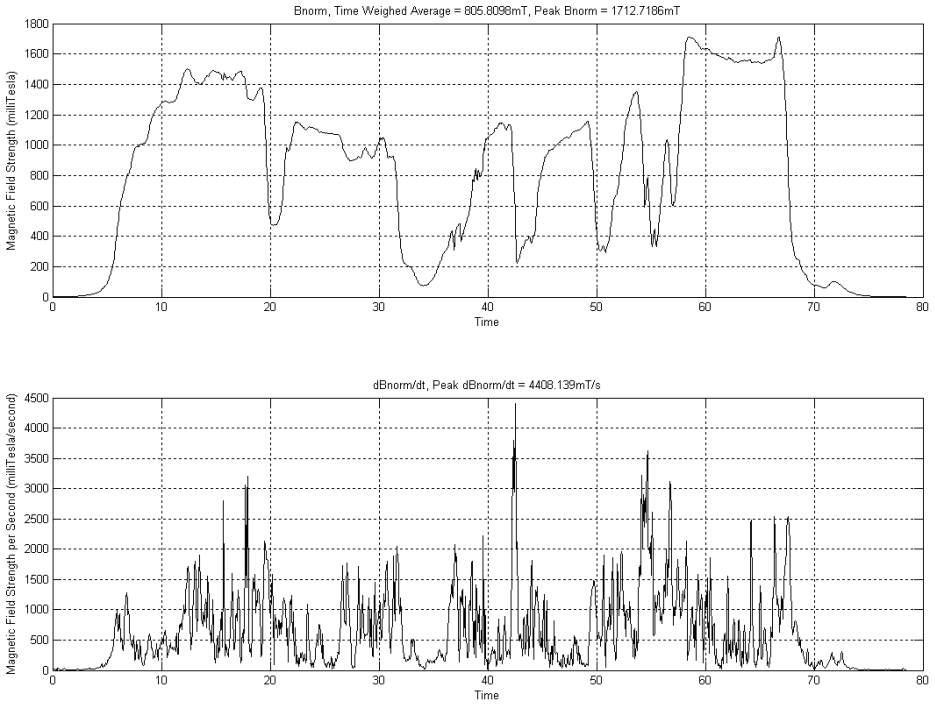

Figure 15 Peak Instantaneous B Field at inner bore at scanner end, 2T magnet

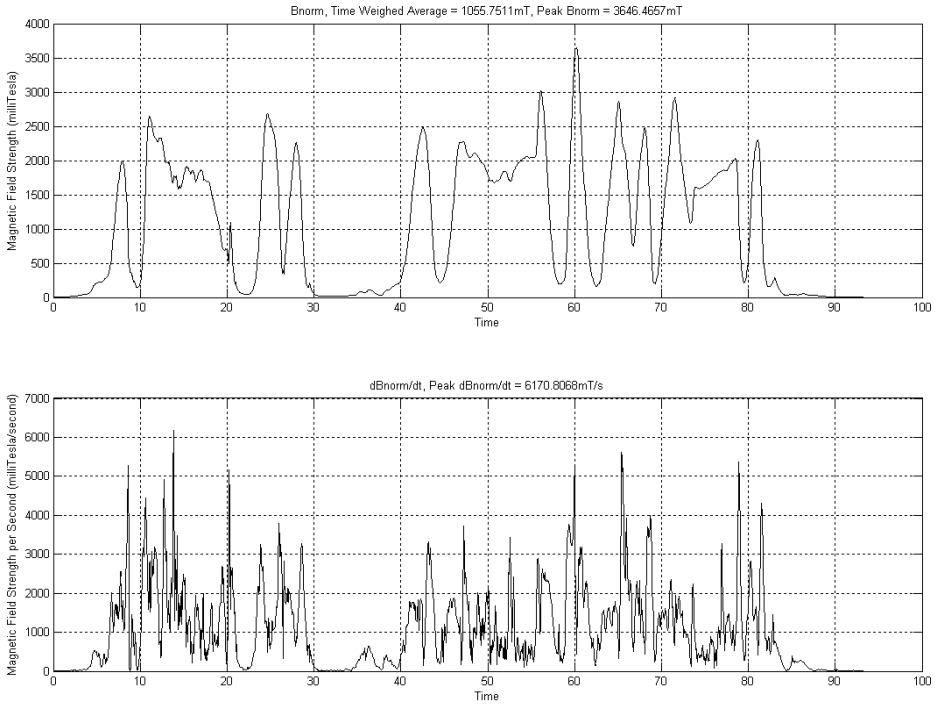

Figure 16 Peak Instantaneous B Field at inner bore at scanner end, 4T magnet

The peak B fields were 1.798T, 1.713T, and 3.646T at 1.5T, 2T, and 4T respectively. However for the 2T system it was not possible to measure right up against the inner bore due to the structure of the gradients and cooling system and may explain why the maximum instantaneous peak at 2T is lower than at 1.5T. Furthermore, inspecting the numerical results in figure 1, we note that the field increase from the centre of the magnet towards the inner bore edges of the magnet end is larger in the 1.5T system than that in the 4T system and as such, the measured peak B-field values show similar behavior as the magnetic field in the 1.5T system near the magnet edges was notably larger than in the Diameter Spherical Volume (DSV) region compared to the 4T system. The measured isotropic magnetic flux density strengths and profiles correspond quite well with the field magnitudes and distributions in figure 1 and at 4T the peak B field value measured exceeds the maximum allowable instantaneous magnetic field exposure for the head and torso. The peak dB/dt's at these field strengths were 7.3T/s, 4.4T/s, and 6.17T/s at 1.5T, 2T, and 4T respectively, exceeding the maximum allowable dB/dt of 767.9mT/s within the measurement bandwidth and therefore, as the radiologist is undergoing a fast translational or bending motion near the magnet bore inner edges, the likelihood for significant *in situ* electric field induction increases due to the spatial (non-uniform field profile) and temporal (movement) change in the impressed magnetic flux density. It is also interesting to note that the peak dB/dt's experienced by workers can approach the types of magnitudes that the measured pulsed gradient fields produce. The dosimeter can be used to alert workers to slow their movements inside the magnet room when dB/dt's approaching the regulatory limits are detected and thus provide a measure of safety against large *in situ* electric field inductions.

4.2 Gradient pulsed magnetic field measurements

Figure 17 illustrates the derived spatial distribution of $|B_{rms}|$ obtained by physically measuring the total magnetic flux density produced by the gradient set of the Bruker 2T system whilst running the EPI sequence illustrated in figure 3. Figure 4 shows the measurement region used to obtain this $|B_{rms}|$ spatial distribution beginning 10cm inside the gradient coil set along the Z direction. The derived spatial distribution of $|B_{rms}|$ (figure 17) shows that the influence of the readout gradient causes the increase in $|B_{rms}|$ amplitude moving radially outwards from the centre at each Z position. Up to Z = 1.26m, measurements could not be conducted beyond a radius of 0.25m due to the cryostat and gradient coil cooling structure but for Z greater than 1.26m, a radial $|B_{rms}|$ maxima occurs at 0.3m at each Z position. For radii greater than 0.3m at each Z position the $|B_{rms}|$ diminishes due to the shielding of the gradient set. The phase encoding gradient and slice encoding contributions to $|B_{rms}|$ is radially constant for any given Z position it diminishes as expected when moving outwards along Z.

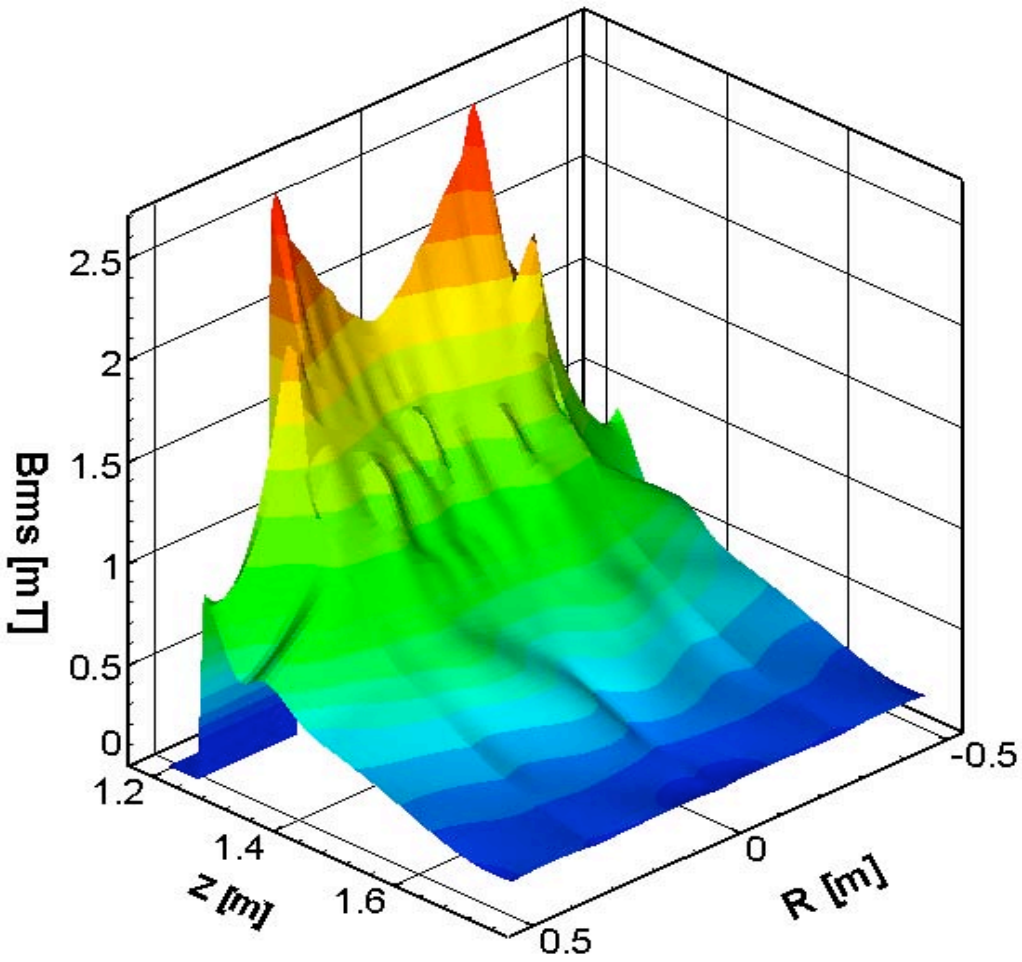

Figure 17 Experimentally measured | B_{rms} | due to the gradient set of the 2 T MRI scanner using the EPI sequence of figure 4

It is the positions outside the cryostat and gradient cooling system structure of the magnet that are important when comparing these measurements to the regulatory limits. Figures 18-24 show the regions where the calculated Brms values exceed the IEEE and ICNIRP MPEs and figures 25-27 show the regions where peak dB/dt's exceed the IEEE and ICNIRP MPEs. Figure 28 shows the experimentally measured peak magnitude dB/dt distribution when the EPI sequence was running.

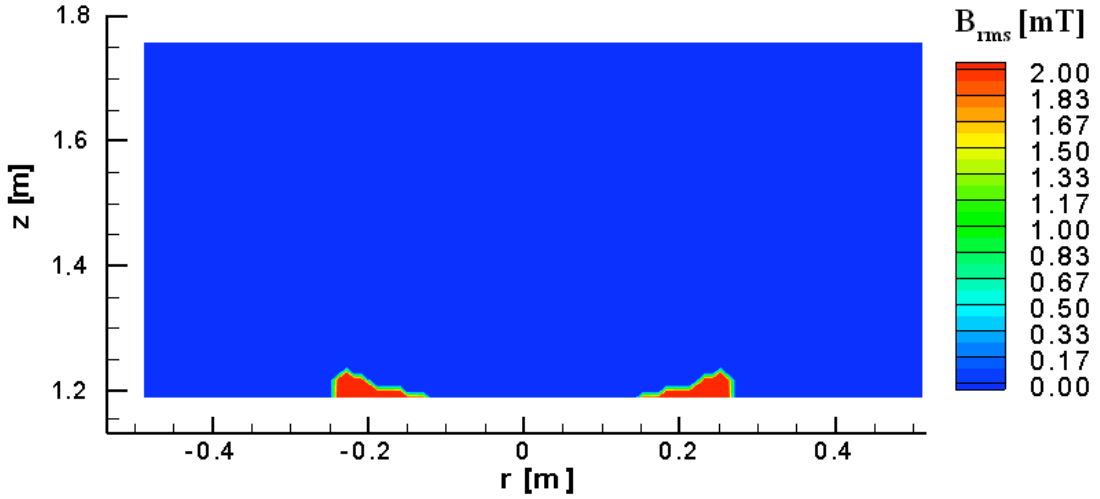

Figure 18 Positions where | B_{rms} | exceeds IEEE for extremities: Readout Gradient

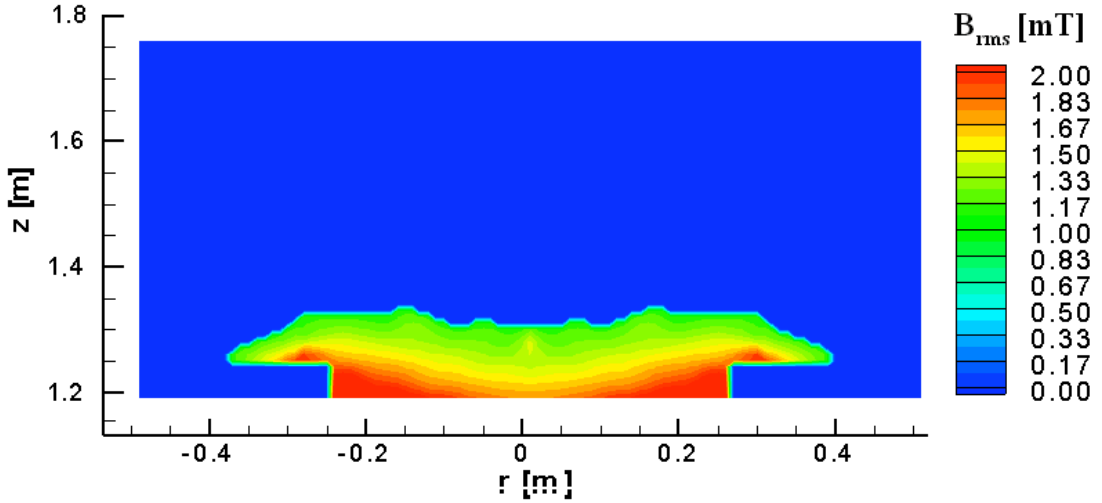

Figure 19 Positions where | B_{rms} | exceeds IEEE for Head and Torso: Readout Gradient

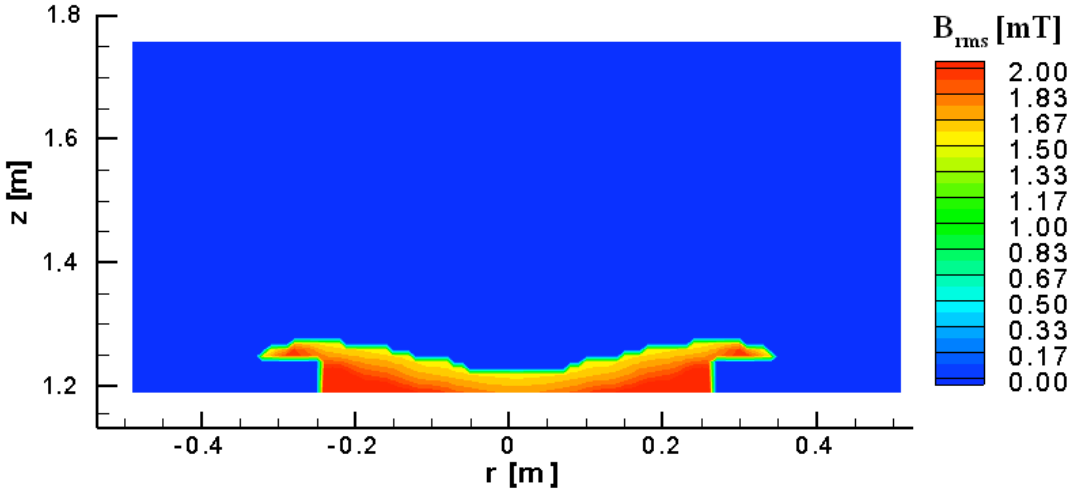

Figure 20 Positions where | B_{rms} | exceeds IEEE for extremities: Phase Encode Gradient

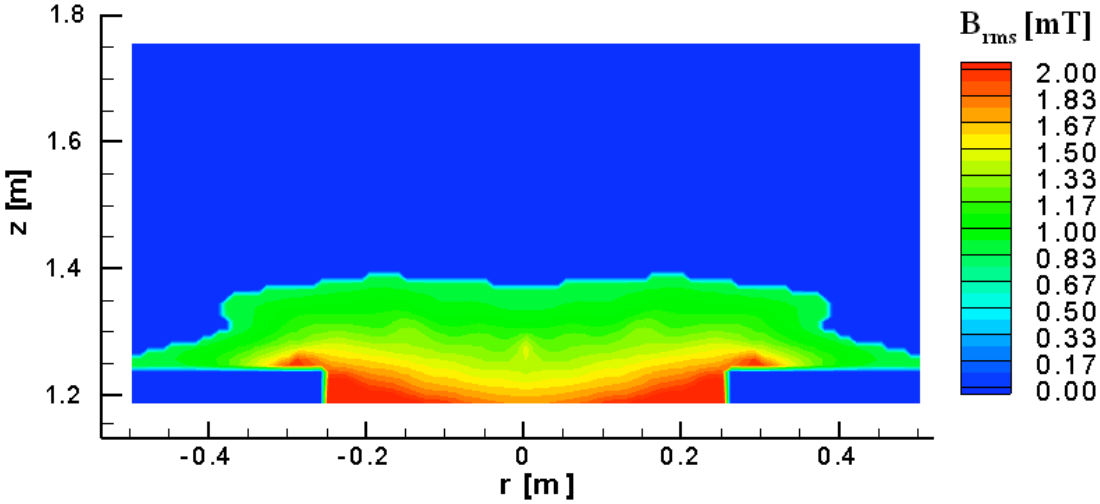

Figure 21 Positions where | B_{rms} | exceeds IEEE for Head and Torso: Phase Encode Gradient

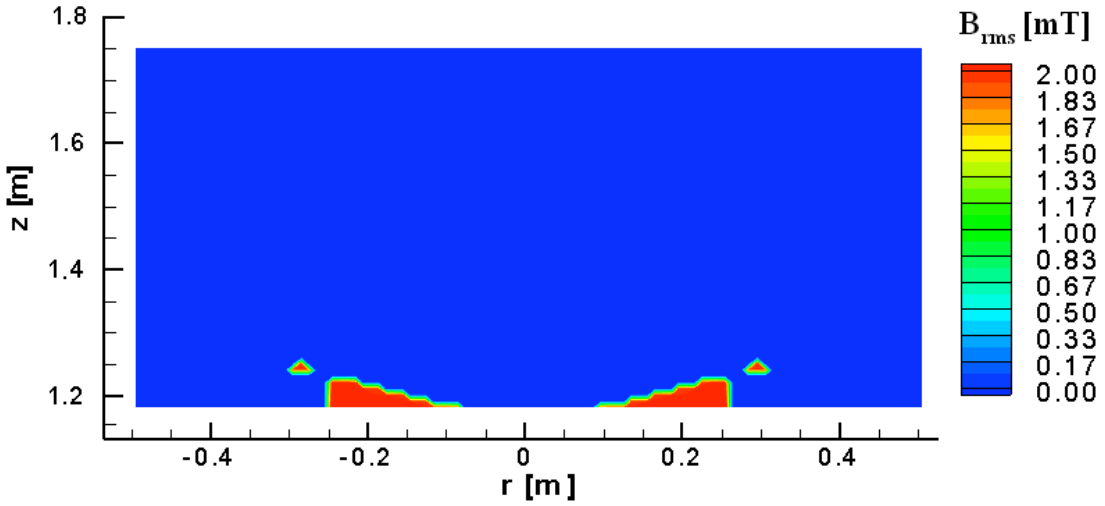

Figure 22 Positions where | B_{rms} | exceeds IEEE for extremities: Slice Select Gradient

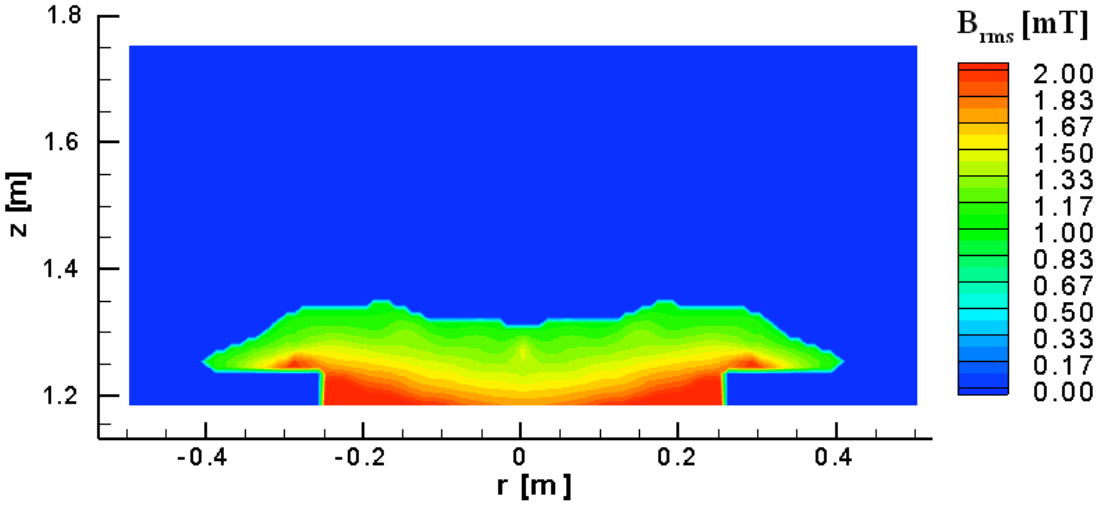

Figure 23 Positions where | B_{rms} | exceeds IEEE for Head and Torso: Slice Select Gradient

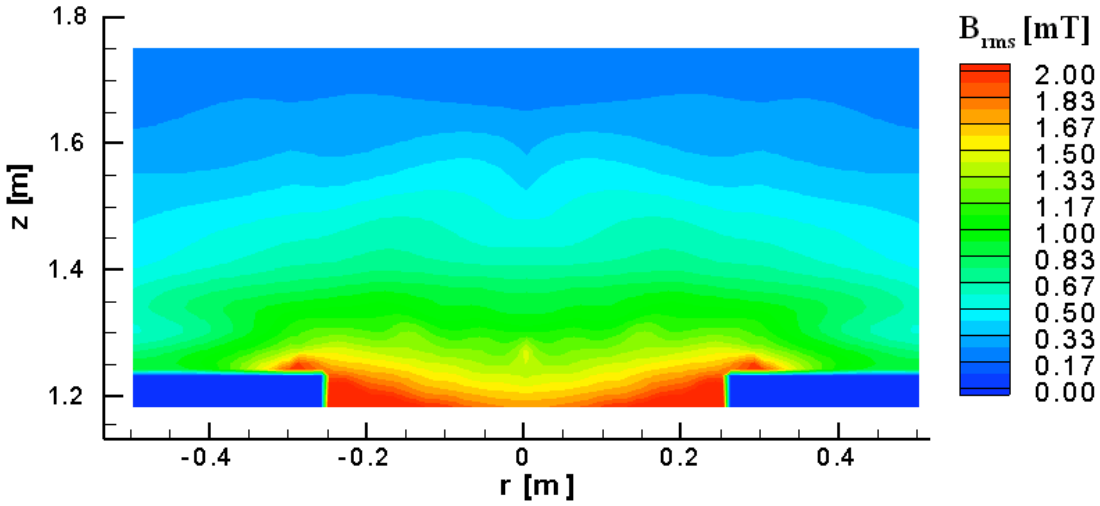

Figure 24 Positions where | B_{rms} | exceeds ICNIRP for Readout, Phase Encode and Slice Select Gradient

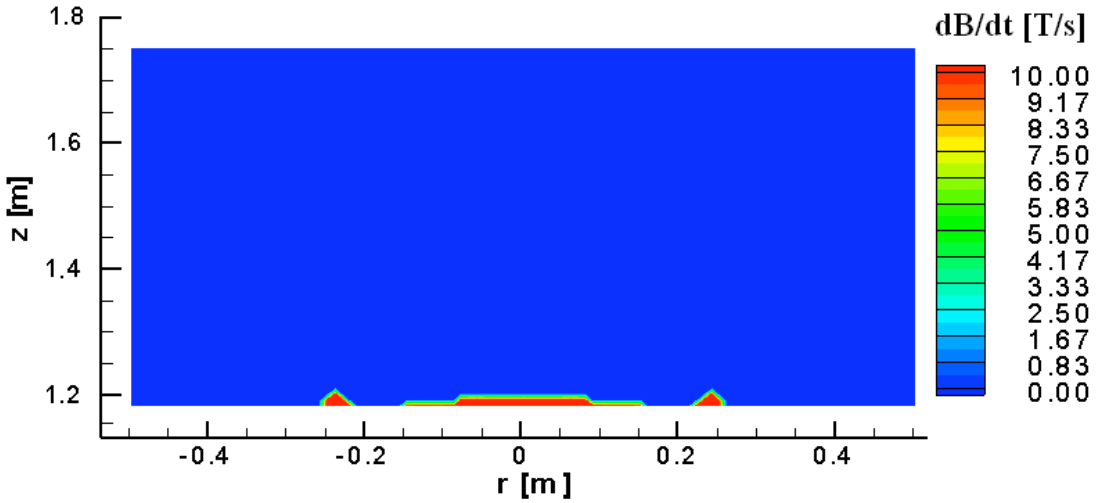

Figure 25 Positions where | dB/dt | exceeds IEEE for extremities

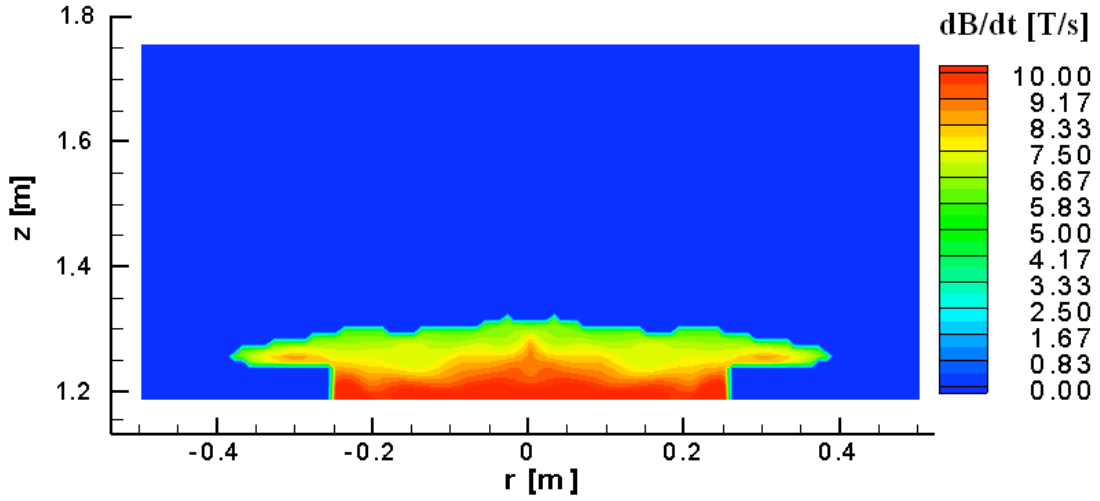

Figure 26 Positions where | dB/dt | exceeds IEEE for Head and Torso

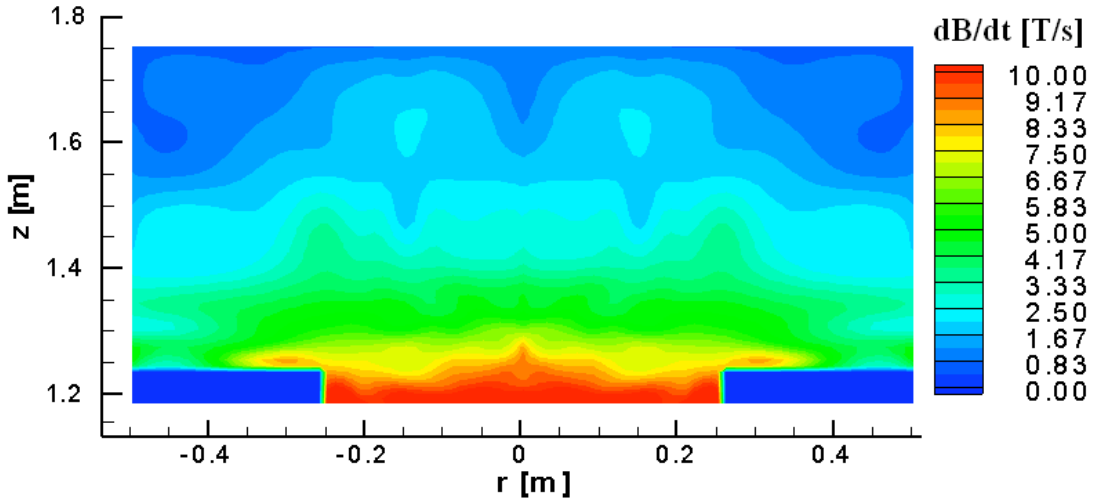

Figure 27 Positions where | dB/dt | exceeds ICNIRP

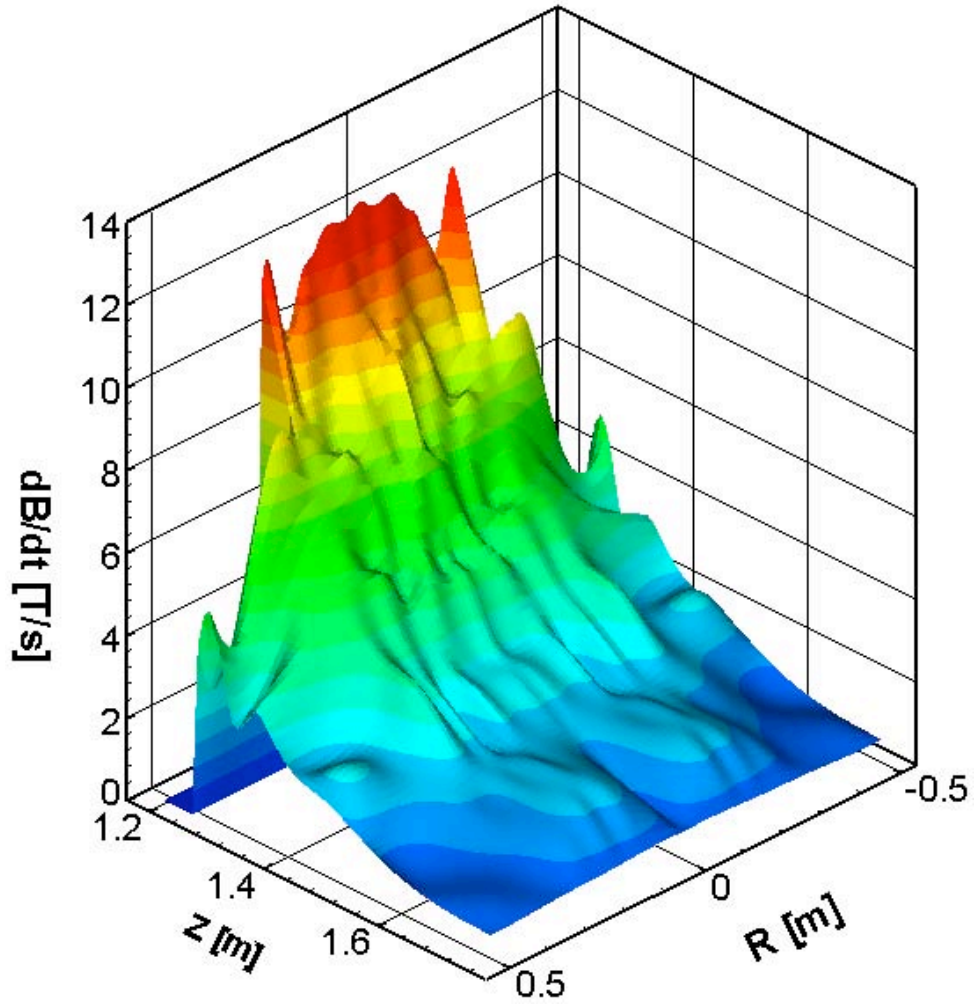

Figure 28 Experimentally measured peak | dB/dt | due to the gradient set of the 2 T MRI scanner using the EPI sequence of figure 4

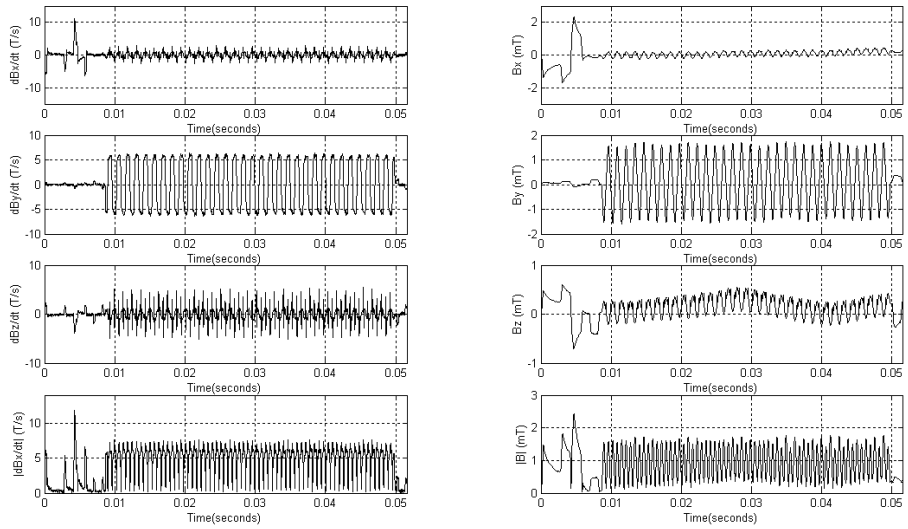

Figure 29 TR period of measured switching gradient data during the EPI sequence of figure 4 at position z = 120cm, x = 3cm, and y = 0cm

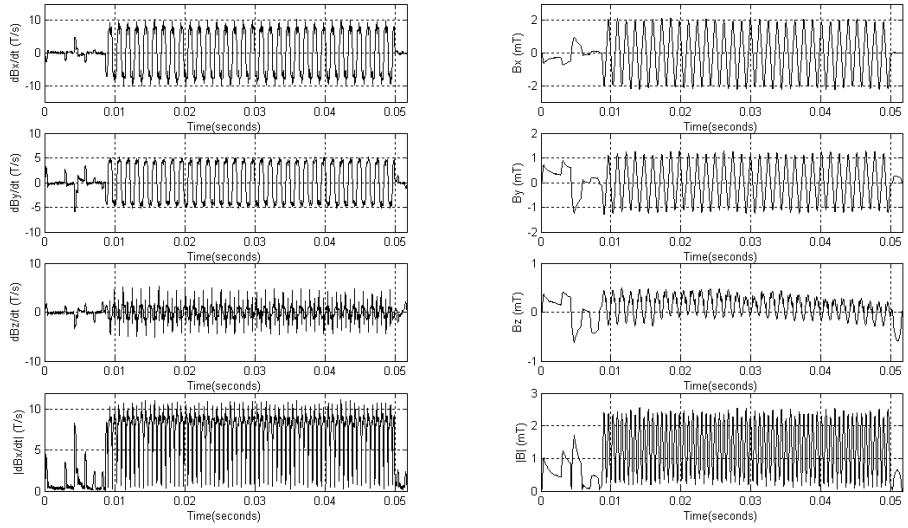

Figure 30 TR period of measured switching gradient data during the EPI sequence of figure 4 at position z = 120cm, x = 25cm, and y = 0cm

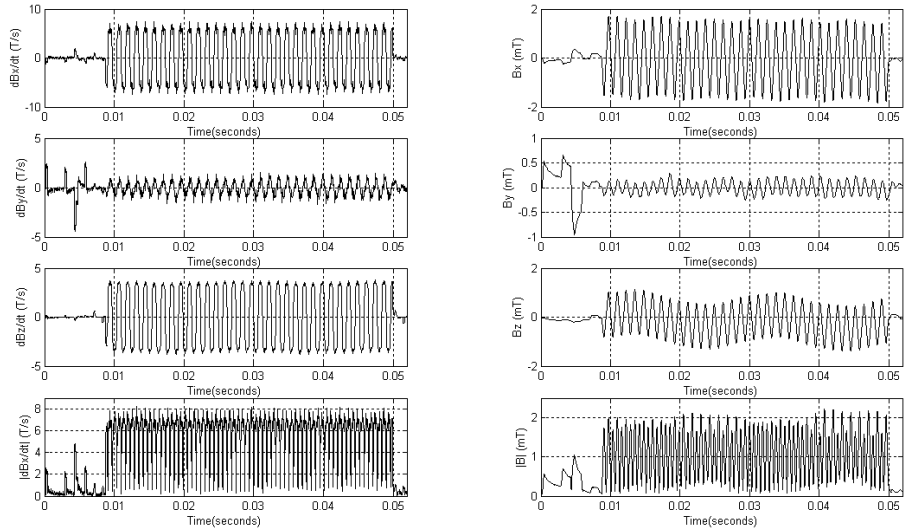

Figure 31 TR period of measured switching gradient data during the EPI sequence of figure 4 at position z = 126cm, x = 30cm, and y = 0cm

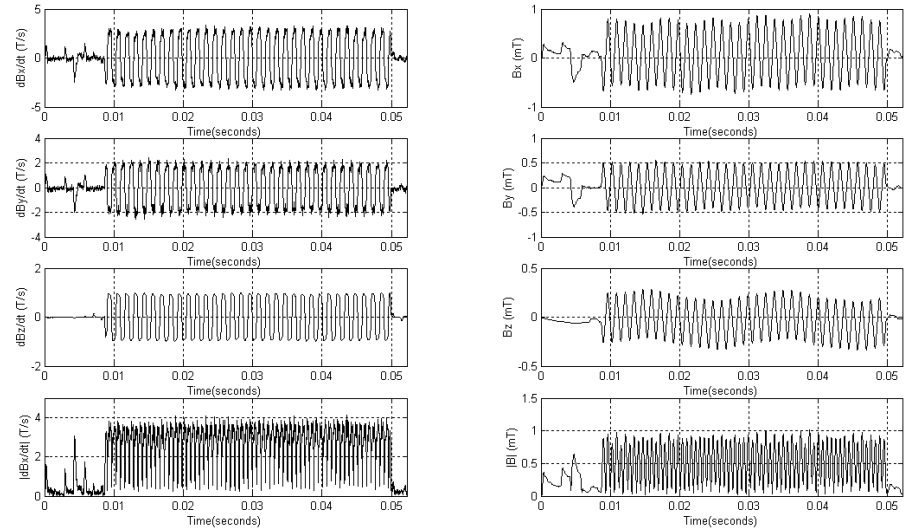

Figure 32 TR period of measured switching gradient data during the EPI sequence of figure 4 at position z = 126cm, x = 50cm, and y = 0cm

Figures 29-32 show a TR period of the EPI sequence measurements at various positions in the XZ plane at Y = 0cm. These figures show B_x, B_y, and B_z components present in all three of the measuring axes due to the misalignment between the measurements coordinate set and the gradient coil coordinate set. This misalignment was not unexpected and because the dosimeter was designed to evaluate the absolute values of the total magnetic flux densities and dB/dt's to get an overall calculation of magnetic field exposure we have used these values to evaluate

against the simulations and the regulations rather than the individual gradient coil contributions. However, by switching the gradient coils individually or otherwise, absolutely aligning the measurement axes to the gradient coil axes, the contribution of each gradient coil pair could to be examined individually.

4.3 Gradient pulsed magnetic field simulations

1. Direct current magnetic fields

Figures 33-37 illustrate the absolute value of total magnetic flux density produced by each theoretical gradient coil with a direct current adjusted to provide a 30mT/m central gradient field strength. To obtain direct correspondence with the experimental measurements, the magnetic fields were numerically evaluated in the X-Z plane (Y=0) and in the same region of interest as performed in the experimental study (see figure 4). From the total magnetic flux density profiles illustrated in figures 33-37, the peak fields are located very close to the gradient coil edges and the field drop off along the z-axis is rapid with the distance away from the gradient end. The magnetic fields are expected to be quite small in magnitude at the sides of the MRI machine, because the highly conducting cryostat vessel attenuates the dynamic fields well. Figure 36 is the absolute value plot of the total magnetic flux density generated by both the read out (x-axis) and phase encode (y-axis) gradient when switched on simultaneously, whereby each coil is prepared to generate central gradient field strength of 30mT/m. Figure 34 indicates that the magnetic field produced by the phase encode gradient is minimal in the X-Z plane when Y=0 and thus there is no significant difference between the field profile of figure 36 (x and y-gradient coil applied simultaneously) and figure 33 (x-gradient applied only). Therefore the influence of the y-gradient in this particular plane is small. Interestingly, for central gradient field strength of 30mT/m, the peak magnetic fields due to the z-gradient coil are around two times larger in magnitude than those produced by the x-gradient coil for instance. When all three gradients with central field strengths of 30mT/m each are switched on simultaneously, as are applied during oblique oriented imaging and diffusion studies, a total magnetic field profile as shown in figure 37 is generated.

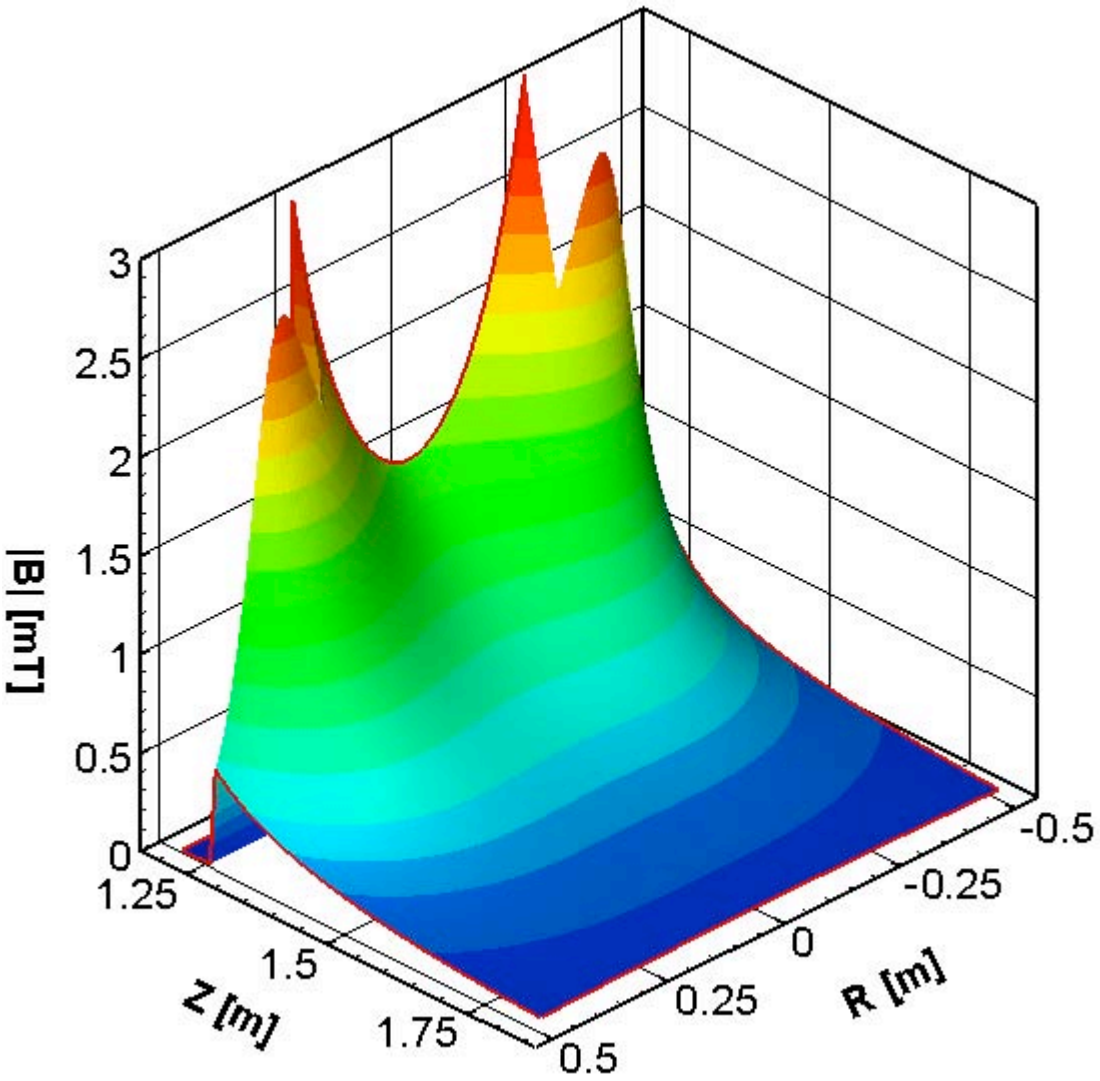

Figure 33 Theoretical |B|-field due to x-gradient with 30mT/m in DSV

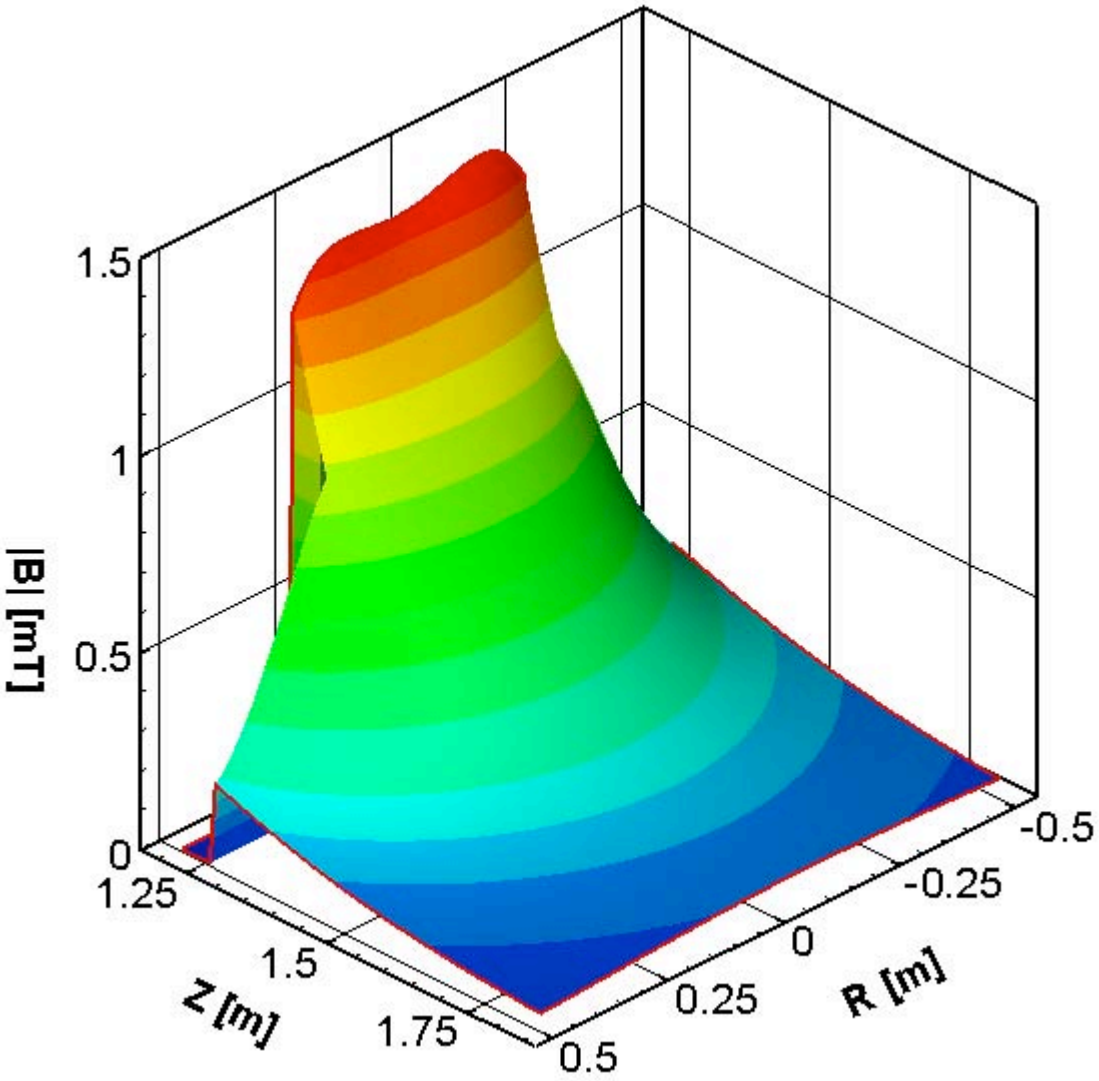

Figure 34 Theoretical |B|-field due to y-gradient with 30mT/m in DSV

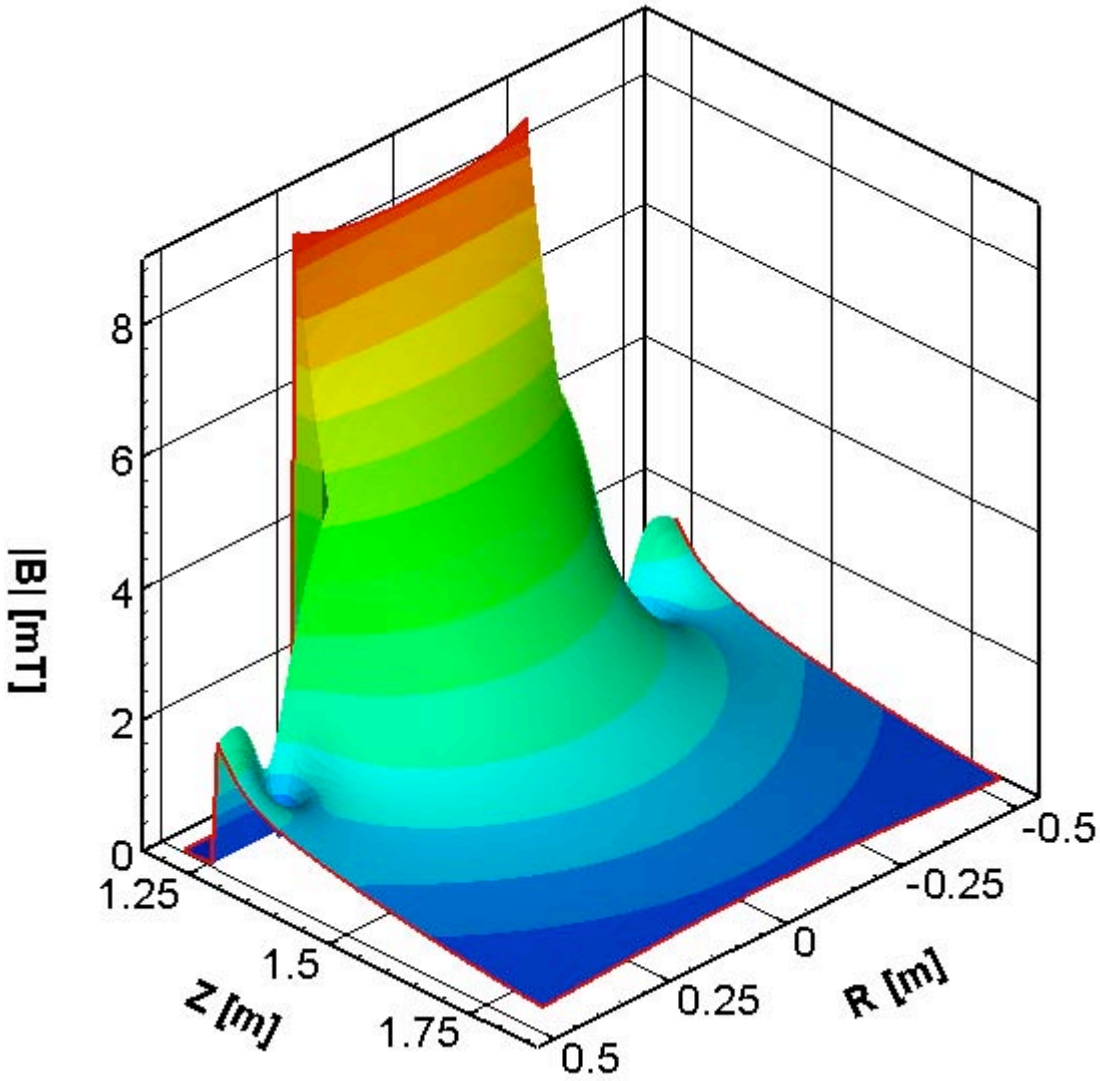

Figure 35 |B|-field due to z-gradient with 30mT/m in DSV

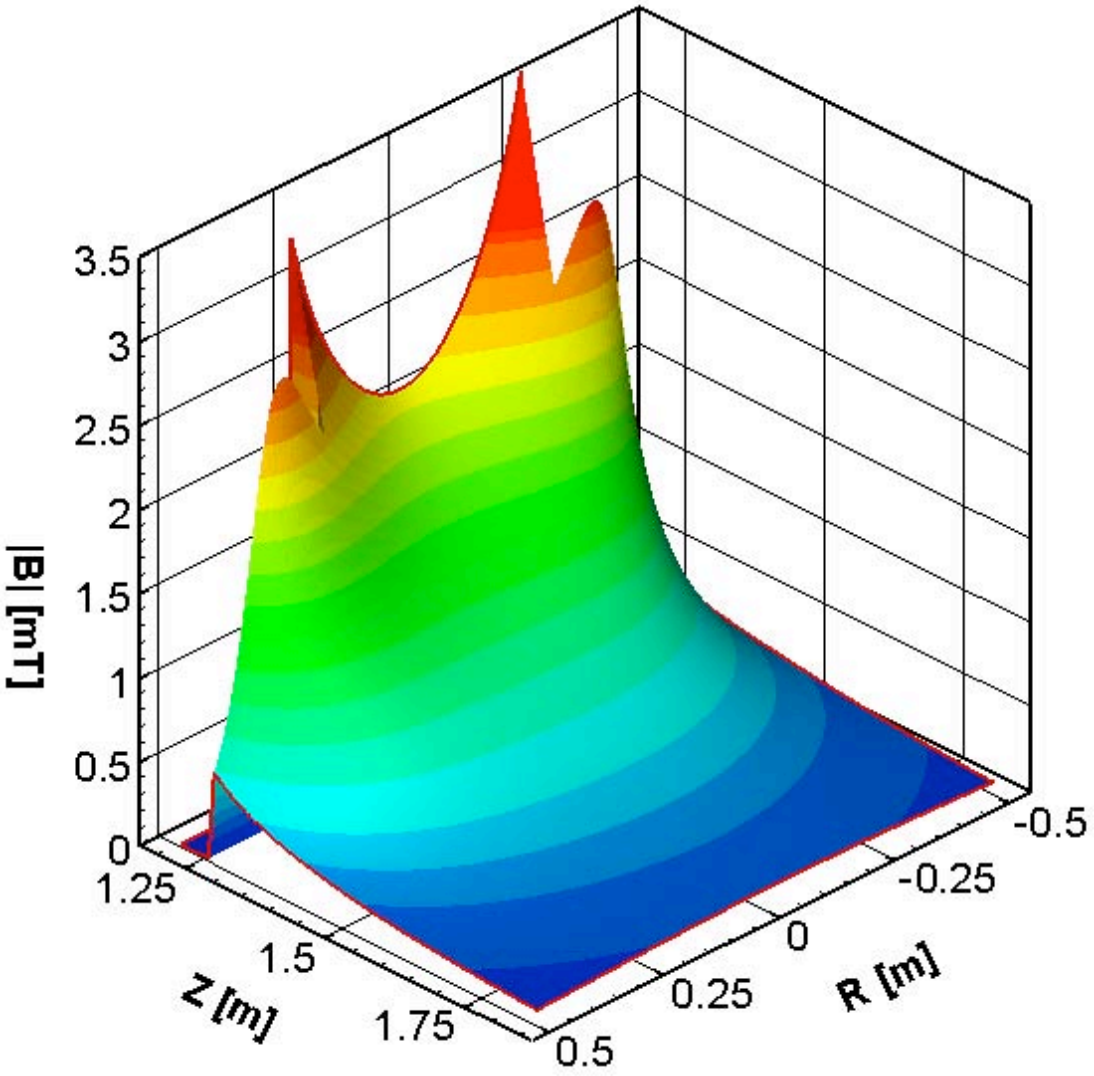

Figure 36 |B|-field due to x and y-gradient with 30mT/m in DSV each

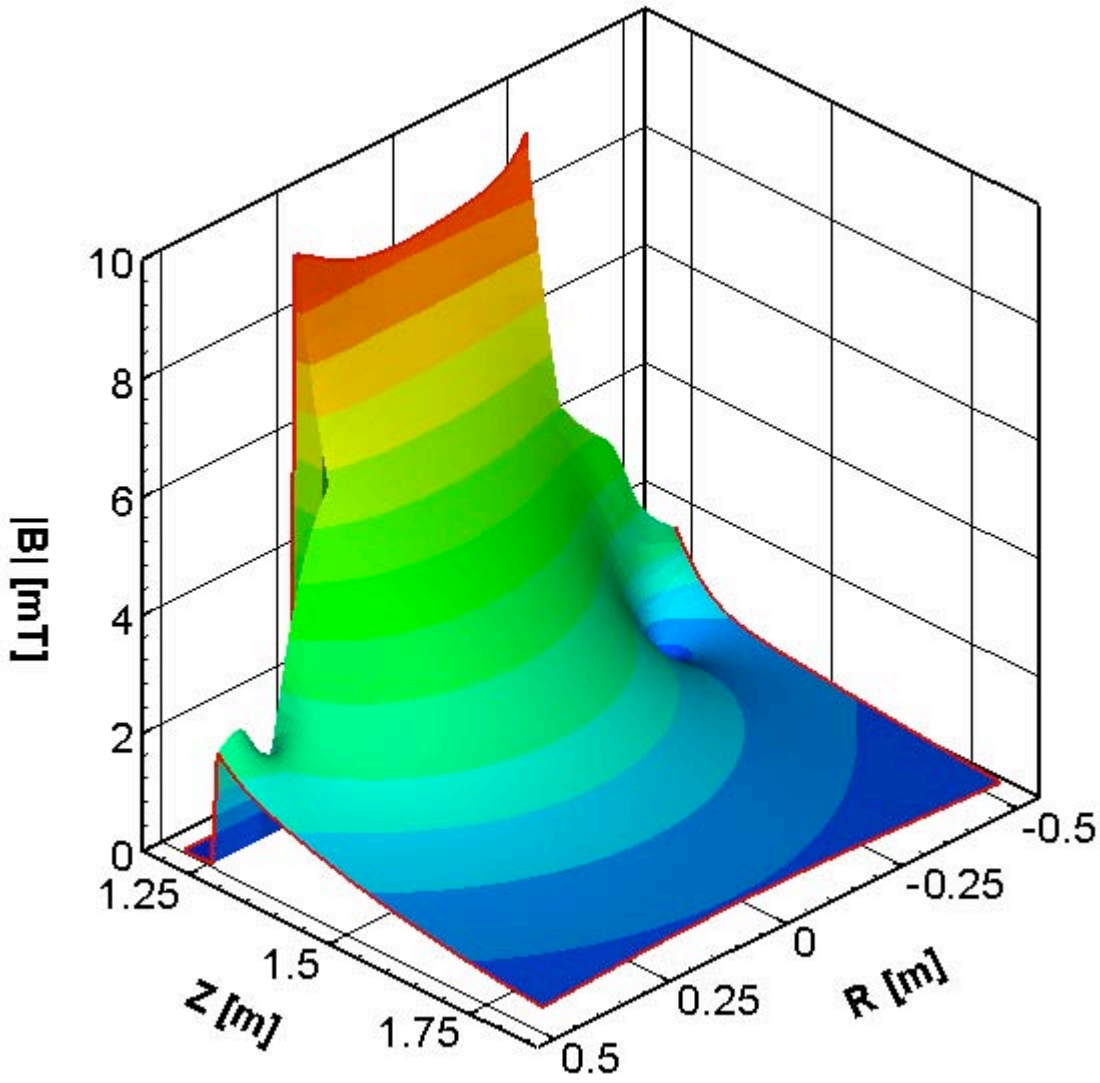

Figure 37 |B|-field due to all three gradients with 30mT/m in DSV each

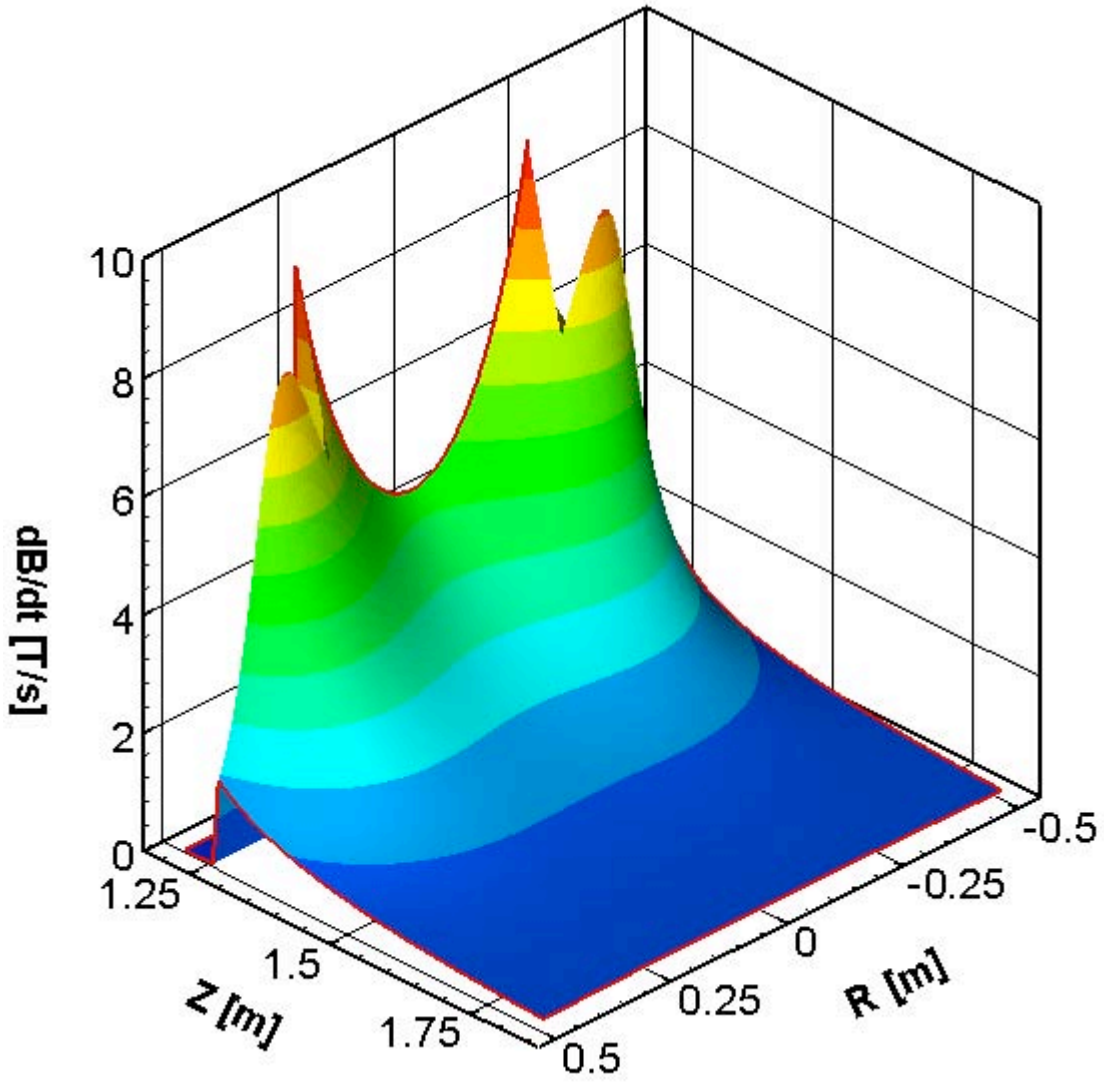

Figure 38 |dB/dt| due to z-gradient with 30mT/m in DSV (40%, see EPI sequence); Here: B is taken as the norm

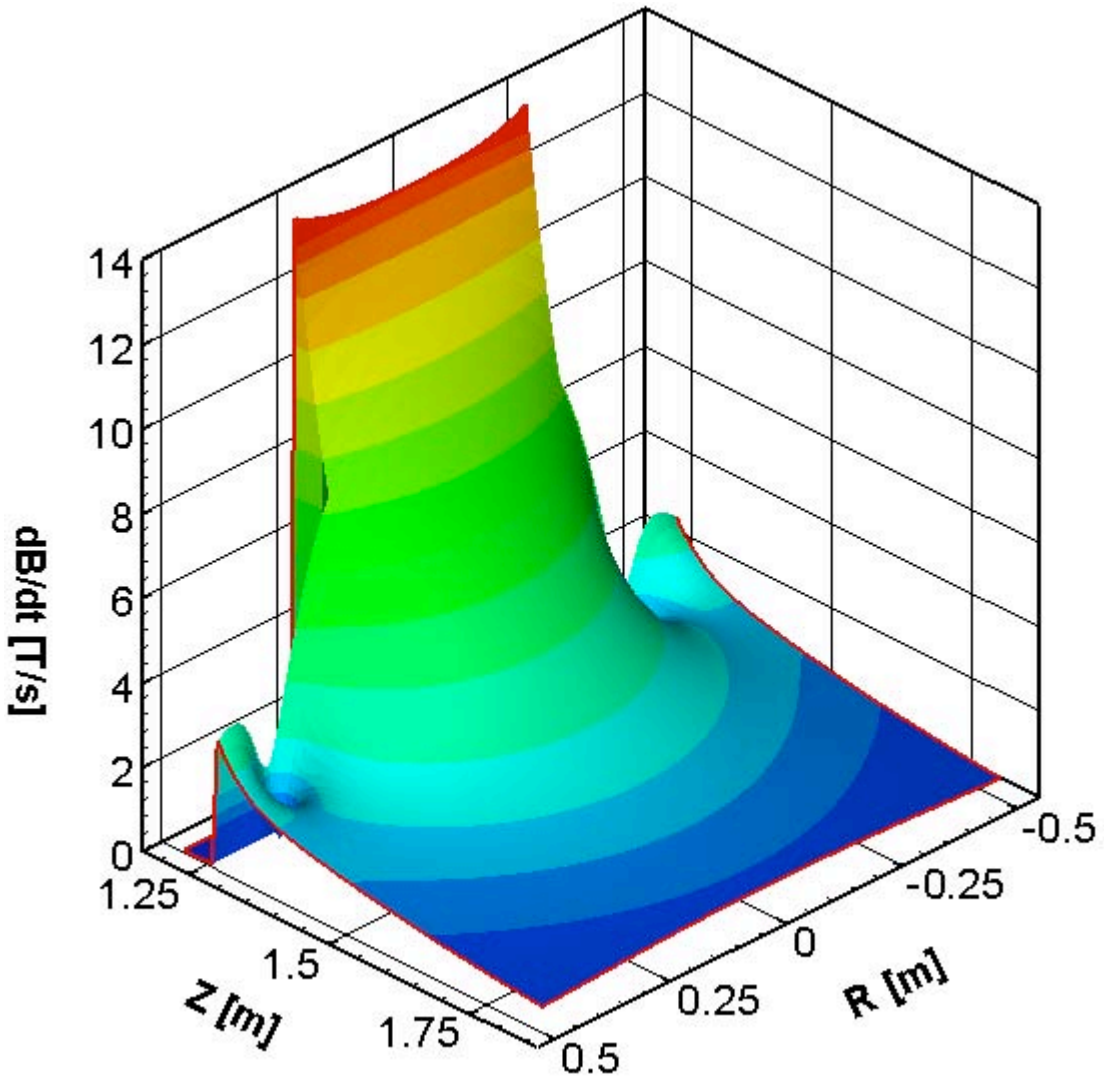

Figure 39 |dB/dt| due to x-gradient with 30mT/m in DSV (80%, see EPI sequence); Here: B is taken as the norm

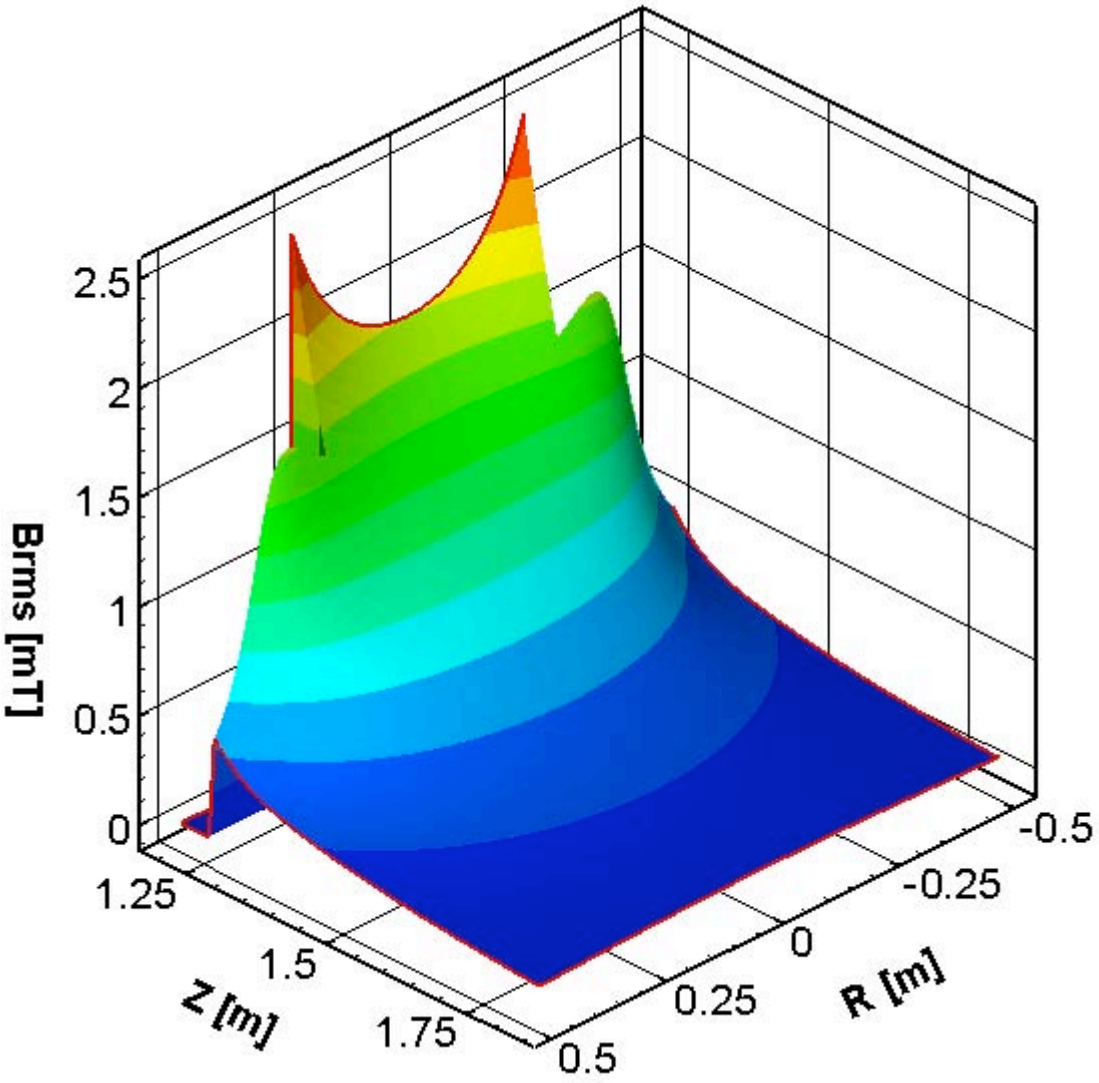

Figure 40 Numerically computed $|B_{rms}|$ due to the theoretical gradient coil set assuming the EPI sequence of figure 4.

2. Field simulation results with the Echo Planar Imaging (EPI) sequence

Figures 38 and 39 illustrate the spatial distribution of dB/dt produced by the z and x-gradient coils respectively. In both plots, the spatial distribution of dB/dt is identical to the magnetic flux density distribution generated by the slice select and frequency encode gradient while they differ in magnitude dictated by the individual gradient strength and rise time used. Figure 40 illustrates a spatial distribution of $|B_{rms}|$ in the x-z plane at the end of the theoretical gradient set starting at 0.1m inside the gradient set bore and extends towards the outside of the bore as portrayed in Figure 4.

4.4 Comparison between measured and simulated gradient fields

The numerically attained field profile of $|B_{rms}|$ in figure 40 agrees quite well in magnitude and reasonably well in spatial distribution to the experimentally derived $|B_{rms}|$ distribution depicted in figure 17. The slight discrepancies in spatial distributions are probably due to the fact that we used a theoretical gradient set that most likely has a different current distribution and therefore

somewhat different magnetic field profile to that of the 2T Bruker's gradient set. Nevertheless, the results indicate that there is a good corroboration between measured and calculated $|B_{rms}|$ field profiles even though a temporally challenging EPI time sequence was engaged during both simulation and measurement. Furthermore, this particular result confirms the validity of numerically evaluated male and female occupational worker exposures to magnetic fields produced by trapezoidally switched gradient coils in the previous study [21]. In the forthcoming research we will aim to utilize the measured values of magnetic fields as major subset of constraints in the optimization of gradient coil current distributions using methods such as stream function and target field. In this study the three measurement axes will need to be absolutely aligned to each gradient coil or each gradient coil switched individually to fully optimize the gradient coil current distributions. Alternatively, the measured field values can facilitate in the development of an equivalent source model based on elementary magnetic dipole moments that generate and mimic the same field pattern of a commercial system. These types of sources can then be used as part of the simulation to evaluate the induction of currents in anatomically equivalent body models analogous to the previous theoretical study.

Figures 18-24 show peak dB/dt's throughout the measurement regions and how they compare to the regulatory limits. In comparison to these simulations we observe that the peak dB/dt's are in the same range of magnitude as the numerical values. The maximum measured dB/dt is 12.25T/s at X=0m, Z = 1.20m, compared to the numerical values of 9.09 T/s for the read out gradient, 1.11 T/s for the phase encode gradient, and 13.63 T/s for the slice select gradient. The values are similar but are not exactly same because we have used different gradient coils in the simulations than those in the real MRI machine and because the largest numerical values occur at sharp corners and are therefore susceptible to changes to the cryostat vessel parameters (i.e. 5mm deviation in cryostat vessel position can noticeably change the dB/dt values). So therefore it is not very robust to directly compare these values to those measured.

4.5 Evaluation against regulatory safety limits

1. Static magnetic fields

The measurements presented show that the time weighted average exposures represent a small fraction of the allowable limits but that the dB/dt's experienced by workers as they move around the magnet room, especially during bending motions near the inner bore at the magnet ends often exceed the maximum allowable dB/dt of 767.9mT/s for the measurement bandwidth (0-7Hz). It was also found that during bending movements towards the imager core, the peak B field values exceed the maximum allowable instantaneous magnetic field exposure for the head and torso at 4T.

These dB/dt's and the associated induction of health-detrimental *in situ* electric fields and currents in terms of magnitude and spatial distribution in the body however, depends on the position of the radiologist relative to the static B-field produced by the imager, the direction of motion, the speed at which this motion is exercised and on the type of motion (jumping up, bending towards the imager bore or simply walking forwards or sideways etc). Therefore, the induced E-field magnitudes and distributions are highly-situation dependant, and as such, information on the measured dB/dt, peak B and cumulative B could be more useful in the assessment of the overall exposure and potentially exceeded limits. If the radiologist is bending towards the imager bore in order to assist the patient lying inside the scanner, the measured dB/dt values can exceed the value specified in the international regulations by a factor of around 4-5. Based on the results of our previous study on numerical simulations involving voxel phantoms of male and female as they undergo different kinds of motion around realistic super conducting magnets (1.5-7T), the induced electric field and current density magnitudes exceeded the limits specified in the ICNIRP and IEEE regulations by similar factors, provided that the body models were involved in movement very close to the magnet inner bore edges.

Therefore, based on current exposure measurements and computations, it is clearly possible to exceed the standards of IEEE, ICNIRP and EU-Directive.

The dosimeter itself can also be used to directly alert a worker that their body movements are causing excessive dB/dt's.

2. Switched gradient magnetic fields

To evaluate the switched gradient magnetic field exposures measured during the EPI sequence against the regulatory guidelines it is important to consider the $|B_{rms}|$ as well as the incident peak magnetic fields at positions outside the cryostat and gradient cooling system structure of the magnet. Figures 18-27 show the regions surrounding the magnet structure where the measured magnetic fields exceed the IEEE and ICNIRP regulations during the EPI sequence in terms of |Brms | and dB/dt. It is illustrated that the IEEE limits are exceeded in regions near the gradient coil ends, as predicted in the numerical models, whereas the ICNIRP limits are exceeded through the whole region that was measured.

We note here that the phase encode gradient provides maximum exposure in the YZ-plane when X=0, and minimum exposure in the XZ-plane when Y=0 (for other values of Y other than 0, the contribution of the phase encode gradient to the overall exposure is higher).

5.0 CONCLUSION

In this study we have developed and engaged an ambulatory tri-axial magnetic field dosimeter to experimentally quantify exposures of radiology personnel to both static and dynamic magnetic fields during normal working shifts within clinical MRI settings. The dosimeter was calibrated and used to measure magnetic field exposures associated with the body movement in static field strengths of 1.5T, 2T, and 4T during routine patient procedures. Similarly, worst-case exposures to pulsed commercial gradient coils were measured assuming the application of a practical Echo Planar Imaging (EPI) sequence. Apart from comparing the static and dynamic field exposures to most-recent international regulatory standards (IEEE, ICNIRP and EU-Directive 2004/40/EC), the field measurements from the gradient field sub-study were assessed against the numerical simulations of Appendices 1&2 with a high degree of corroboration. Our measurements confirm that workers can be exposed to magnetic fields exceeding the guidelines at positions near the main magnet and gradient coil ends during clinical imaging. The time weighted average magnetic field exposures in 1.5T, 2T, and 4T were all within the regulatory limits during static magnetic field measurements. The peak static field to the head of a healthcare worker leaning into a 4T MRI can exceed 3T. Nevertheless, some of the dB/dt values attributed to human movement through strong static magnetic fields exceeded the regulatory limits at all field strengths examined and therefore cannot be ignored. Similarly the magnetic field gradients generated when magnetic field gradient coils are pulsed at low frequencies exceed the regulatory limits at specific locations surrounding the main magnet and gradient coil ends.

More data and detailed situational studies need to be undertaken and compiled to fully understand the extent and nature of these exposures. We have shown that magnetic field dosimetry can be achieved in a practical manner and will be useful in providing workers with instantaneous warnings about over-exposure to magnetic fields. In addition, the results of these experimental measurements have confirmed the validity of the recent simulation outcomes on the exposure of tissue-equivalent body models in MRI environments.

6.0 ACKNOWLEDGEMENTS SPECIFIC TO THIS SECTION

The authors would like to thank Dr. Katie McMahon from the UQ Research Facility at the Wesley Hospital, Dr Gary Cowin from the Centre for Magnetic Resonance at UQ, Dr Melanie Fuentes from the Royal Brisbane Hospital, and Mr Ross Holt From Southern X Imaging Pty Ltd for arranging and overseeing the dosimetry studies at the testing sites. All studies were subject to approved ethics protocols governed by University of Queensland guidelines.

7.0 REFERENCES

[1] Stehling, SMK, and Turner, R Echo-planar imaging theory, technique and application, Springer, 1998.

[2] Crozie,r S, and Liu, F Numerical evaluation of the fields caused by body motion in or near high-field MRI scanners, *Progress in Biophysics and Molecular Biology*, **87**: 267-278, 2005

[3] Trakic, A, Crozier, S. and Liu, F Numerical modelling of thermal effects in rats due to high-field magnetic resonance imaging (0.5-1GHz) *Physics in Medicine and Biology*, **49:** 5547-5558, 2004

[4] Purves, GJ, Ausustine, D, Fitzpatrick, LC, Katz, A.–S, LaMantia, and. McNamara,. JO *Neuroscience*. Sinauer, Sunderland, Massachusetts, 1997

[5] Budinger, TF, Fischer, H, Hentschel, D, Reinfelder, H, and Schmitt, F Physiological effects of fast oscillating magnetic field gradients, *J. Computer Assisted Tomography*, **15**(6): 909-914, 1991

[6] Cohen, MS, Weisshoff, RM, Rzedzian, RR, and Kantor, HC Sensory stimulation by timevarying magnetic fields, *Magnetic Res. Med*., **14**: 409-414, 1990.

[7] Hebrank, FX SAFE model—a new method for predicting peripheral nerve stimulation in MRI, *Proc. Intl. Soc. Mag. Res. Med*., **8**, p. 2007, 2000.

[8] Mansfield, P and Harvey, PR Limits to neural stimulation in echo-planar imaging, *Magnetic Res. Med.*, **29**: 746-758, 1993.

[9] Schaefer, DJ, Bourland, JD, and Nyenhuis, JA Review of patient safety in time-varying gradient fields, *Jl. Mag. Res. Imag.*, **12**: 20-29, 2000.

[10] The **I**nstitute of **E**lectrical and **E**lectronics **E**ngineers (IEEE), C95.6: Standard for Safety Levels with Respect to Human Exposure to Electromagnetic Fields (0–3 kHz), New York, 2002

[11] **I**nternational **C**ommission on **N**on-**I**onizing **R**adiation **P**rotection (ICNIRP), Guidelines for limiting exposure to time varying electric, magnetic and electromagnetic fields (up to 300 GHz) *Health Phys.* **74**: 494–522, 1998

[12] Directive 2004/40/EC of the European Parliament and of the Council, *Official Journal of the European Union*, L **159**, 2004

[13] A Magnetic Field Dosimeter - PCT/AU2005/001495

[14] Liu, HW, Zhao, H, and Crozier, S On the Induced Electric Field Gradients in the Human Body for Magnetic Stimulation by Gradient Coils in MRI *IEEE Transactions on Biomedical Engineering*, **50** (7): 804-815, 2003

[15] Feng, L, Zhao, H, and Crozier, S Induced fields by body movement and head-shake in High-Field MRI, J. Magn. Reson. 161/1 pp 99 - 107, 2003

[16] Minetti, AE, et al Energetics and Mechanics of Human Walking at Oscillating Speeds *Journal of American Zoology*, Vol 41: 205–210, 2001

[17] Giansanti, D, et al The Development and Test of a Device for the Reconstruction of 3-D Position and Orientation by Means of a Kinematic Sensor Assembly With Rate Gyroscopes and Accelerometers *IEEE Transactions on Biomedical Engineering*, **52** (7): 1271-1277, 2005

[18] Keshner, EA Head-Trunk Coordination During Linear Anterior-Posterior Translations *Journal of Neurophysiology* 89: 1891-1901, 2003

[19] Kavanagh, JJ, et al Coordination of head and trunk accelerations during walking *European Journal of Applied Physiology* 94: 468–475, 2005

[20] Glover, PM, et al Static B_0 Field Monitoring at 3T and 7T: An MRI Dosimeter *Proceeding of ISMRM 14th Scientific Meeting,*, 2006

[21] Crozier, S, Wang, H, Trakic, A, and Liu, F Numerical evaluation of occupational worker exposures to pulsed magnetic field gradient coils in MRI, *Journal of Magnetic Resonance Imaging*, [in press]

HSE

Health and Safety Executive

Assessment of electromagnetic fields around magnetic resonance imaging (MRI) equipment

This report describes the results of an investigation of operator exposure to static and switched-gradient fields from magnetic resonance imaging (MRI) systems. The project involves both computational modelling and the measurement of personal exposure using dedicated magnetic field dosemeters. The work was undertaken by Professor Stuart Crozier of the University of Queensland acting as an MCL consultant.

The computational modelling has three strands: modelling of the static and switched-gradient magnetic fields from MRI systems with 1.5 T, 4T and 7T magnets; modelling of induced current densities and internal electric field strengths arising from motion through static field spatial gradients; modelling of induced current densities and internal electric field strengths from time-varying switched-gradient fields.

Close to the ends of the three MRI systems modelled, relevant occupational exposure could be exceeded by movement through the static field, or directly by the switched-gradient fields.

This project has shown that the MRI personal dosemeter is capable of indicating, in real-time, situations which might lead to exposure guidelines being exceeded.

This report and the work it describes were funded by the Health and Safety Executive (HSE). Its contents, including any opinions and/or conclusions expressed, are those of the authors alone and do not necessarily reflect HSE policy.

RR570

www.hse.gov.uk